MASSACHUSETTS INSTITUTE OF TECHNOLOGY

RE-23

ANALYTICAL AND EXPERIMENTAL INVESTIGATIONS OF LOW LEVEL ACCELERATION MEASUREMENT TECHNIQUES

by

S. Ezekiel, P.K. Chapman
and J.T. Egan

GPO PRICE $ ______

CFSTI PRICE(S) $ ______

Hard copy (HC) 3.00

Microfiche (MF) 1.00

ff 653 July 65

FACILITY FORM

N66 37305
(ACCESSION NUMBER)

144
(PAGES)

CR-78050
(NASA CR OR TMX OR AD NUMBER)

(THRU)

1
(CODE)

14
(CATEGORY)

EXPERIMENTAL ASTRONOMY LABORATORY
MASSACHUSETTS INSTITUTE OF TECHNOLOGY
CAMBRIDGE 39, MASSACHUSETTS

RE-23

ANALYTICAL AND EXPERIMENTAL INVESTIGATIONS OF LOW LEVEL ACCELERATION MEASUREMENT TECHNIQUES

by

S. Ezekiel, P.K. Chapman
and J.T. Egan

Experimental Astronomy Laboratory
Massachusetts Institute of Technology
Cambridge, Massachusetts, 02139

Approved W. Markey
Director,
Experimental Astronomy Laboratory

ACKNOWLEDGMENT

The authors wish to express their appreciation to the following persons: Professor Winston R. Markey, Mr. C. Louis Lothrop, Mr. Richard J. Jankins, Mr. Walter L. Littlewood, Mr. Eric A. Mattson, Miss May I. Fraser, and Miss Jean K. Harris of the Experimental Astronomy Laboratory without whose cooperation this program would have been impossible; Professor Samuel C. Collins and Mr. Robert P. Cavileer of the M.I.T. Cryogenic Laboratory for their advice and their tireless ministering to LLAMA's thirst for liquid helium.

This program was supported by DSR 4526 under NASA Grant NGR 22-009-080.

RE-23

ANALYTICAL AND EXPERIMENTAL INVESTIGATIONS OF LOW LEVEL ACCELERATION MEASUREMENT TECHNIQUES

ABSTRACT

An investigation has been made of techniques for the measurement of acceleration in the range 10^{-6} to 10^{-9}g. In developing an experimental apparatus, the approach was to seek unconventional mechanizations of the various components of a simple, linear, single-axis accelerometer, with considerable emphasis on system compatibility and with explicit provision of a means for calibration of the instrument. The resultant design choices are briefly outlined. Problems encountered in the design of a superconducting (Meissner effect) test mass suspension are described, together with results obtained from a feasibility demonstration model of the suspension. A laser interferometer was developed for the displacement detector and design principles for such a device are discussed. Restoring forces are generated by means of small coils within the suspension, and calibration is effected by means of controlled radiation pressure.

Shaoul Ezekiel
Philip K. Chapman
J. Thomas Egan

April 1966

TABLE OF CONTENTS

TABLE OF CONTENTS (cont.)

TABLE OF CONTENTS (cont.)

LIST OF FIGURES

LIST OF FIGURES (cont.)

CHAPTER I

INTRODUCTION

1.1 Applications of Very Sensitive Accelerometers

At the present time, devices are available for the reliable measurement of acceleration down to about 10^{-6} g. Sensitivities approaching 10^{-9} g have on occasion been claimed, but the calibration and stability of such instruments is open to serious question.

The development of a capability of making routine acceleration measurements in the micron/sec^2 (10^{-7}g) range and below would be useful in a number of areas, for instance:

i) Inertial guidance of electrically propelled space vehicles. This requires threshold sensitivities of about 10^{-7}g.

ii) Microseismology, including the detection of remote explosions. The accelerations of interest are of the order of 10^{-8}g, with periods of 1-100 seconds(1).

iii) The levelling of test tables during the precise test and calibration of other inertial components and the establishment of statistical models for the errors in such components.

iv) Vertical indication in orbit by active tracking of the gravity gradient. Thresholds below 10^{-10} g are required(2).

v) Various important physical experiments, such as tests of the principle of equivalence and the detection of gravitational waves(3).

1.2 The LLAMA Concept

LLAMA (for Low Level Acceleration Measurement Apparatus) is a system which has been developed in the Experimental Astronomy Laboratory of the Massachusetts Institute of Technology. The object of this program is the investigation of techniques for the construction of an accelerometer with a threshold sensitivity well below 10^{-6}g. While the present system is intended for laboratory use only, it is hoped that the technology developed will be of use in constructing operational acclerometers.

The first application of the system under development will be as a sensor for use in the dynamic levelling of an inertial test table: i.e., a component of an active filter of microseismic disturbances.

In a terrestrial calibration facility, it is extremely difficult to produce known accelerations of the magnitude of interest here. As an example, tilting a test table from the horizontal through one arc second gives an acceleration component parallel to the table of 5 μg. For this reason, a primary design consideration in the present program was that the system should be absolute in the sense that it did not require calibration in terms of a known acceleration input.

The simplest form of accelerometer consists of a damped, elastically suspended test-mass, with some form of readout of the displacement of the mass under an applied acceleration. For single axis operation, the test-mass must be supported, in directions perpendicular to the sensitive axis, by means of forces which are essentially decoupled from the sensitive axis.

Fig. 1.1 is a diagram showingthe various components of this type of accelerometer, in an elementary form. As mentioned above, a suitable calibration system (shown schematically by the balance pan and weights at the right in the figure) is of fundamental importance if the instrument is to be of use at very low acceleration levels.

The design approach used in the LLAMA program is to take each component of a simple accelerometer of this type and seek a new mechanization which will substantially improve performance.

1.3 General Design Considerations

It is a relatively simple matter to design a very sensitive accelerometer for use under free-fall conditions, as long as it is also possible to conduct any required test and calibration of the instrument under zero-gravity conditions. For a laboratory system, however, it is necessary to support the test-mass in the gravitational field of the Earth: as it is hardly possible that one could devise a support system with an adequate vertical stability, this implies that the instrument should be sensitive to horizontal acceleration only.

Microseisms constitute a background noise in all terrestrial acceleration measurements. Typically, the peak activity in the horizontal plane consists of a vibration with an amplitude of a few microns and periods of the order of a few seconds, giving rms accelerations of about 10^{-7}g. Because of this problem, the initial LLAMA system is being designed for operation in the vicinity of 10^{-6}g, so as to check the feasibility of the techniques used without undue complication of the test appratus. The instrument is, however, theoretically capable of operation at much lower levels.

1.4 Support of the Test-Mass

The primary goal in the design of a test-mass suspension for an accelerometer is control of the interaction between support forces and the dynamics along the sensitivie axis. In general, the following types of force-coupling may occur:

i) Threshold effects, static friction, etc. Any threshold which is present clearly imposes a lower limit on the attainable sensitivity of the instrument. For

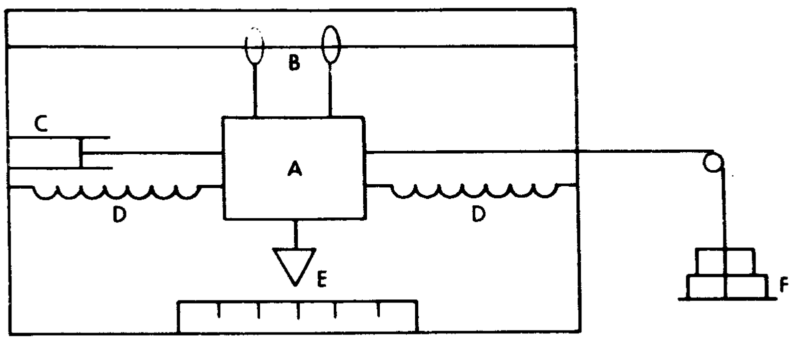

A: TEST - MASS
B: TEST - MASS SUSPENSION
C: DAMPING
D: RESTORING FORCE GENERATOR
E. DISPLACEMENT READOUT
F: CALIBRATION

Fig. 1.1 An Elementary Accelerometer

the purposes of LLAMA, such effects must bekept below 10^{-9} dynes, if at all possible.

ii) Conservative (position-dependent) forces: Assuming that no sharp non-linearities (e.g., mechanical hysteresis) are present, the level of force of this type which is acceptable depends on the expected amplitude of displacement. For instance, if the displacement is kept within 1 micron of the null position, an initial "spring constant" due to the suspension of 0.1 dynes/cm would allow operation at least down to the 10^{-6}g range. For high sensitivity of the instrument, a trade-off must be made between the difficulty of providing low conservative forces along the sensitive axis and the difficulty of detecting very small displacements.

iii) Dissipative (velocity-dependent) forces: It is, of course, essential that any motion of the test-mass in directions other than the sensitive axis be reasonably well damped. A small amount of natural damping of motion along the sensitive axis is also acceptable, although a fixed time constant means that the test-mass will be more than critically damped at sufficiently low acceleration levels.

For the present purposes, force-coupling corresponding to higher time derivatives of the test-mass displacement may be ignored.

Because almost any conceivable mechanical suspension would exhibit threshold and/or hysteretic effects beyond the stringent LLAMA tolerances, it was decided that some form of electromagnetic suspension would be used.

1.4.1 Magnetic Suspension

It can be shown quite generally that no configuration of permanent magnets is capable of stably supporting a magnetised test mass (Earnshaw's theorem). However, a ferromagnetic object may be suspended in a magnetic field if the field intensity be controlled by feedback from the position of the object. This principle has been used(4) to suspend models in wind tunnels, so as to avoid interference from support structures.

This technique is quite complex and expensive, and it is difficult to create sufficient spatial homogeneity of the fields along the sensitive axis for use in a low-level accelerometer.

A variant of this method is the magnetic resonant suspension(5) commonly used in floated inertial instruments. While avoiding the complexities of suspension feedback loops, this system suffers from the same type of field homogeneity problem, and in addition it is difficult to damp oscillations in directions other than the sensitive axis.

1.4.2 Electric Suspension

The electrically suspended gyro (ESG) demonstrates the feasibility of this type of support for inertial instruments(6). For use in an accelerometer, a typical design is shown in Fig. 1.2. A light conducting cylinder of radius a, constituting the test-mass, is contained within an outer electrode cylinder of radius b. The outer cylinder consists of four electrodes, numbered 1 to 4 in the figure.

Application of a voltage between any adjacent pair of electrodes produces a stress at the surface of the test-mass which is given by $0.442\ E^2$ microdynes/cm^2, where E is the voltage gradient at the surface in volts/cm, attracting the float to the excited electrodes. It is clear that, in order to support a float of reasonable weight in the Earth's gravitational field, quite high voltage gradients are required. The clearances around the float must therefore be very small, of the order of 25 microns, and the system must operate in a high vacuum (10^{-8} torr or better) so as to prevent electrical flashover.

As in the case of the magnetic suspension, this device is inherently unstable: the float height must be stabilized by feedback techniques. A convenient error signal may be obtained by comparing the capacitance between one pair of adjacent electrodes with that of the opposite pair in a high frequency bridge. For horizontal and vertical stabilization, two servo loops are of course required.

A resonant suspension technique is also possible in this case, the main disadvantage being the difficulty of providing adequate damping.

The dissipative forces in this type of suspension are extremely low, being mainly due to drag from residual gas in the system. If the outer cylinder be sufficiently long, so that end effects may be ignored, the only source of axial conservative forces is geometrical imperfection of the electrode and float cylinders. In particular, because of the very small separation between the float and the electrodes, surface roughness may produce axial forces which are significant at the levels under consideration for LLAMA.

While electric suspension is quite attractive (especially for use in the space environment, where the low support forces required allow much larger clearances), rather elaborate facilities are needed in order to construct the device. In the first place, the float should have as low a density as possible; beryllium is the usual choice, despite the machining problems introduced. Secondly, the tight dimensional tolerances make a pressurized clean room mandatory for construction.

1.4.3 Charged- Particle Suspension

In the electric suspension systems described above, the test-mass carries no net charge, the support forces being generated by polarization of the float under an applied electric field. It is also possible to support a charged particle in an electric field(7), if some provision be made so that the charge does not leak away too rapidly.

Apart from the difficulty of adequate position detection, support of a charged particle by servo control of an applied electric field is a relatively simple matter.

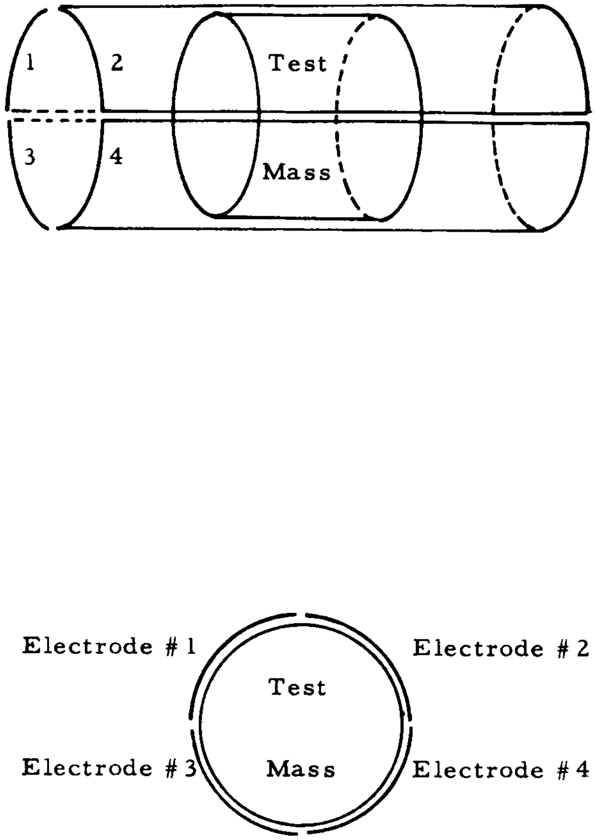

Fig. 1.2 Geometry for Electric Test-Mass Suspension

A more interesting possibility is that of a semi-passive suspension, using alternating fields.

The equation of motion of a charged particle in an alternating electric field is a variant of Matthieu's equation. Given some damping, quasi-stable solutions are possible, in which the particle executes a small oscillation about a stable mean position.

1.4.4 Cryomagnetic Suspension

A superconductor is perfectly diamagnetic (the Meissner effect): it is repelled by a magnetic field. It is therefore possible for a small permanent magnet to be stably suspended over a superconducting surface, without requiring any ancillary stabilization equipment. This phenomenon provides the basis for a simple and effective suspension system.

Despite the difficulty of operation at cryogenic temperatures, it was considered that this type of suspension offered the simplest mechanization and also the best compatibility with the other LLAMA components of all the possible field supports. Later chapters of this report describe the development of this concept into an operational system.

1.4.5 Displacement Detection

Starting from rest at 10^{-6}g 0.45 seconds are required to move through a distance of one micron. For a given acceleration, the bandwidth of an accelerometer depends strongly on the sensitivity of the displacement detection system. In order to maintain an adequate bandwidth, an accuracy of 0.1 micron was set as the design goal for the displacement detector in LLAMA.

An additional reason for limiting the test-mass displacement to very small values is that this minimises the effects of spatial non-linearity of any axial forces. It would otherwise be necessary to obtain a calibration curve for the instrument over the whole range of displacements.

The precision required of the displacement detector is such that interferometric methods offer the most practical solution. A specialized Twyman Green laser interferometer has been designed for LLAMA, in which, by means of a folded optical system, interference is obtained between light beams reflected from small, optically flat and parallel mirrors attached to either end of the test-mass. This technique gives twice the displacement sensitivity of a conventional interferometer and also allows the design of a system which is insensitive to the inevitable small oscillations of the test-mass about transverse axes.

1.4.6 Restoring Force Generation

At the acceleration levels for which LLAMA is designed, the maximum restoring force required is of the order of one microgram, for a test-mass of about one gram. Since the test-mass is a permanent magnet, the easiest technique is to control its position by means of currents in suitably placed small coils, and this approach has been adopted in the initial LLAMA system.

1.4.7 Calibration

As noted in Section 1.2, a primary consideration in the design of LLAMA was that it should not require an externally applied acceleration for calibration. The alternative, is of course, to apply a known small force directly to the test-mass. The most convenient source of such a force is radiation pressure from a mercury arc lamp. The maximum power needed in the calibration beam is of the order of one watt.

1.4.8 Damping

In the LLAMA suspension as finally developed, an adequate damping of transverse motion of the test-mass is provided by eddy-current generation in a surrounding copper jacket. The same mechanism gives some axial damping, which may be increasing by suitable filtering in the restoring force generation servo (see below).

1.4.9 System Aspects

Fig. 1.3 shows the manner in which the components described above are combined in the LLAMA system. The test-mass is a small permanent magnet, which is freely suspended inside a superconducting tube. Small optically flat mirrors are attached to the ends of the magnet, to form the fundamental mirrors in an interferometric displacement detection system. The interferometer produces an output signal whenever the test-mass is displaced from the null position in the center of the tube, and this signal is used to control the differential current in two small coils inside the superconducting tube, so as to provide a restoring force which keeps the test-mass very close to the null position. The ouput of the accelerometer consists of a measurement of the differential current in the coils, in the steady state.

Provision is made to calibrate the instrument periodically by allowing the beam of light from a mercury arc lamp to fall directly on the test-mass and noting the resultant output. The calibration and displacement detection beams are distinguished by color separation. The interferometer uses a helium-neon CW laser at 6328 Å: the mercury arc has a low output at this wavelength, which is further reduced by a rejection interference filter centered on the laser wavelength.

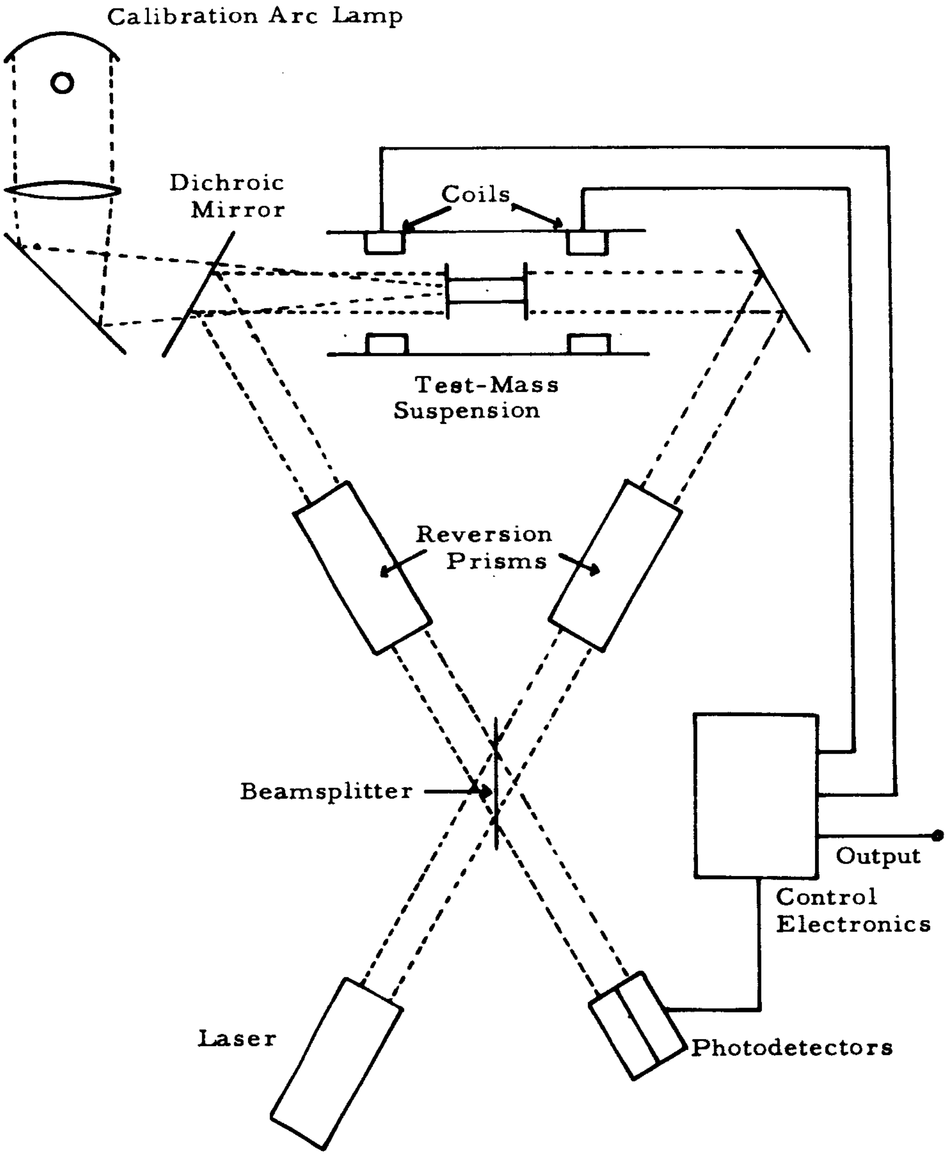

Fig. 1.3 The LLAMA System

CHAPTER II

THE MEISSNER EFFECT SUSPENSION

2.1 Superconductivity and the Meissner Effect

The phenomenon of superconductivity was discovered by H. Kamerlingh-Onnes at the University of Leiden in 1911(8), when he observed that the electrical resistance of mercury disappeared at a temperature of 4.15° K. While of course it cannot be stated categorically that a superconductor exhibits truly zero resistivity, an upper limit of 10^{-23} ohm. cm has been established(9).

A total of 24 elements and a great number of alloys and compounds(10) are now known to exhibit superconductivity. For bulk samples of pure metals, the change from the normal to the zero-resistance state is abrupt as the temperature is reduced (see Fig. 2.1), at least in the absence of a magnetic field, and the transition temperature is characteristic of the material, ranging from 0.35° K for hafnium (although lower transition temperatures will undoubtedly be found as cryogenic technology allows lower temperatures to be explored) to about 18° K for certain alloys of niobium and zirconium.

The transition temperature of a given sample is strongly affected by the magnitude and direction of any applied magnetic field. For a given specimen shape and orientation with respect to the the field, the critical field (defined as that field above which the material is in the normal state) has an approximately parabolic dependence on the temperature:

$$H_e \cong H_o \left[1 - \left(\frac{T}{T_c}\right)^2\right] \tag{2.1}$$

where T_c is the transition temperature at zero field and H_o is the critical field at zero temperature.

Because superconductors are perfectly diamagnetic (see below), when a given specimen is inserted into a constant field the actual field intensity at the surface will vary in a way which is dependent on the specimen shape and it orientation with respect to the field. The actual critical field is then given by

$$H_e = (1-n)\, H_c \tag{2.2}$$

where H_c, the maximum possible critical field for a given temperature and material, is obtained when the specimen is a long cylinder oriented

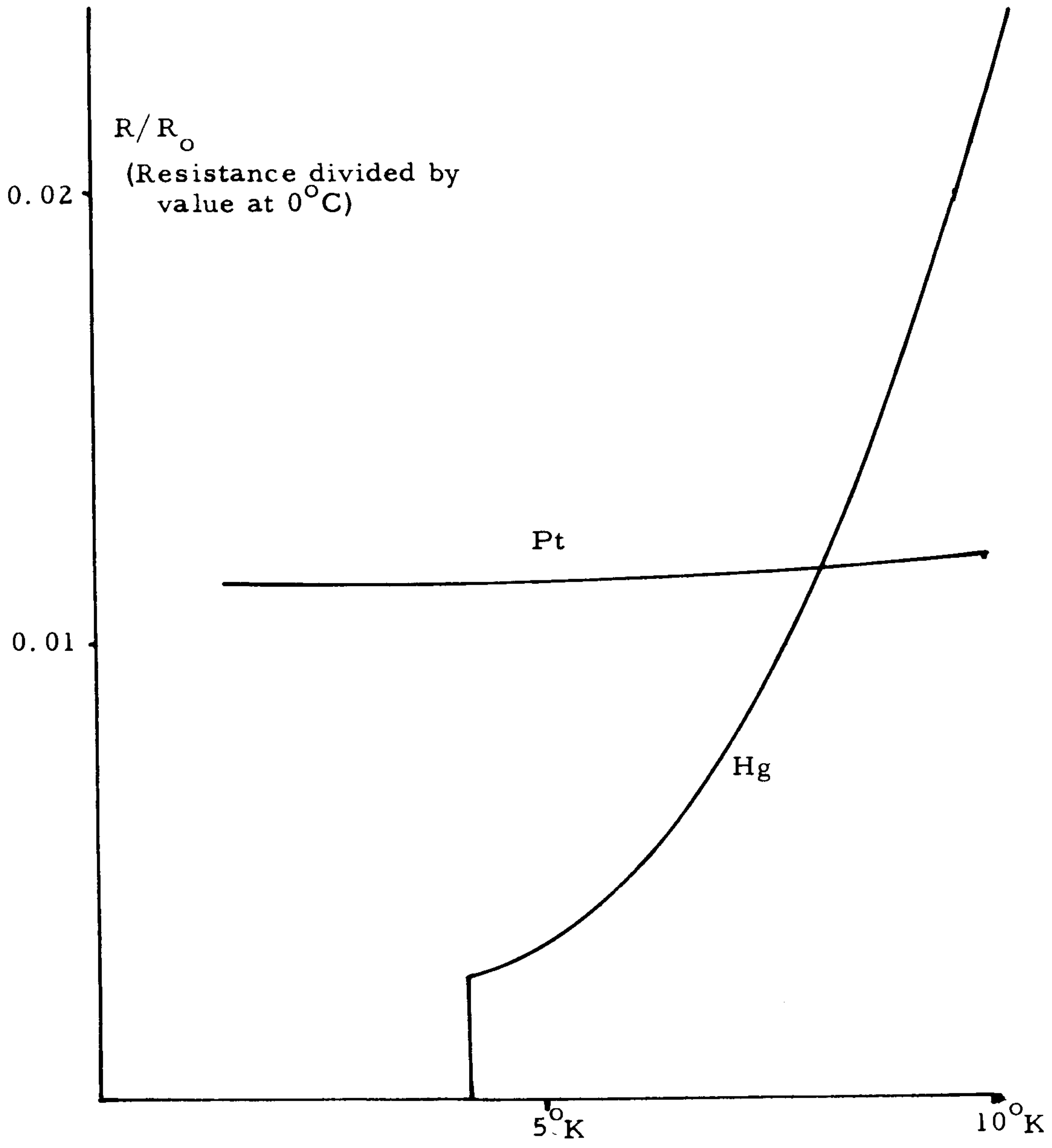

Fig. 2.1 Resistance vs Temperature for Platinum and Mercury(8)

parallel to the applied field (i.e., $n = 0$ for this case). For a cylinder perpendicular to the field, $n = 1/2$; for a sphere, $n = 1/3$; this parameter is known as the demagnetizing coefficient for the specimen.

When the field is between H_e and H_c, the specimen is in a complex state wherein some regions are superconducting and some are normal(11).

For the purpose of suspending a magnet over a superconducting surface, these complexities may fortunately be ignored. It is sufficient to state the the field due to the magnet at the surface of the superconductor must not exceed H_c, which is of course related to the temperature by an equation similar to (2.1), with H_o replaced by H_o', the critical field at zero temperature and demagnetizing coefficient.

Fig. 2.2 shows H_c versus temperature for several materials.

Apart from the above magnetic effects, until 1933, it was assumed that the magnetic properties of a superconductor were those of a perfect conductor. In that year Meissner and Ochsenfeld found that all magnetic flux is expelled from the interior of a superconductor as it makes the transition from the normal state(12). The Meissner effect was a radical discovery, which could not be predicted on the basis of any previous experiments. The implication for the present purpose is that any external magnetic field has a zero normal component at the surface of a superconductor, so that it behaves like a perfect diamagnet.

There have been many attempts at theoretical explanations of superconductive phenomena. One result from the Londons' theory(13) which is of interest in the present context is that the magnetic field inside a superconductor is not identically zero, but decreases from the surface according to

$$\nabla^2 \underline{H} = \underline{H} / \lambda^2 \tag{2.3}$$

If supercurrents are flowing, the current density obeys a similar law:

$$\nabla^2 \underline{J} = \underline{J} / \lambda^2 \tag{2.4}$$

For bulk specimens, these equations lead to an exponential decrease of magnetic field and current density with distance from the surface. The penetration depth λ is of the order of 10^{-5} to 10^{-6} cm, depending on the material.

For the present application, the significance of this result is that the superconducting sheet used in the test-mass suspension must be at least several microns thick. This fact can be of importance when the use of a thin superconducting plating over a normal base is considered (see Section 5.2).

The Londons' theory, in common with most other more-or-less successful descriptions of superconductive phenomena, was phenomenological in that rather

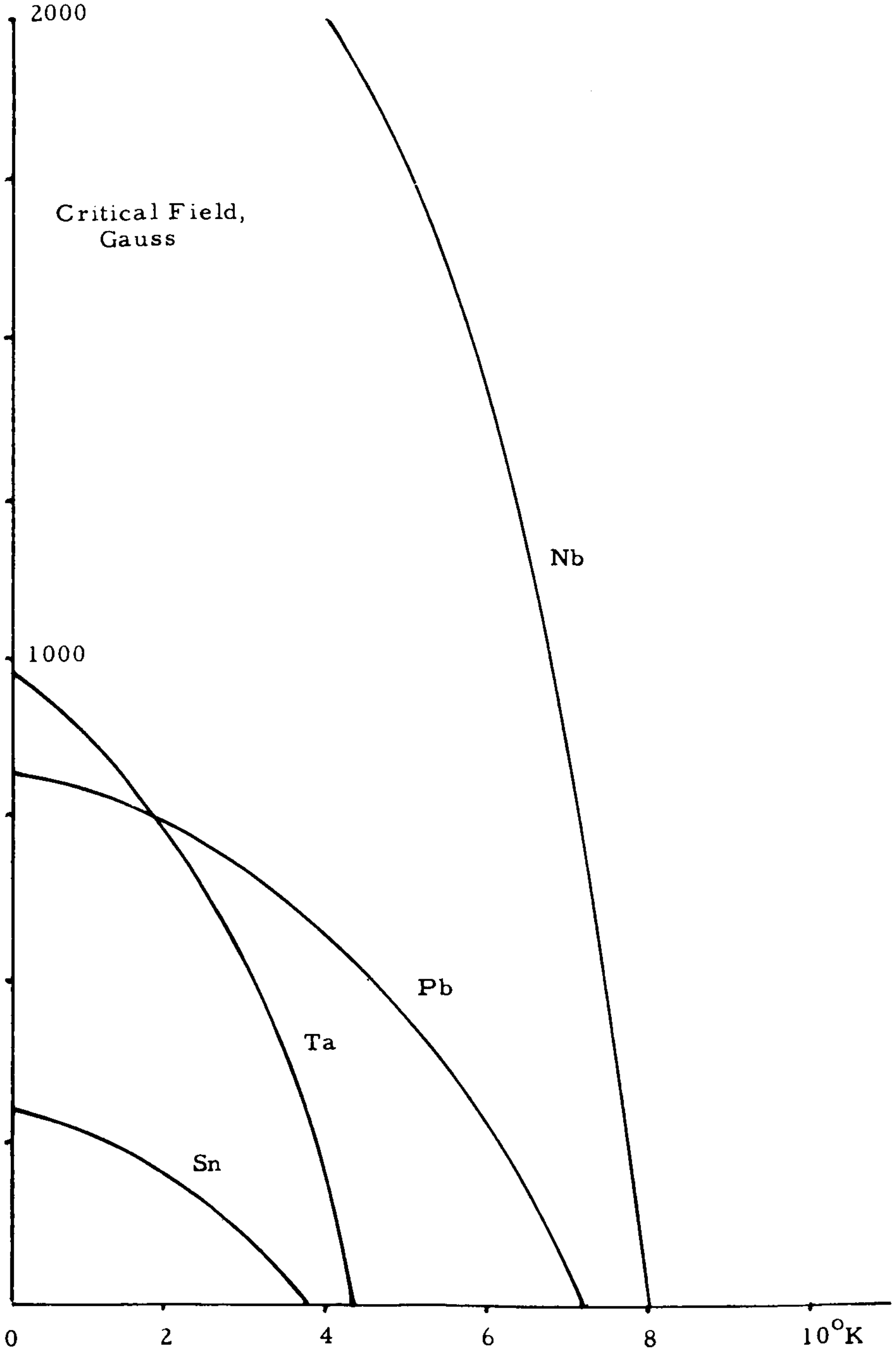

Fig. 2.2 Critical Field of Several Superconductors

arbitrary assumptions were made in order to explain experimental results. It is only quite recently that several microscopic (i. e. quantum mechanical) theories have been proposed which hold promise of explaining the observed effects in a detailed and self-consistent way. Of these, probably the most successful is the BCS theory (so called because it was developed by Bardeen, Cooper and Schrieffer(14) at the University of Illinois in 1957), which makes a basic advance in that it recognises the importance of electron-phonon interactions. In a pure conductor, the conduction electronics are fermions (i. e., have half-integral spin), so that they obey Fermi-Dirac statistics, at least at normal temperatures. If one considers the conduction electronics to be a gas of Coulomb-repulsive fermions ("Fermi sea") with negligible interaction with the crystal lattice of the metal, no explanation of the onset of superconductivity is forthcoming. At low temperatures, however, as the average momentum of the electronics decreases, lattice interactions become increasingly important, leading to an attractive two-electron (Fröhlich) interaction by phonon interchange (i. e., energy exchange via crystal lattice vibrations). An attractive interaction can of course lead to a bound two-electron state, but the decisive step in modern theories is the demonstration that the appropriate concept, for an ideal metal at very low temperatures, is instead a "pairing" of single-electron states; the pair of state behaves in some respects like a quasi-molecule in particular exhibiting integral spin, so that the electron gas can be considered as being composed of bosons, obeying Bose-Einstein statistics instead of the Fermi-Dirac model. As was shown long ago by Einstein(15), such particles exhibit an anomalous condensation into the single-particle ground state at low temperatures. Furthermore, it can be shown that an ideal Bose-Einstein gas, below its condensation point, exhibits a Meissner effect (16).

An adequate description of modern quantum theories of superconductivity is beyond the scope of this report, but several excellent texts have been recently published(17).

2. 2 The Floating Magnet

Consider a small permanent magnet placed over a large, horizontal superconducting plane. As was first demonstrated by Arkadiev(18), the diamagnetism of the superconductor may produce a repulsion which is sufficient to overcome the weight of the magnet, causing it to be stably suspended.

A more pictorial way of thinking of this phenomenon is the following: At this macroscopic level, the small penetration of the field into the superconductor may be neglected. The lines of force near the superconductor must therefore be parallel to the surface. The resulting field distribution is identical to that which would be produced (without the superconductor) by the magnet together with an "image" of the same sign an equal distance below the surface. The height at which the magnet will float over the superconductor is therefore equal to half the height at which it could just be supported by an identical magnet.

When the magnet moves over the superconducting surface, the image moves with it. The system is therefore neutrally stable with respect to horizontal displacement, and constitutes an essentially "stictionless" suspension.

Once a means of establishing a suitable superconducting surface has been provided, the Meissner effect suspension is extremely simple, as compared with the systems discussed in Sections 1.4.1 to 1.4.3, because it does not require feedback techniques to ensure vertical stability. In addition, quite substantial float heights (at least 1 cm) may be obtained, minimising forces due to surface roughness, etc.

2.2.1 The Cryogenic Gyro

A considerable amount of effort has been devoted during the last decade to the application of the Meissner effect as a frictionless bearing for gyros and small instrument motors. In general, the approach has been the converse of that suggested for LLAMA, in that a superconducting body has been levitated in a magnetic field.

The advantage of this technique, of course, is that one is not limited by the flux densities available from a permanent magnet, so that fairly heavy bodies may be floated. For example, Harding and Tuffins(19) have experimented with a niobium sphere weighing 300 gm: as the low friction support allows such rotors to be spun at speeds in excess of 20,000 rpm, the potentialities for gyroscopic applications are obvious.

For stable support of a spherical rotor, a mechanical potential minimum must be exhibited, which is quite simple to arrange with a suitable array of coils. For the LLAMA application, however, it is very difficult to obtain a sufficiently homogeneous field, in the direction of the sensitive axis of the accelerometer, using this technique.

An even more serious difficulty arises because the suspended body is very effectively thermally isolated from its surroundings, including the cooling system, so that any radiant heat influx may cause it to go normal. In fact, Simon(20) found that too low a gas pressure in a superconducting ball bearing of this type caused his suspended ball to cease superconducting, due to a lack of convective dissipation of the small heat influx through an observation port. In general, a compromise must be found between low gas drag on the one hand and adequate cooling of the suspended body on the other.

In the LLAMA system, it is proposed to use radiation pressure for calibration, with a consequent power influx to the test-mass of up to one watt. It is most unlikely that it would be possible to obtain sufficiently reflective end mirrors and sufficiently good radiative and/or convective cooling to maintain a superconductive test-mass under these circumstances. However, as discussed in the next Section, it may be desirable to abandon radiation pressure calibration in some applications of LLAMA, in order to be able to use a test-mass consisting of a small coil of superconducting wire, carrying a high supercurrent and arranged so as to simulate a permanent bar magnet, as far as its external field is concerned.

2.3 Choice of Magnet

The most powerful permanent magnetic material readily available in the form of small bars is Alnico V, which has an attainable BH product of 0.21 ergs/cc. Cylindrical magnets of diameter 0.318 cm (1/8") were chosen. From the manufacturer's published data, magnets with a permeance coefficient of 20, corresponding to a length to diamter ratio of 5, exhibit the maximum value of BH product.

The data presented by the manufacturer allow the calculation of the flux density at the center of a given bar magnet. However, the pole strength, and hence the expected float height, is not derivable directly from these data. In addition, once cannot be certain that the magnets being used are actually magnetised to saturation.

In order to evaluate realistically the height at which the magnet could be expected to float, as a function of its length, bars cut to various lengths in pairs were obtained. These were freshly magnetised, and the jig shown in Fig. 2.3 was used to determine the height at which each magnet would just support its mate. In these experiments, the upper magnet was raised very slowly until the lower one dropped, the separation at this time being twice the float height at the bar under test. The results are plotted in Fig. 2.4.

It is apparent that the float height does not depend very critically on magnet length. In order to minimise the power required in the calibration light beam, the test mass should be as light as possible, so bars of length 1.6 cm and mass 0.9 gm were chosen.

As a rough check on this choice, a shallow lead dish was placed in a transparent dewar, as sketched in Fig. 2.5 The inner vessel was filled with liquid helium, and the chosen magnet was lowered into the dish by means of non-magnetic tongs. It was observed that the magnet floated at a height of about 1 cm over the lead surface. Boiling of the helium caused the little bar to dash about at random in the dish.

2.4 Suspension Geometry

The superconducting plane discussed so far allows the magnet to move freely in two dimensions. In order to make a single-axis device, a superconducting trough may be used. The magnet then encounters a restoring force on displacement in any direction except along the axis of the trough.

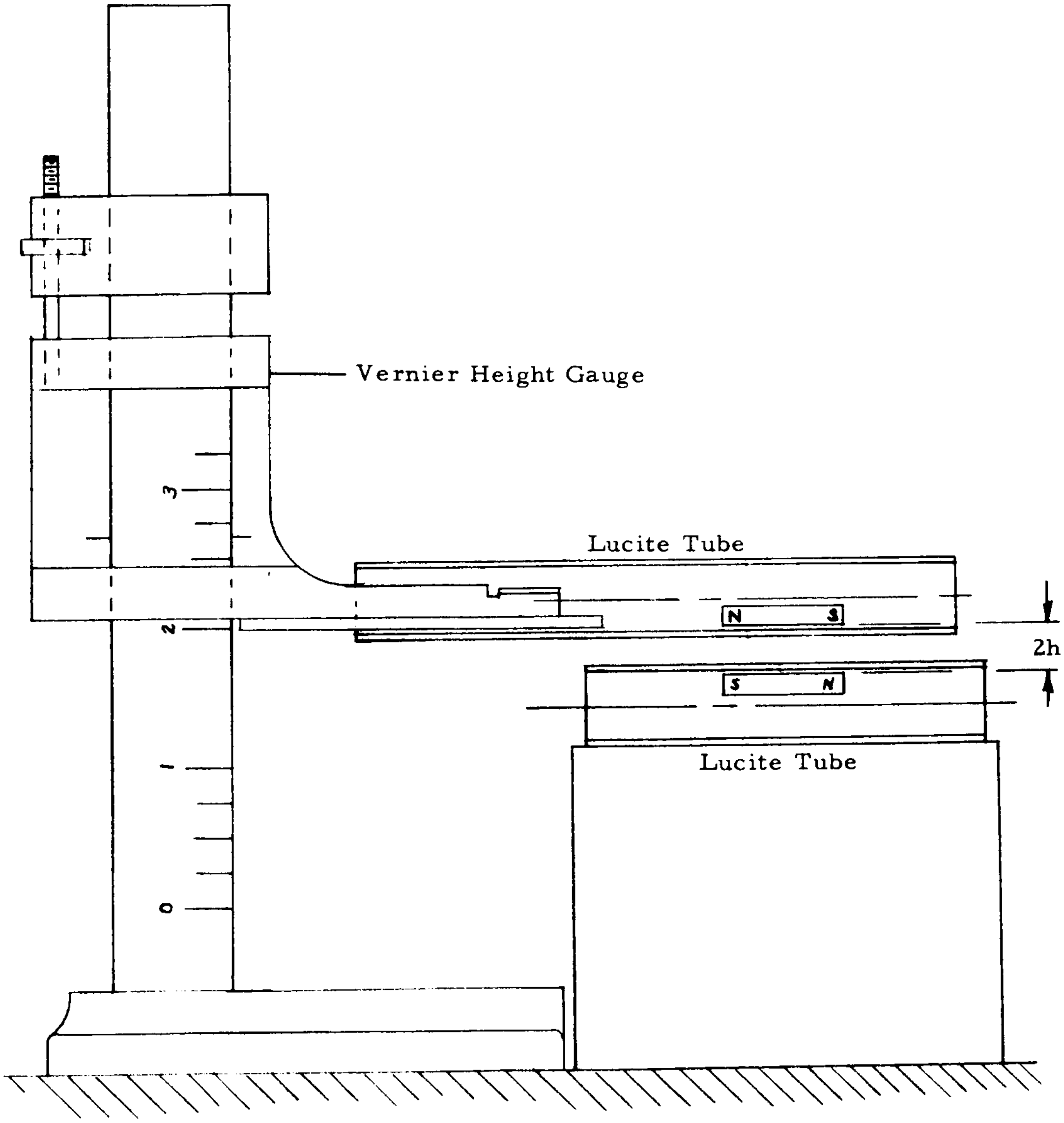

Fig. 2.3 The Float-Height Test Jig

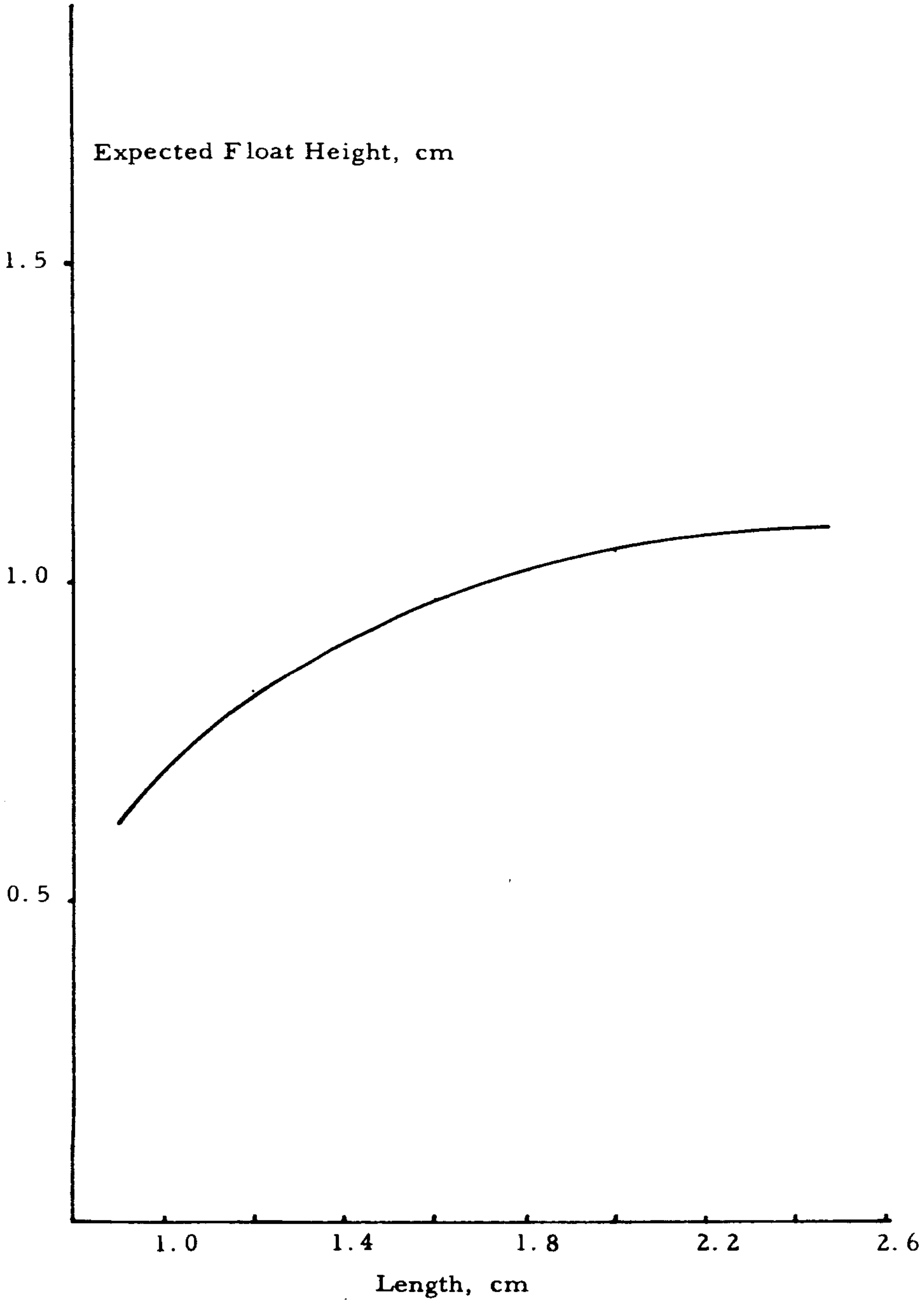

Fig. 2.4 Float Height vs Magnet Length

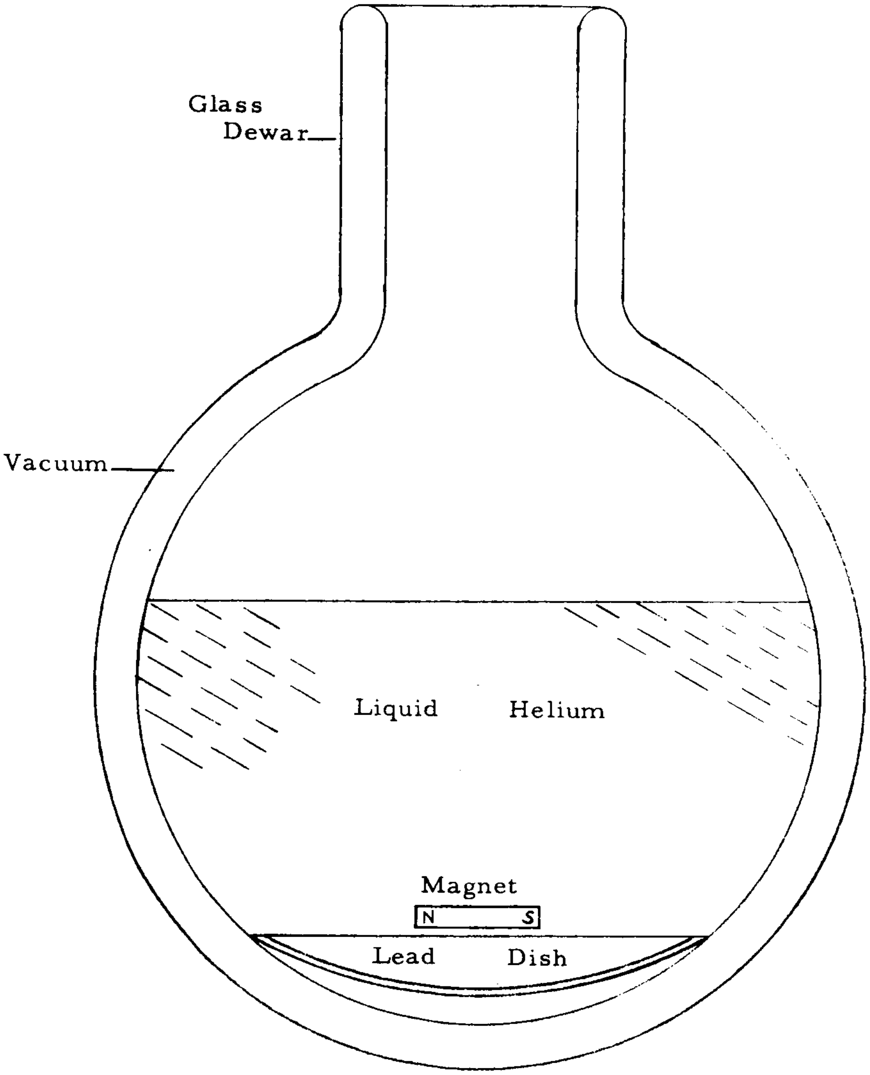

Fig. 2.5 The First Flotation Experiment

Unfortunately, the image concept used in discussing the superconducting plane is not applicable to this case. Qualitatively, however, one might expect that the float height would be greater in the case of a trough of semicircular cross-section than in the case of the plane.

For discussing qualitatively the behavior of the floating magnet, another simple mental picture may be used to replace the image concept. Since the energy stored locally in the magnetic field is proportional to the square of the field strength, the magnet tends to move in such a way that the lines of force are separated as widely as possible, this being the minimum-energy configuration. The magnet therefore behaves as though there were a repulsion between the lines of force in its field.

In particular, this concept allows a discussion of edge effects. When the magnet is near an edge of the superconducting surface, some of the field "spills over", forcing some of the lines of force to double back on themselves, as sketched in Fig. 2. 6. The repulsion between the lines then has a component parallel to the surface of the superconductor, and the magnet is attracted to the edge. A finite plane therefore gives a suspension which is unstable in the horizontal direction.

In a semicircular trough of small radius, the magnet may float near or even above the axis. Because of the edge effect, the suspension is then unstable with respect to transverse horizontal displacement, and the magnet will be ejected. The obvious solution to this problem is to use a superconducting tube rather than a trough.

A tubular geometry has two incidental advantages as compared with a trough: (a) the suspension is "tighter" with respect to transverse displacements, so that transverse oscillations have a higher frequency and hence may be damped more readily, and (b) since the magnet is almost completely surrounded by superconductor, of permeability zero (which of course what is meant by perfect diamagnetism), it is well shielded from external fields.

Topologically speaking, a tube is a doubly-connected structure, which means that any motion of the magnet will set up persistent currents, so that support itself will develop a magnetic moment. A singly-connected tube may be constructed by introducing a barrier consisting of a narrow slit along the upper surface of the tube*. A small amount of flux from the magnet will then leak out through the slit, and variations in the width of the slit will produce axial forces, which cannot be tolerated. The slit must therefore be made with great care.

The magnet will of course always float at a lower height in a tube than in a trough of the same radius of curvature. Indeed, for a tube with a slit of negligible

---

*A possible use of a multiply-connected suspension is discussed in Chapter IX.

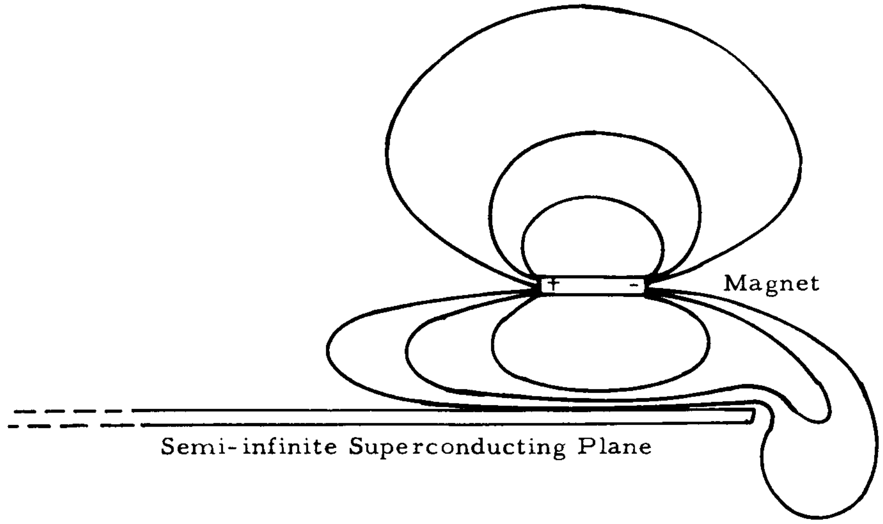

Note: This figure is not intended to be an accurate representation o the field, but simply to give a qualitative impression of why a floati magnet is drawn to the edge of a superconducting surface.

Fig. 2.6 Field Distortion at Edge of Superconducting Plane width, the magnet will always float below the axis, regardless of the radius, since it would, by symmetry, float on the axis in the absence of gravity.

A slitless tube creates sufficiently simple boundary conditions for analytical treatment (see Appendix), but the introduction of a slit complicates the field distribution considerably. Because of the compression of the field inside the tube, there is a strong tendency for flux to be "squeezed" out through even a narrow slit. This produces a levitating force on the magnet, so that, as far as float height is concerned, there exists an optimum slit width.

Because of the end effects, a tubular suspension is normally axially unstable, and some means must be found of compensating the inherent axial forces. The introduction of a slit greatly complicates the situation, but, for the purposes of discussion, it will be assumed that the end effects produce axial forces which vary with the displacement in the manner prescribed by Eq. (A. 33) of the Appendix:

$$F = \alpha \sinh 2c_1 x \qquad (2.5)$$

where x is the displacement, c_1 is a constant equal to 3.83 divided by the radius of the tube, and α is to be regarded as an experimentally determined constant.

2.5 End-Effect Compensation

Several different end-effect compensation techniques were conceived during the development of LLAMA. Because of their simplicity and flexibility, stabilization is achieved by means of small coils inside the suspension in the first model of the instrument. These coils also serve as the source of restoring force in closed-loop operation.

A permanent magnet may be attracted or repelled by a current-carrying coil depending on the sense of the current relative to the orientation of the magnet. If coils are placed on either side of the center of the suspension, with their axes coincident with the axis of the tube, and fed with an appropriate current, it is possible to overcome the forces due to the suspension and produce a mechanical potential minimum. This implies that the magnet is repelled by the coils, which normally would give rise to a rotationally unstable situation; however, reaction from the sides of the tube prevents this problem from arising in normal operation. This effect does limit the current which can be used to fairly small values, but effective end-effect compensation is quite possible.

According to Eq. (A. 37) of the Appendix the force produced by a pair of stabilizing coils is of the form

$$F_c = -\beta I \sinh c_1 x \qquad (2.6)$$

It is only possible to produce exact compensation for displacements which are so small that both (2.5) and (2.6) are effectively linear. For a tube of radius 1.25 cm, this condition holds within 0.02% up to a displacement of 60 microns, and within 1% to 400 microns. If the displacement can be held within one micron, as is expected when the entire LLAMA system is operational, the maximum uncompensated end effect force would, according to this model, be no more than $3 \times 10^{-11}\ \alpha$ dynes. This is so small that in practice essentially perfect compensation may be achieved.

The non-linearity of these equations does however have some important consequences in the test of the suspension (Section 7.2).

2.6 The Flux-Trap Problem

The the discussion so far, it has been tacitly assumed that the superconducting surface was continuous. This is only true if certain precautions are taken during the cooling process.

Suppose that a sheet of superconducting material, in the normal state, is immersed in a magnetic field, which for simplicity is taken to be normal to the surface. If there exists a local maximum of field intensity, the region near the maximum will remain normal after the rest of the sheet is superconducting, as the sheet is cooled uniformly, because of the dependence of transition temperature on the applied field (Section 2.1). There will thus be a "hole" in the superconductor with flux passing through it. As the magnetic field cannot penetrate the superconductor, there is no way for this flux to escape. As the sheet is cooled further, the size of the hole will decrease, but the same amount of flux will pass through it; the field intensity in the hole will increase until it reaches the critical field corresponding to the temperature of the sheet.

If now the source of the field be removed, a current will be induced around the hole. Since there is no resistance, Faraday's law gives (in m.k.s. units)

$$V = L\frac{dI}{dt} = -\frac{d\Phi}{dt} \tag{2.7}$$

where L is the self-inductance of the circuit around the hole and Φ is the flux due to the external source.

Thus, by the definition of self-inductance, the flux in the hole due to the induced current is

$$\Phi' = LI = \Phi_o - \Phi \tag{2.8}$$

which is just sufficient to maintain the total flux at the value it had before the source was removed: Φ_o.

Once flux has been trapped by a superconductor, there is thus no way to eliminate it short of raising the temperature above the zero-field transition value and recooling.

The conclusion, then, is that there must be no closed contours of magnetic field intensity surrounding maxima on the surface of the superconductor at the time that it is cooled. If it is desired to have the test-mass magnet in the vicinity of the suspension during the cooling process, it must be located so that the nearest part of the superconductor is an edge of the surface.

A similar problem arises if the cooling is not uniform. If a sheet of superconductor be immersed in a uniform field and cooled from the edges, the peripheral region will superconduct first, trapping the flux passing through the center of the sheet. Thus the cooling technique must be such that no local maximum of temperature occurs at any time.

The influence of these phenomena on the design of the LLAMA suspension is discussed in Chapter V.

2.7 Preliminary Experiments

In order to gain some familiarity with the problems of cryogenic suspension operation, a series of experiments were performed in the transparent glass dewar sketched in Fig. 2.5 Because this dewar was unsilvered, there was a large radiant influx of heat from the surroundings, with the result that the liquid helium boiled away quite rapidly, limiting the duration of each experiment to about ten minutes. The boiling helium produced rather turbulent conditions inside the dewar, so that it was difficult to make estimates of the forces on the floating magnet. In addition, the rapid efflux of cold helium from the top of the dewar caused a heavy fog, which at times prevented photography or even observation of the interior.

For these reasons, the experiments were generally rather qualitative; however, a great deal of experience and some quite significant information was obtained.

The first experiment consisted simply of a demonstration that a small magnet would indeed float over a lead dish, as described in Section 2.3.

For the next experiment, a lead tube was constructed, as shown in Fig. 2.7. The upper edges were separated by a sliver of cardboard, so as to make the superconductor singly connected. In order to keep the magnet in the tube, the ends were closed with a grid of (non-superconducting) wires. The magnet was prepared by attaching to the ends lucite discs, about a centimeter in diameter, to simulate the mirrors which would be present in the actual device.

The magnet was then inserted into the cylinder, and the whole assembly lowered on strings into the dewar full of liquid helium. As the lead cooled, the magnet did not lift itself off, but it was possible to get it floating by flicking it with a

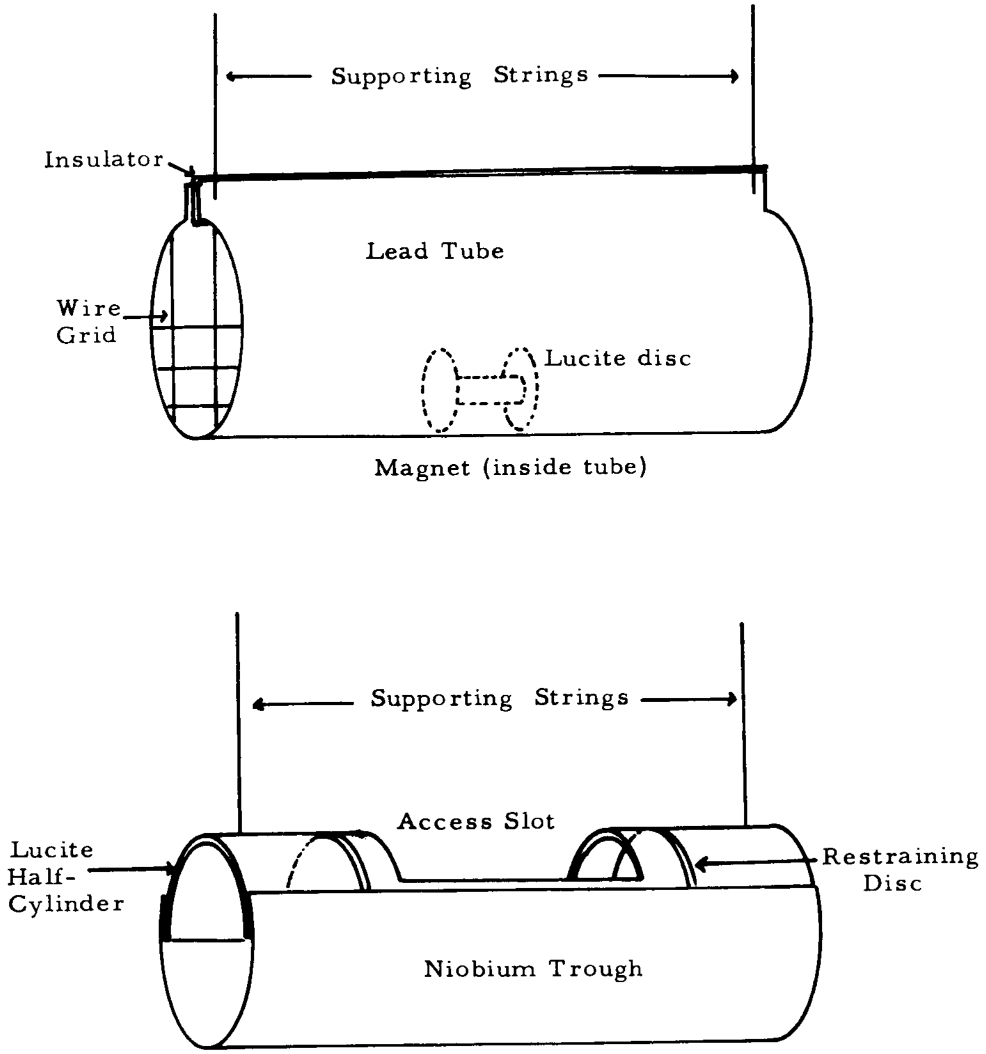

Fig. 2.7 Early Experimental Suspensions

bent probe lowered into the dewar. However, the float height was very disappointing; the lucite discs barely cleared the surface. It was found that by shaking the tube, it was possible to start the magnet spinning about its long axis, which showed that it was freely suspended.

The reason for the poor float height in this experiment was, of course, the flux-trapping problem discussed in Section 2. 6. This hypothesis was confirmed by a later experiment (see below).

A new tube was now constructed, as shown in Fig. 2. 7. A lucite tube of suitable diameter was cut in half lengthwise, and a wide slot was cut in the top, near the center. Lucite discs were glued to the inside of this semi-cylinder, the purpose being to keep the magnet in the low-force region near the center of the suspension. The device was completed by attaching to the outside a sheet of niobium formed into a section of a cylinder, with a gap about 60° wide at the top.

This assembly was suspended on strings inside the dewar of helium. When it was certain that the niobium was superconducting, the magnet was lowered with non-magnetic tongs and inserted into the support through the slot in the lucite.

The magnet floated just below the axis, and moved very easily between the lucite discs when the tube was tilted slightly. While it was not possible to make a quantitative estimate of the axial forces, this experiment did indicate that there were no unexpected gross phenomena which might prevent the operation of the system.

In order to confirm the importance of the flux-trapping effect, this experiment was repeated, with the magnet placed in the tube before it was inserted into the dewar. It was observed that the magnet did not lift off the superconducting surface, and when it was flicked with a probe, it floated with a very small clearance. Movement of the magnet in the axial direction was very sluggish.

2. 8 The LLAMA Dewar

The overall configuration of LLAMA, together with the lessons learned in the preliminary experiments, dictated the following requirements for a dewar which would permit quantitative performance measurements:

i) The suspension itself should consist of a superconducting cylinder, with an axial slit along the top to prevent circulating supercurrents.

ii) The inside of the cylinder, where the magnet would float, should be evacuated to at least 10^{-6} torr, to prevent radiometer effect from interfering with light-pressure calibration of the instrument(18).

iii) Optically flat windows should be provided at the ends of the cylinder, to allow access of the light used in the calibration and in the interferometric displacement detector.

iv) Some means should be provided for storing the magnet externally to the suspension during the cooling process, to avoid flux-trapping.

v) The ratio of liquid helium capacity to total heat input should be such that operation for at least two hours would be possible, to allow time for careful measurements.

vi) No magnetic materials should be used in the construction of the dewar.

The construction of a dewar meeting these specifications is examined in detail in Chapter V. However, a brief description of the apparatus is given here.

A cross section of the metal dewar is shown in Fig. 2.8. A thin walled copper cylinder (O.D. 2.2 cm.) is inserted lengthwise in a hollow copper block, attached to the bottom of the inner vessel of the dewar. The superconductor is a sheet of niobium wrapped around the outside of this cylinder, so that it is in contact with liquid helium when the dewar is filled. An axial gap is left at the top of the superconductor to prevent super currents. The ends of the cylinder are open to the dewar vacuum. In operation, the test mass floats just below the center line of the cylinder, (See Fig. 2.9). To avoid the flux trapping, the magnet is stored in a room temperature evacuated ante-chamber before cooling takes place. When the niobium is superconducting, the magnet is inserted into the suspension by means of a lucite spoon which can be manipulated from outside the dewar via a vacuum feedthrough.

The dewar is equipped with windows opposite the ends of the cylinder, which are used for observation of the test mass and for access by the displacement detection system. A photograph of the dewar is shown in Fig. 2.10.

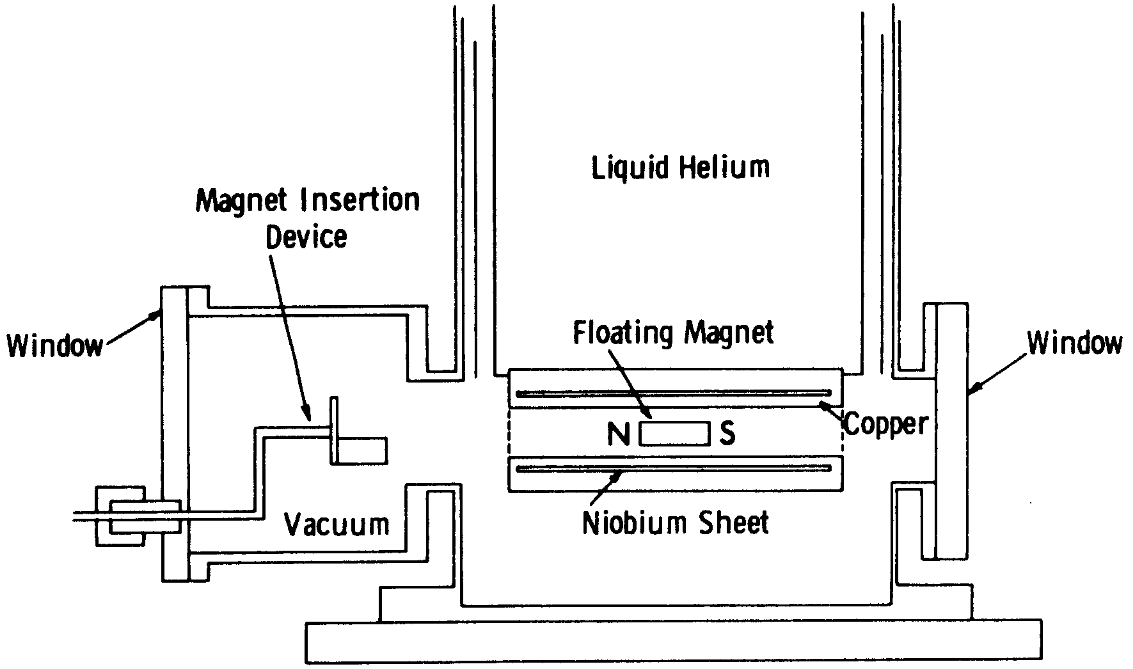

Fig. 2.8 Basic Construction of Metal Dewar

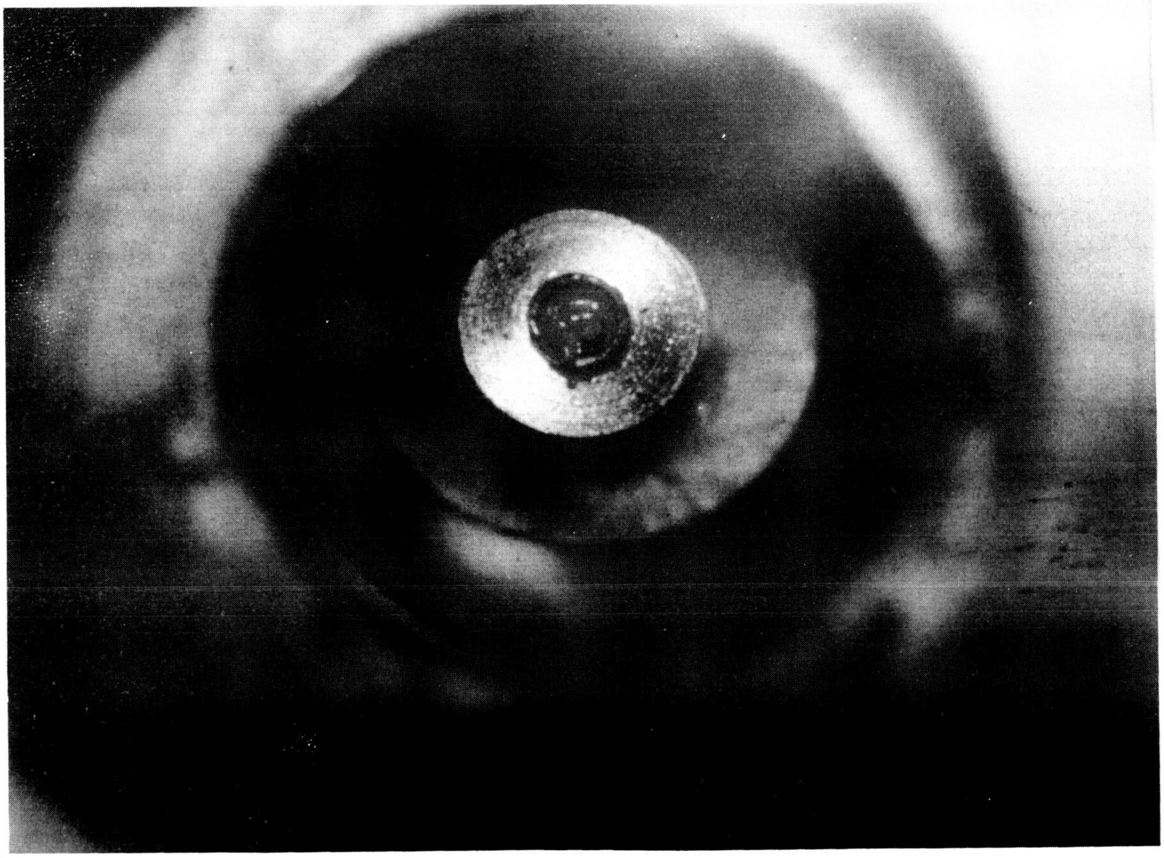

Fig. 2.9 Magnet Floating in LLAMA Suspension

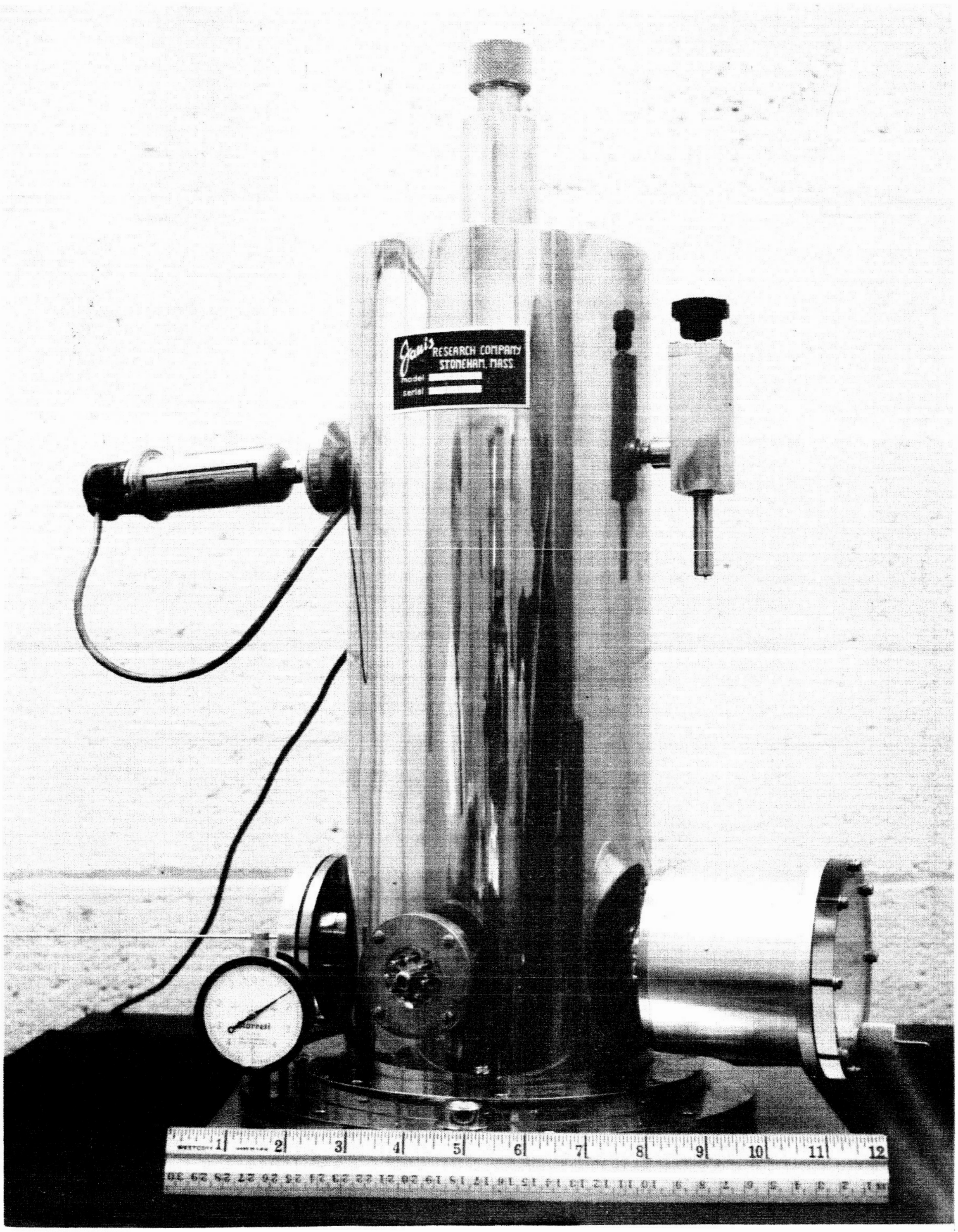

Fig. 2.10 The LLAMA Dewar (early model)

CHAPTER III

DISPLACEMENT DETECTION

3.1 General

Very small axial displacements, on the order of a fraction of a micron, of the magnet must be detected in order to preserve an adequate bandwidth at low acceleration levels. For example, if the acceleration is 10^{-6}g the time taken to move, say, 1 mm is about 14 seconds or 0.45 seconds for a displacement of 1 micron. When lower acceleration levels are considered, say, 10^{-9}g, the time taken to move 1 micron is 14 seconds. Other reasons for desiring high sensitivity displacement detection are (a) to tolerate a larger axial suspension spring constant and (b) to avoid non-linearities in the suspension and in the detector.

3.2 Displacement Detector Design Goals

The ideal displacement detector for LLAMA is a device that:

(a) is capable of sensing axial displacements way below 1 micron.
(b) is insensitive to displacement along or tilts about other axes.
(c) is linear.
(d) does not exert any force on the magnet.
(e) maintains its sensitivity for long periods.
(f) is compatible with the LLAMA system.

3.3 Interferometric Displacement Detector (IDD).

At present, the test mass is a permanent magnet which must be inserted inside the superconducting cylinder after the temperature of the niobium has dropped below its critical value, as explained in Chapter II. This imposes yet another restriction on the design of the displacement detector.

Several methods of displacement detection have been considered and an interferometric scheme was found suitable and highly compatible with the rest of the LLAMA system. An interferometric scheme does not depend on fixtures mounted inside the superconducting cylinder which might hamper the insertion or the withdrawal of the magnet. In addition, the IDD allows the null position of the magnet to be varied as desired which is useful in the early stages of experimentation.

3.3.1 The Michelson Twyman-Green Interferometer

Interferometric principles may be illustrated simply with the aid of Fig.3.1. One part of a collimated monochromatic beam of light of frequency ν, passes

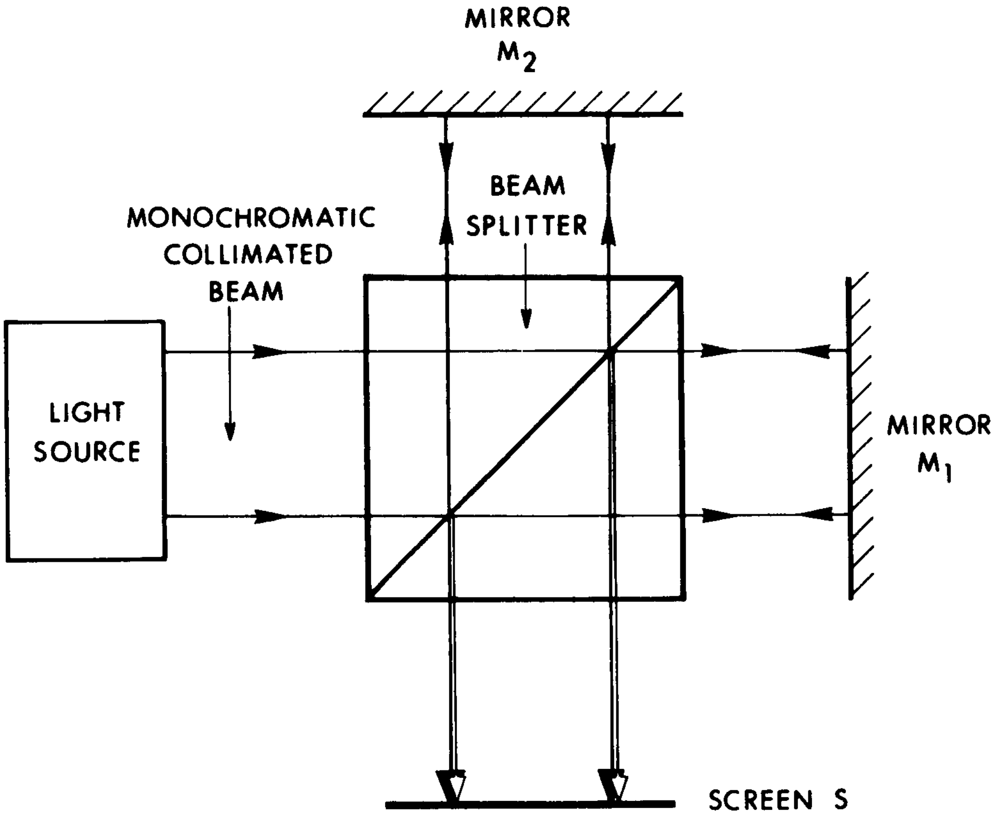

Fig. 3.1 Simple Illustration of Interferometric Principles

through a beam splitter BS, is reflected from mirror M_1, normal to the beam, and then impinges on a screen S after reflection at the beam splitter. Similarly, the other portion of the beam is reflected from mirror M_2, also normal to the beam, so that the two portions of the beam overlap at the screen S.

The intensity at S of beam # 1 in the absence of beam # 2 is given by

$$I_1 = \frac{c}{4\pi} \cdot \sqrt{\frac{\epsilon}{\mu}} \langle \vec{E}_1^{\,2} \rangle$$

or

$$I_1 = k \langle \vec{E}_1^{\,2} \rangle$$

where $\langle \vec{E}_1^{\,2} \rangle$ is the time average of the square of the amplitude of the electric field vector at S; ϵ, μ, are the permittivity and permeability of free space and c is the velocity of light; k is a constant which equals

$$\frac{c}{4\pi} \cdot \sqrt{\frac{\epsilon}{\mu}} \quad .$$

Generally,

$$\vec{E}(\vec{r}, t) = \text{Real}\left[(\vec{A}(\vec{r})e^{-i2\pi\nu t}\right] = \frac{1}{2}\left[\vec{A}(\vec{r})\, e^{-i2\pi\nu t} + \vec{A}^{\,*}(\vec{r})\, e^{+i2\pi\nu t}\right]$$

where $\vec{A} = ae^{ig}$ is the amplitude vector for a linearly polarized wave and a is the amplitude and g is the spatial phase angle.
Then,

$$\langle \vec{E}_1^{\,2} \rangle = \frac{1}{2} \vec{A}_1 \vec{A}_1^{\,*} = \frac{1}{2} A_1 \cdot A_1^{*}$$

Now when the two beams are superposed, the total electric field vector becomes

$$\vec{E} = \vec{E}_1 + \vec{E}_2$$

and

$$\langle \vec{E}^{\,2} \rangle = \langle \vec{E}_1^{\,2} + \vec{E}_2^{\,2} + 2\vec{E}_1 \cdot \vec{E}_2 \rangle \ ,$$

hence the total intensity I is given by

$$I = I_1 + I_2 + J_{12}$$

where $I_1 = k \langle \vec{E}_1^{\,2} \rangle$; $I_2 = k \langle \vec{E}_2^{\,2} \rangle$ and

$$\begin{aligned} J_{12} &= 2k \langle \vec{E}_1 \cdot \vec{E}_2 \rangle \\ &= 2k \left\langle \tfrac{1}{2} \left(\vec{A}_1 e^{-i2\pi\nu t} + \vec{A}_1^{\,*} e^{+i2\pi\nu t}\right)\left(\tfrac{1}{2}\right)\left(\vec{A}_2 e^{-i2\pi\nu t} + \vec{A}_2^{\,*} e^{+i2\pi\nu t}\right)\right\rangle \\ &= \frac{k}{2}\left(\vec{A}_1 \vec{A}_2^{\,*} + \vec{A}_1^{\,*} \vec{A}_2\right) \\ &= \frac{k}{2}\left(a_1 e^{ig_1} a_2 e^{-ig_2} + a_1 e^{-ig_1} a_2 e^{ig_2}\right) \\ &= \frac{k}{2} a_1 a_2 \cos\psi \end{aligned}$$

where $\psi = g_1 - g_2$ = difference in optical path length traversed by beam # 1 and # 2.

Hence

$$\begin{aligned} I &= k\left[\tfrac{1}{2}\left(E_1 E_1^{*}\right) + \tfrac{1}{2}\left(E_2 E_2^{*}\right) + a_1 a_2 \cos\psi\right] \\ &= k\left[\tfrac{1}{2} a_1^2 + \tfrac{1}{2} a_2^2 + a_1 a_2 \cos\psi\right] \end{aligned}$$

But $\frac{1}{2} k a_1^2 = I_1$, etc.

$\therefore$ total intensity I is given by

$$\boxed{I = I_1 + I_2 + 2\sqrt{I_1 I_2}\cos\psi}$$

It is evident that I varies between

$$I_{max} = I_1 + I_2 + 2\sqrt{I_1 I_2} \quad \text{for } |\psi| = 0,\ 2\pi,\ \cdots$$

and

$$I_{min} = I_1 + I_2 - 2\sqrt{I_1 I_2} \quad \text{for } |\psi| = \pi,\ 3\pi,\ \cdots$$

In the case where the intensities in the two beams are equal i.e. $I_1 = I_2$; then

$$\begin{aligned} I &= 2 I_1 + 2 I_1 \cos\psi \\ &= 4 I_1 \cos^2 \frac{\psi}{2} \end{aligned}$$

then $$I_{max} = 4I_1$$

$$I_{min} = 0$$

Fig. 3.2 illustrates the variation of intensity with path length difference for $I_1 \neq I_2$ and for $I_1 = I_2$.

In terms of path length difference Δx,

$$\psi = g_1 - g_2 = 2\pi \frac{\Delta x}{\lambda_o}$$

where λ_o is the wavelength of the monochromatic light so that

$$I = 2I_1 + 2I_1 \cos \frac{2\pi}{\lambda_o} \Delta x \tag{3.1}$$

Eq. (3.1) states that for a collimated monochromatic light the intensity at the screen S varies from dark to bright as the path length difference Δx is varied, in other words, as M_1 is moved relative to M_2 in the direction of the beam.

In terms of frequency ν_o, where $\lambda_o = \frac{c}{\nu_o}$

$$I_{\nu_o} = 2I_1 + 2I_1 \cos\left(2\pi \frac{\nu_o}{c} \Delta x\right)$$

Now if this frequency ν_o does not remain constant but changes to, say, $\nu_o + \Delta\nu$, then

$$I_{\Delta\nu} = 2I_1 + 2I_1 \cos\left[2\pi \frac{(\nu_o + \Delta\nu)}{c} \Delta x\right]$$

This change in frequency can be interpreted as a change in Δx given by

$$\frac{2\pi(\nu_o + \Delta\nu)}{c} \Delta x = \frac{2\pi\nu_o}{c} \Delta x'$$

where $\Delta x' - \Delta x = \epsilon$ = change in Δx due to $\Delta\nu$

$$= \frac{(\nu_o + \Delta\nu)}{\nu_o} \Delta x - \Delta x$$

$$\therefore \epsilon = \frac{\Delta\nu}{\nu_o} \Delta x \tag{3.2}$$

Eq. (3.2) indicates that a change in frequency can only cause an error if there is a finite path length difference. For example, if $\frac{\Delta\nu}{\nu_o} = 10^{-7}$

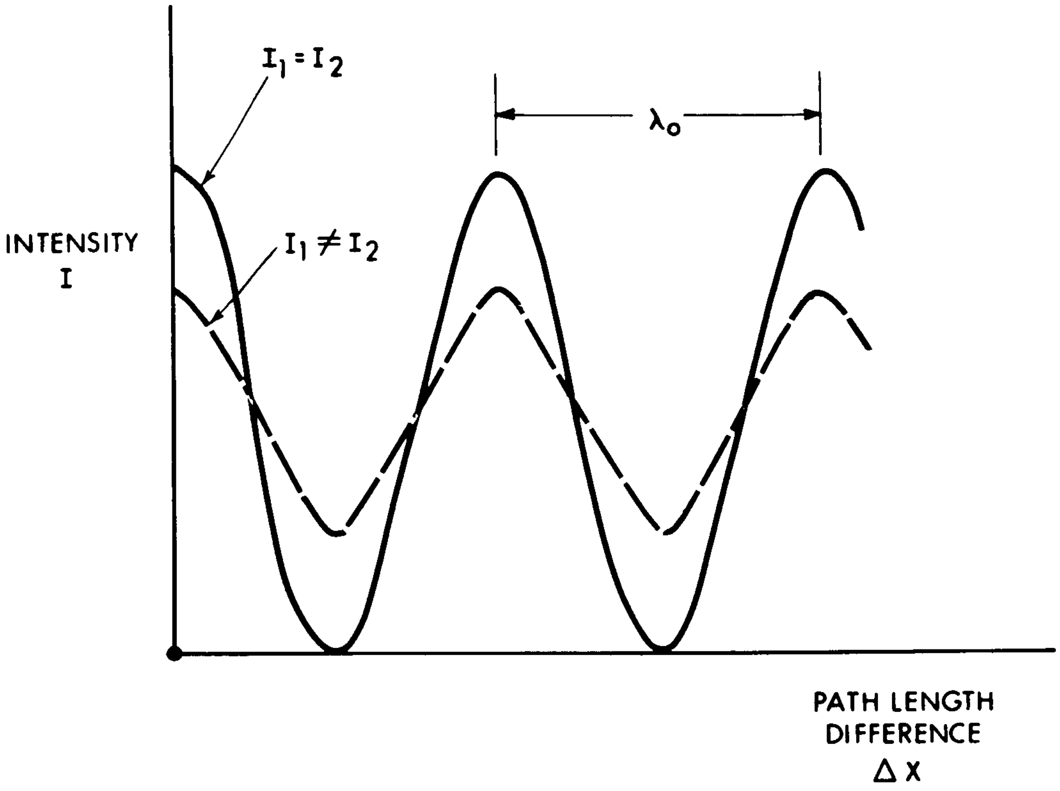

Fig. 3.2 Variation of Output Light Intensity with Path Length Difference

[for a typical non-stabilized laser] and $\Delta x = 10\text{cm}$ then $\epsilon = 10^{-2}$ microns.

Now the path length difference that causes the interference pattern to change from dark to bright (i.e. one fringe) corresponds to $\Delta x = \frac{\lambda o}{2}$ or a mirror displacement of $\frac{\Delta x}{2} = \frac{\lambda o}{4} \approx 0.15$ micron, for $\lambda o = 6000\,\text{Å}$. ϵ in this case is about 0.03 of a fringe.

The visibility of the fringe is defined by

$$V \triangleq \frac{I_{max} - I_{min}}{I_{max} + I_{min}}$$

$$= \frac{2\sqrt{I_1 I_2}\ \cos 2\pi \frac{\Delta\nu}{c}\ \Delta x}{I_1 + I_2}$$

Fig. 3.3 illustrates the influence of $\Delta\nu$ on fringe visibility. A full treatment of interference with partially coherent light is given by Born and Wolf.(23).

The effect of tilts of the reference mirrors will now be examined. Fig. 3.4 shows mirror M_1 tilted by angle θ about its center. The beam reflected by M_1 will be rotated by 2θ. The interference at the screen S will no longer be a uniform field and will only take place over the area of overlap of the two spots. If θ is large the spots will no longer overlap and hence all interference information will be lost.

For small θ it can be noticed from Fig. 3.4 that one part of the beam reflected from M_1 will traverse a longer path than for $\theta = 0$ and another part of the beam will traverse a shorter path.

Consider a ray in the beam situated at a distance y above the axis of the beam.

Let $d_1 = AB$, $d_2 = BA$, $d_3 = AD$ and

$d_1' = AB'$ $d_2' = B'A'$, $d_3 = A'D'$

The change in path length of this ray is given by

$$\Delta d_y = d_1' + d_2' + d_3' - (d_1 + d_2 + d_3)$$

It can be shown that

$$\Delta d_y = (d_1 + d_3)\left(1 - \frac{1}{\cos 2\theta}\right) + y \tan\theta \left(1 + \frac{1}{\cos 2\theta}\right)$$

The displacement of the ray along the screen is given by

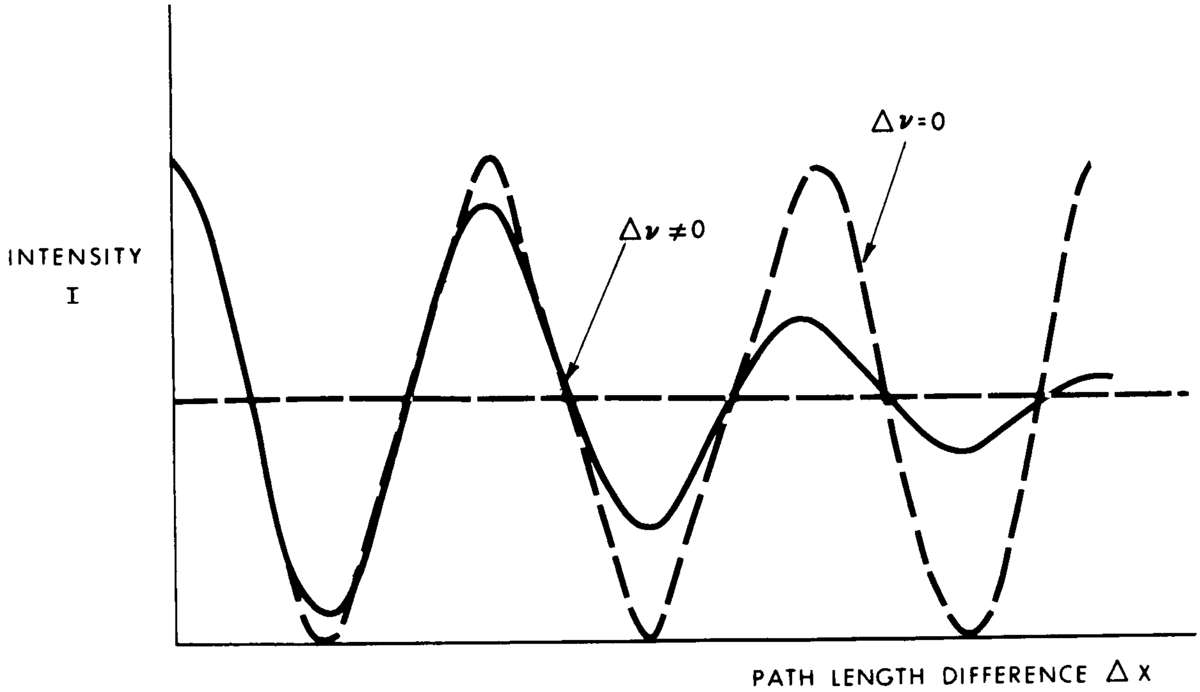

Fig. 3.3 Effect of Frequency Uncertainty $\Delta\nu$ on Intensity vs. Path Length Difference

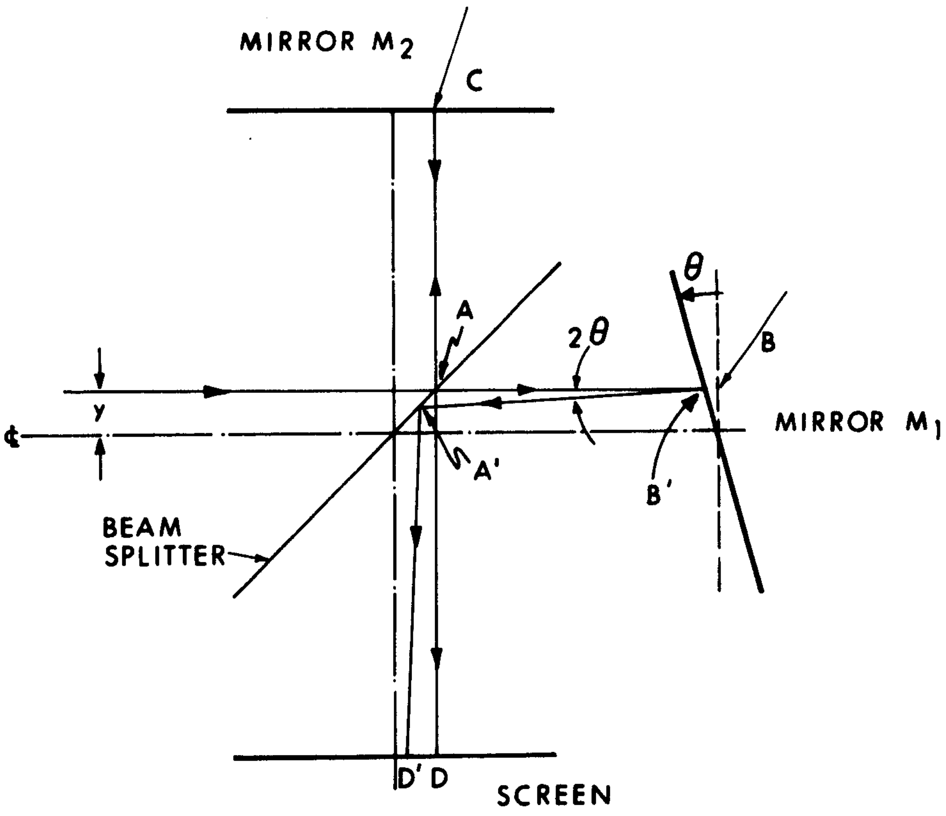

Fig. 3.4 The Effect of Tilt of One of the Reference Mirrors

$$\Delta S_y = (d_1 + d_3 - y \tan\theta) \tan 2\theta$$

$$= (d_1 + d_3) \tan 2\theta - y \tan\theta \tan 2\theta$$

For interference, ΔS_y must be less than $2\overline{y}$ where $2\overline{y}$ is the diameter of the collimated beam. Therefore for interference to take place

$$\theta \lesssim \frac{\overline{y}}{(d_1 + d_3)}$$

For $2\overline{y} = 4$ mm. and $d_1 + d_3 = 100$ cm, then $\theta < 2 \times 10^{-3}$ rads.

Another limit on θ is imposed by the sensitivity desired. If Δd_y must be less than one hundredth of a fringe, i. e., $\Delta d_y < \frac{\lambda o}{200}$ then

$$\theta \lesssim \frac{\Delta d}{2\overline{y}}$$

For a beam of diameter 4 mm. and $\Delta d = \frac{\lambda o}{200}$ or 1/100 of a fringe, $\lambda o = 6000$ Å, then

$$\theta < 0.75 \times 10^{-6} \text{ radians}$$

Generally, therefore, the limit on θ imposed by sensitivity desired is usually more stringent than that imposed by spot overlap.

3.3.2 Interferometric Configurations for Detection of Displacement

Several interferometric configurations may be examined for the detection of the displacement of a test mass such as that in LLAMA. One scheme is illustrated in Fig. 3.5(a), where a plane mirror attached to one end of the magnet serves as the second reference mirror in the interferometer discussed above. The distance moved by the test mass, corresponding to a shift of one fringe, is $\frac{\lambda o}{4}$. This configuration subjects the reference mirrors to different environments which makes a stable interference pattern difficult to achieve. In addition, any tilts of the magnet will cause an optical wedge to be set up between the reference mirrors. Instead of a uniform field the interference pattern will now exhibit an intensity gradient. With increase in the angle of tilt, straight line fringes will appear in the interference pattern.

In Fig. 3.5(b) two interferometers are shown, one for each end of the magnet. Although this set up is twice as sensitive as that in Fig. 3.5(a), it suffers from the same problems. Fig. 3.5(c) shows a configuration that subjects both reference mirrors to the same environment, has double the sensitivity of (a) and uses only one light source and one detector. However, this scheme still suffers

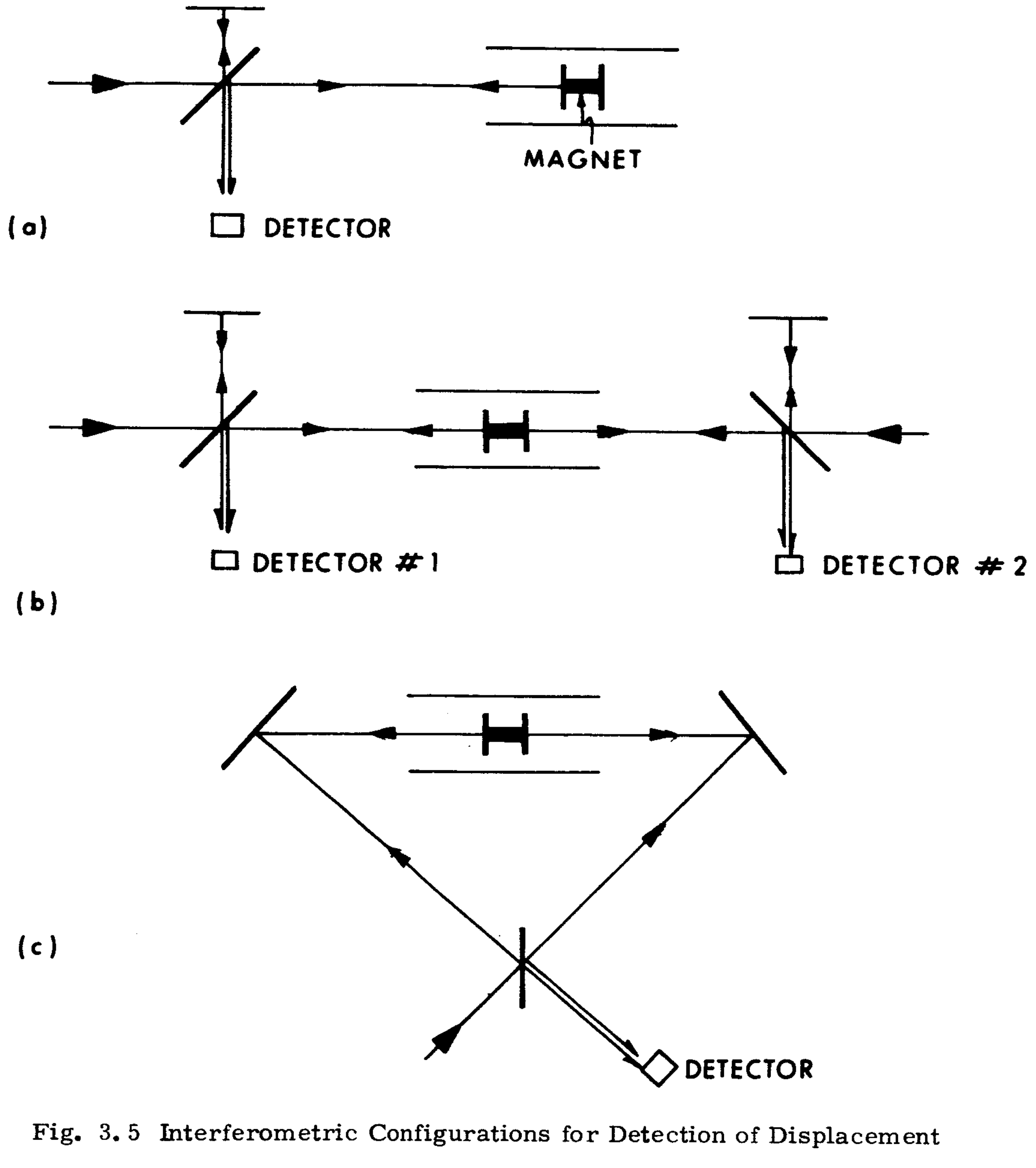

Fig. 3.5 Interferometric Configurations for Detection of Displacement

from a wedge effect that is caused by slight tilts of the magnet.

It will be shown later that if the image of one of the reference mirrors in Fig. 3.5(c) is optically completely reverted, top to bottom and left to right, the beams will not be misaligned by any tilt of the magnet. The beams will remain superposed but will move together over the surface of the detector, preserving the interference pattern in spite of magnet tilts.

3.3.3 LLAMA Interferometer Displacement Detector

Because the test mass in LLAMA has six degrees of freedom and control is only exerted along the sensitive axis, the output of any displacement detector must be sensitive only to displacements along this axis. The interferometric configuration adopted is that shown in Fig. 3.6 and will now be analyzed.

Optically flat mirrors are attached to the ends of the magnet so that they are parallel and concentric with the magnet axis. Any displacement of the magnet will change the intensity of the uniform field interference pattern with twice the sensitivity of a normal interferometer, since both reference mirrors are on the test mass. As one path gets shorter, the other gets longer. The intensity I after interference, assuming equal intensity I_1 in each arm of the interferometer is given by

$$I = 2 I_1 \left[1 + \cos \left(\frac{2\pi}{\lambda o} 2 \Delta x \right) \right]$$

Since the test mass is operated in a null configuration and the path lengths in each arm of the interferometer can be made equal, there is no error due to change in frequency when at null.

The distance the test mass has to move to cause the interference pattern to go from dark to bright (i.e., one fringe) is now $\frac{\lambda o}{8}$ or .075 micron for $\lambda o = 6000 \text{Å}$. It should be possible to detect from 1/10 to 1/100 of the change between dark to bright so that displacement thresholds as small as 7.5×10^{-4} micron can be detected using suitable readout techniques, (see Sec. 3.3.4).

Because the reference mirrors are parallel any displacement of the magnet vertically or laterally does not change the interference pattern. Similarly, any rotation of the test mass about its longitudinal axis does not cause an error. However, any rotation or tilt of the magnet about a transverse axis causes a wedge effect which in this case would be twice that given in Section 3.3.

The problem of rotation and its compensation will now be analyzed with the aid of Fig. 3.7. Let A, B and C, D represent the extremities of the two reference mirrors which are attached to the test mass. Let x be the difference in path length between the two arms of the interferometer. A clearer representation is shown in Fig. 3.7(b). Simplifying still further, A, B can be reflected in the beam splitter so that A, B and C, D are on the same side. The separation between these lines is x, but in Fig. 3.7 x is assumed zero for clarity.

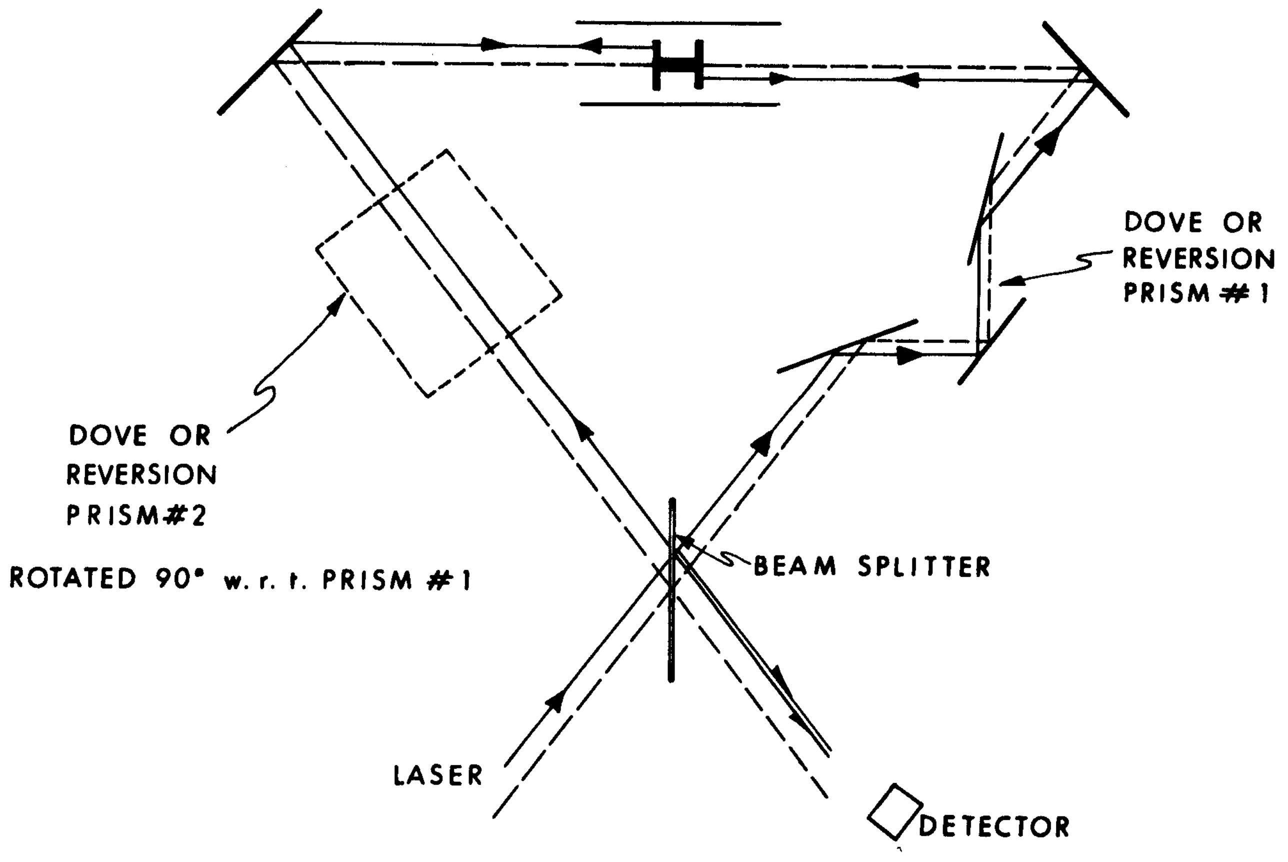

Fig. 3.6 LLAMA IDD With Dove Prisms

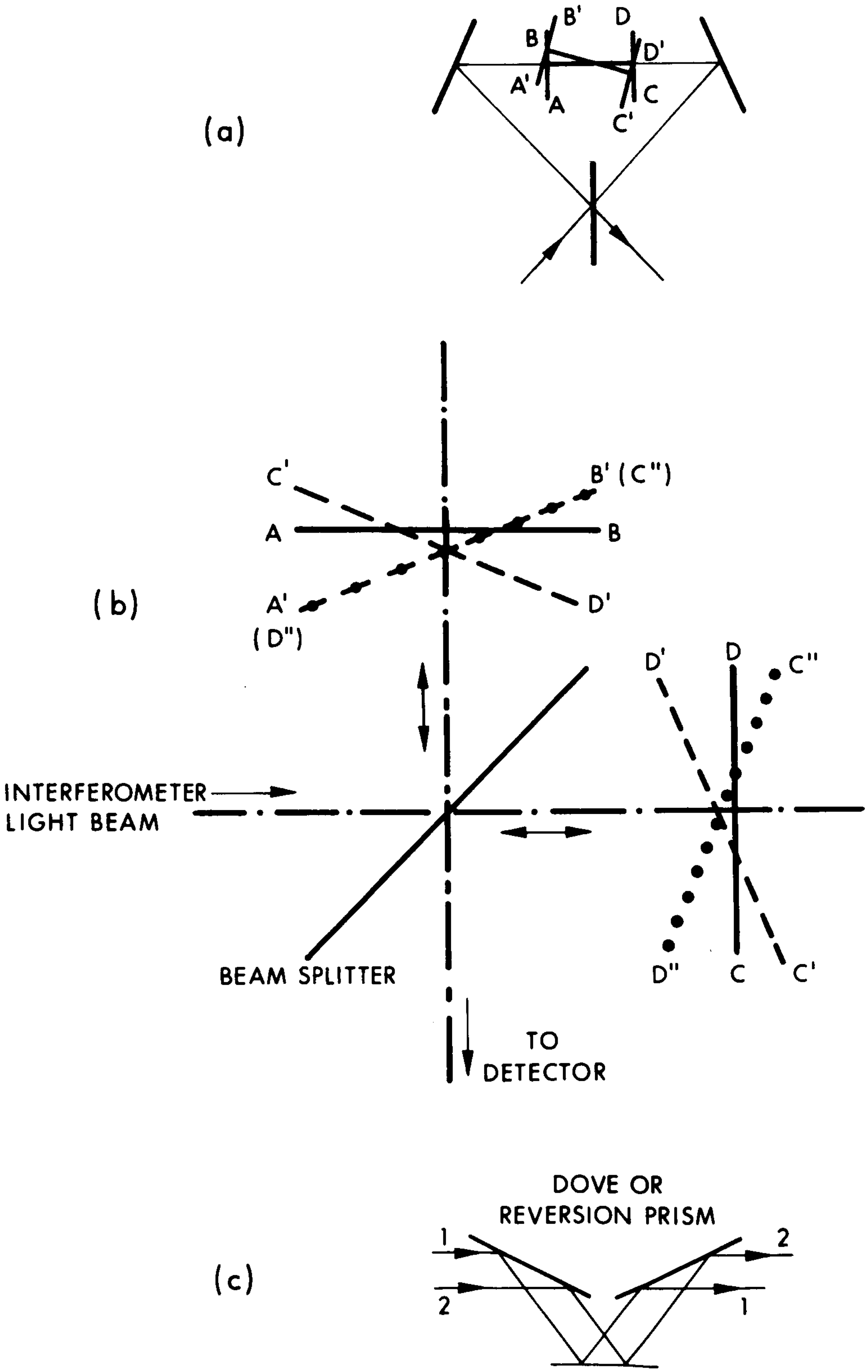

Fig. 3.7 Analysis of IDD Tilt Compensation

Now if the magnet rotates about a transverse axis normal to the paper by an angle θ. The mirror extremities will now move to A', B' and C', D'. This is represented in Fig. 3.7(b) and the wedge effect is clearly seen.

To avoid this wedge, A', B' have to be inverted with respect to axis ZZ to obtain A'', B''. C', D' are now parallel to A'', B'' and the wedge has been removed. The inversion of A', B' may be achieved by means of a dove prism as shown in Fig. 3.7(c). For rotations about the other transverse axis C', D' are reverted in a similar way by means of another dove prism oriented with its axis rotated through 90° with respect to the first dove prism. By placing a dove prism in each arm the path lengths are again equal. If the path lengths are not equal a second order effect in θ will affect the interference but this is neglected here.

With the use of dove prisms, rotation of the test mass will result in the interference beams moving together over the surface of the detector but the interference pattern is preserved.

Analysis of Fig. 3.8 shows that the limit on angle of rotation in a scheme with dove prisms is that due to spot overlap. If the path lengths in each arm are exactly equal, i.e., $x = 0$ then complete overlap will result irrespective of tilt angle. However, when a difference in path length x exists, the limit on tilt angle is given by

$$\theta < \frac{2\overline{y}}{2x}$$

where $2\overline{y}$ is the beam diameter. For $2\overline{y} = 4$ mm. and $x = 10$ cm., $\theta < 3^\circ$.

Another method of eliminating rotation effects is to attach corner cubes to the ends of the magnet instead of parallel plane mirrors. A corner cube has the property that an axial incident beam is reflected back along the same direction independent of any rotations of the corner cube about its apex. For a non-axial beam, the reflected beam is parallel to but laterally displaced from the incident beam. This displacement varies with rotation about the apex. If rotation is not about the apex then the incident and reflected beams are no longer parallel.

3.3.4 Readout Scheme

A suitable readout scheme should provide information as to phase and magnitude of the displacement of the test mass. For operation within a fringe, the position of the test mass is set so that the intensity of the interference pattern is half-way between dark and bright. The sense of the displacement of the magnet will be indicated by a decrease or increase in intensity. The extent of the change in intensity represents the magnitude of the displacement.

A suitable intensity reference for this setup can be derived from the interferometer light source as shown in Fig. 3.9, rather than from an external stable voltage source.

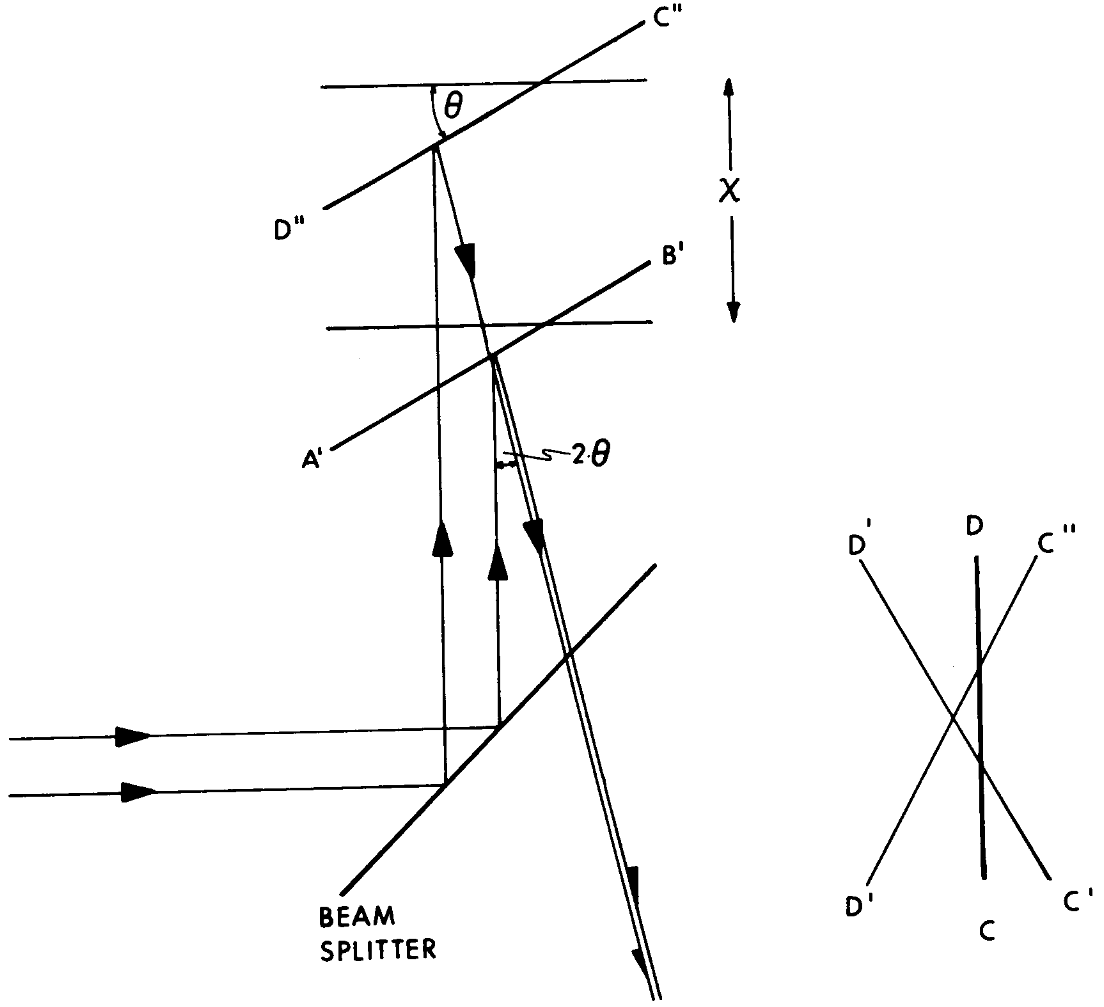

Fig. 3.8 Limitations of Tilt Compensated IDD

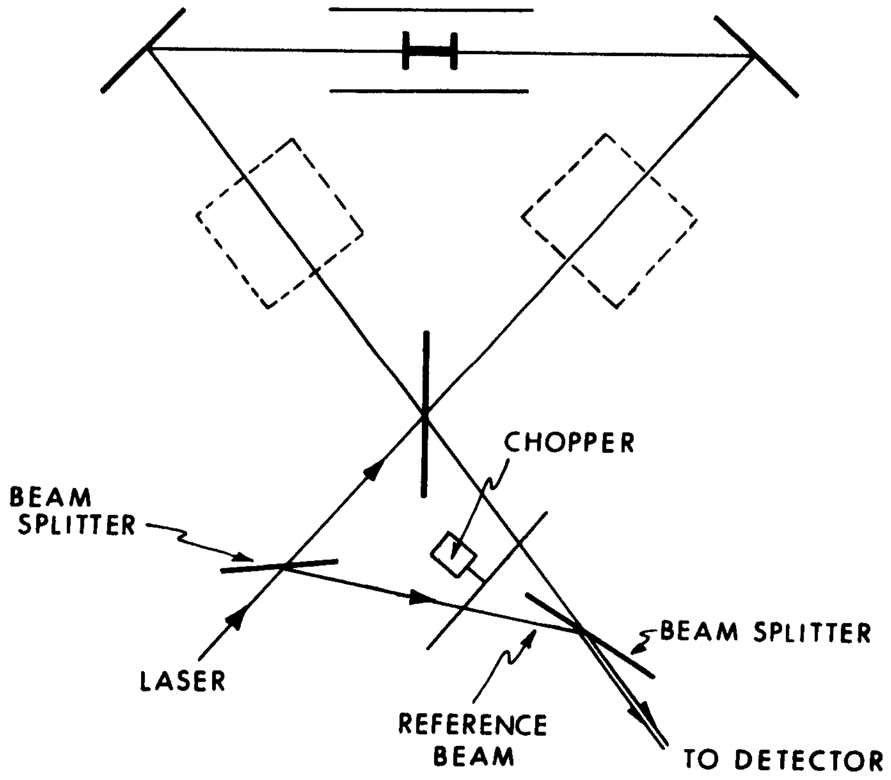

Fig. 3.9 IDD Readout Scheme

This makes the null position independent of intensity fluctuations in the light source. For a given displacement from null, any fluctuations in the intensity of the light changes only the amplitude of the error signal. This is of little consequence in a null-operation scheme.

By choosing a beam splitter with a suitable transmission-reflection ratio the intensities of the interference beams and the reference beam at the detector can be made as desired. A chopper can be used to interrupt the beams alternately so that only one photo detector need be used. The signal from the detector is then fed into a phase sensitive demodulator to get a d. c. signal proportional in magnitude and phase to the displacement of the test mass. The use of the chopper greatly enhances the sensitivity of the readout because a. c. coupling in the detector circuits minimizes drift and noise problems.

The sense of the displacement depends on which side of the interference pattern the null position happens to be. There is a sign reversal every half of a wave of the interference pattern. This ambiguity is taken care of in the servo. If the magnet happens to be at null but on the wrong slope of the interference pattern, the error signals fed into the servo due to slight displacement will drive the magnet away from null instead of restoring it back. The magnet moves to the next null position, a half of an interference wave further away, where there is a reversal in sign of the error signal and the servo will stabilize the magnet around this new null position.

Other schemes using mirrors of various shapes on the ends of the magnet may be considered. Because the magnet weighs only one gram, severe weight limitations are placed on any attachments to the magnet. The scheme using plane end mirrors and dove prisms seemed feasible and least complicated and preliminary experiments were carried out using this scheme.

Different methods for test mass tilt compensation have been suggested by Scott(24) and Steel(25). Both schemes involve out of plane tilt compensation which tends to complicate the setting up and alignment of the interferometer. The dove prism method used in LLAMA is generally a one plane scheme, which simplifies alignment procedures.

3.3.5 Interferometer Light Source

The interferometric scheme described above assumed a highly collimated beam of light, i. e., a beam with a plane wavefront. The resulting interference pattern when using such a beam and assuming that there is no wedge effect between the reference mirrors is a uniform field, modulated in intensity by motion of the test mass. The readout scheme for such an interference pattern is thus relatively simple as discussed in Section 3. 6.

Lack of collimation of the beam complicates the pattern. For example, a beam with a spherical wavefront causes an interference pattern with the familiar concentric rings of bright and dark fringes. (Strictly speaking, this pattern becomes a uniform field when the optical path lengths in each leg of the interferometer are exactly equal.)

A gas laser in the TEM_{00} mode is clearly a good source for this application. The high frequency stability(better than one part in 10^7 for the common free running gas laser) enables high contrast fringes to be obtained with unequal path lengths. This greatly simplifies the setting up of the interferometer and the location of the fringes. The high spectral intensity of the laser beam coupled with a uniphase wavefront makes the fringes readily visible and simplies the method of readout.

Transverse modes in the laser beam distort the interference pattern only if there are non-symmetrical rotations of the wavefronts of the beams in each arm of the interferometer.

The laser used was a Perkin Elmer model 5200, helium neon, 0.5 mw optical power TEM_{00} mode, with a cavity in a hemipsherical configuration.

In order to increase the sensitivity of the interferometer even more, say, to less than one thousandth of a fringe, a means of modulating either the displacement of the magnet or one of the optical paths could be incorporated. If the frequency of modulation is chosen outside the frequency range of the 1/f noise then a virtually noise free output can be obtained where the only significant source of noise is the Poisson noise of the photons arriving at the detector.

It is clearly impractical to oscillate the test mass at frequencies in the kilocycle range, but the optical path length could be modulated at a high frequency, for example, by inserting a rotating wedge in the optical path.

3.4 Spot Occultation Displacement Detector (SODD)

Although the interferometric displacement detector (IDD) discussed above is capable of sensing displacements within a fringe (or $\frac{\lambda}{8}$), it is not able to remember where the null position with respect to the superconducting tube must be, unless large capacity fringe counters are used. A coarse detector, the Spot Occultation Displacement Detector (SODD) has been designed which can position the magnet within a few microns from the desired null and can bring the magnet back to this position for excursions not exceeding two centimeters. When the magnet is brought to the desired position, the IDD takes over for operation within a fringe.

A schematic diagram of the SODD is shown in Fig. 3.10. The principle of operation is based on the occultation of a beam of light by the magnet, so that the received intensity depends on the position of the magnet. Fig. 3.10 shows an incident beam of light reflected across the magnet by means of a mirror mounted inside the superconducting tube. If the magnet is not present the entire beam is reflected back on to a photodetector. One end of the magnet is allowed to occult the beam so that at "null", half the beam is reflected back to the detector. Any displacement of the magnet from null will modulate the received intensity. Any rotation of the

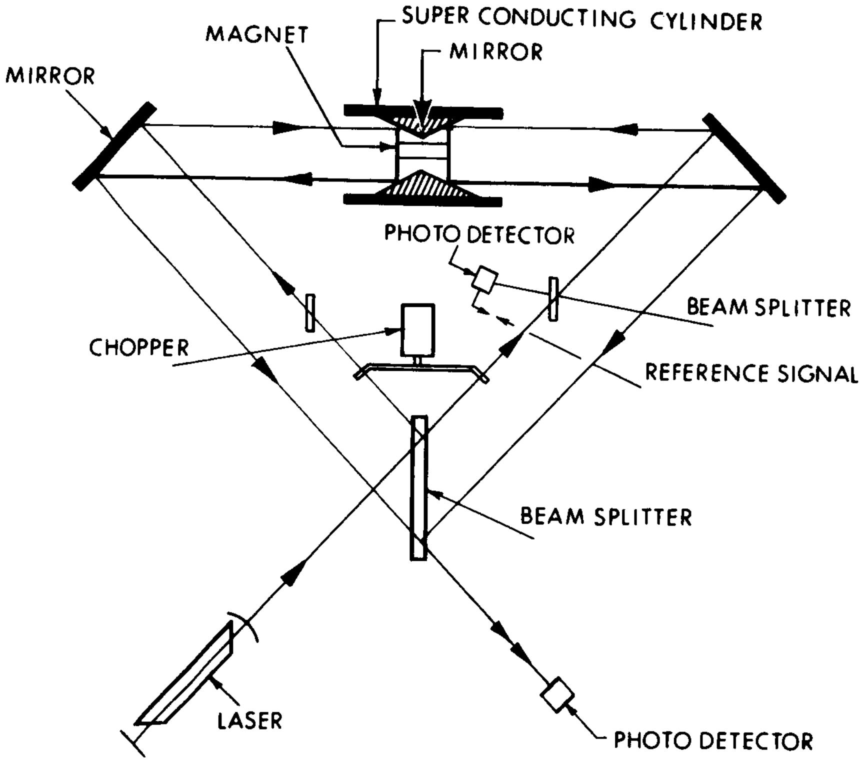

Fig. 3.10 Spot Occulation Displacement Detector (SODD)

magnet about a transverse axis will reduce the intensity because the projected area perpendicular to the beam is always increased and hence more occultation.

To eliminate rotation effects, the other end of the magnet is used to occult another beam in a similar way. This two-ended scheme gives twice the sensitivity because as the intensity in one beam is increased the other is reduced. At null this differential signal is zero. Now if rotation takes place when at null, the differential output remains zero because the intensities in both beams are reduced by the same amount.

To eliminate the use of two detectors, both return beams are brought together onto one detector as shown in Fig3.10. In order to extract the sense of the displacement the incident beams are chopped alternately so that the detector views each beam separately. The output of the detector is fed into a phase sensitive demodulator so as to obtain a signal proportional in magnitude and phase to the displacement of the magnet.

Any variation of the brightness of the light source does not affect the position of null because both beams are affected equally.

Using a test mass suspension simulator, see Chapter V, an output voltage vs. displacement plot was obtained, see Fig. 3.11. The linear range of the detector was found to be 0.62 mm and the peak signal to noise ratio was 160. This indicates that the uncertainty range of the SODD is ± 2 microns.

A helium-neon laser was used as the light source.

A reduction in the uncertainty range may be achieved by preceding the phase sensitive demodulator by a tuned amplifier tuned to the chopping frequency, so as to reduce noise and the effect of harmonics.

Another way of increasing the sensitivity is to reduce the diameter of the beams at the magnet. Control of the size of the beam, however, affects the extent of the linear range.

An early form of the SODD was used in preliminary experiments, see Chapter VII, and this is shown in Fig. 3.12. This displacement detector was a one ended SODD which was sensitive to both rotation of the magnet and to intensity variations in the light source. The linear range was around one millimeter.

3.5 Integration of SODD With IDD

It is highly desirable to choose a configuration for the SODD that shares as much of the IDD optics as possible. The triangular layout of the IDD is also suitable for the SODD. Ideally, the beam splitter and the two side mirrors can be used for both detectors. However, in practice, it is necessary to make adjustments in the SODD that are independent from the IDD and vice-versa. Two small adjustable beam splitters are added on either side of the main beam splitter solely for the SODD as shown in Fig. 3.12.

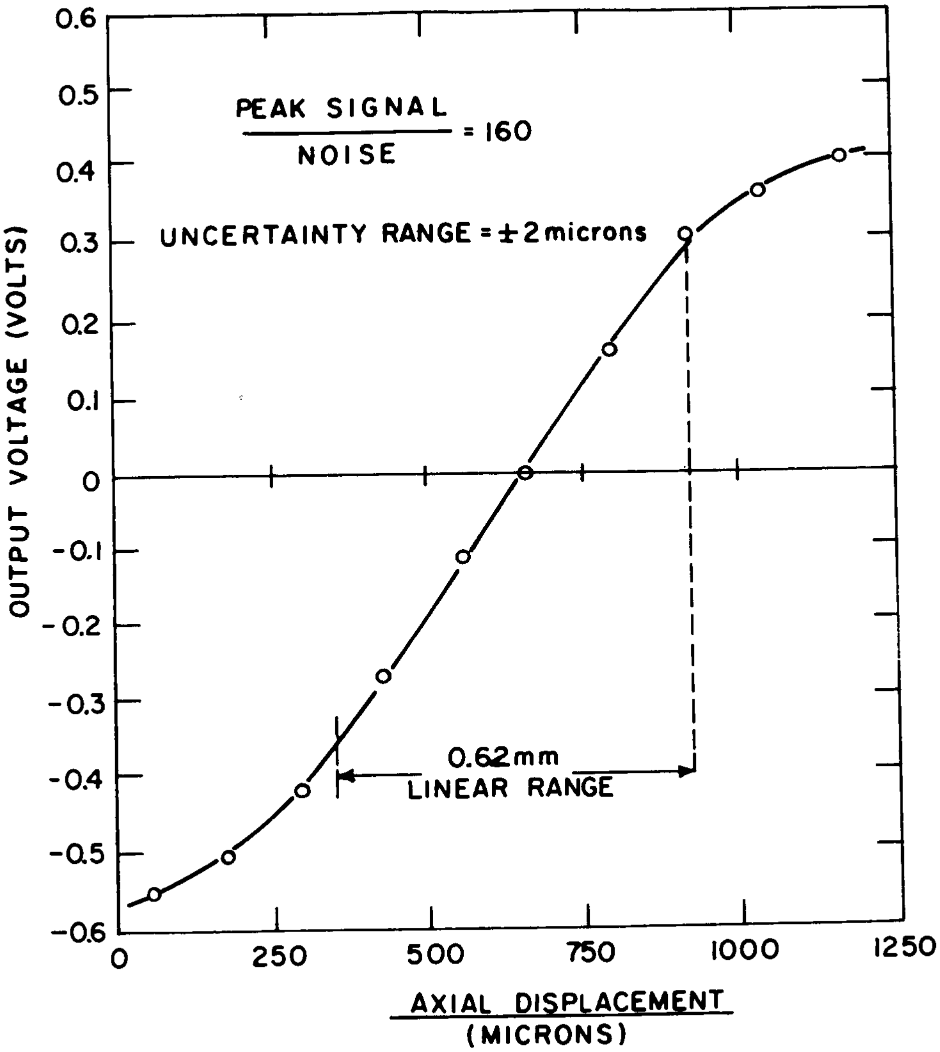

Fig. 3.11 SODD Output Voltage vs Displacement

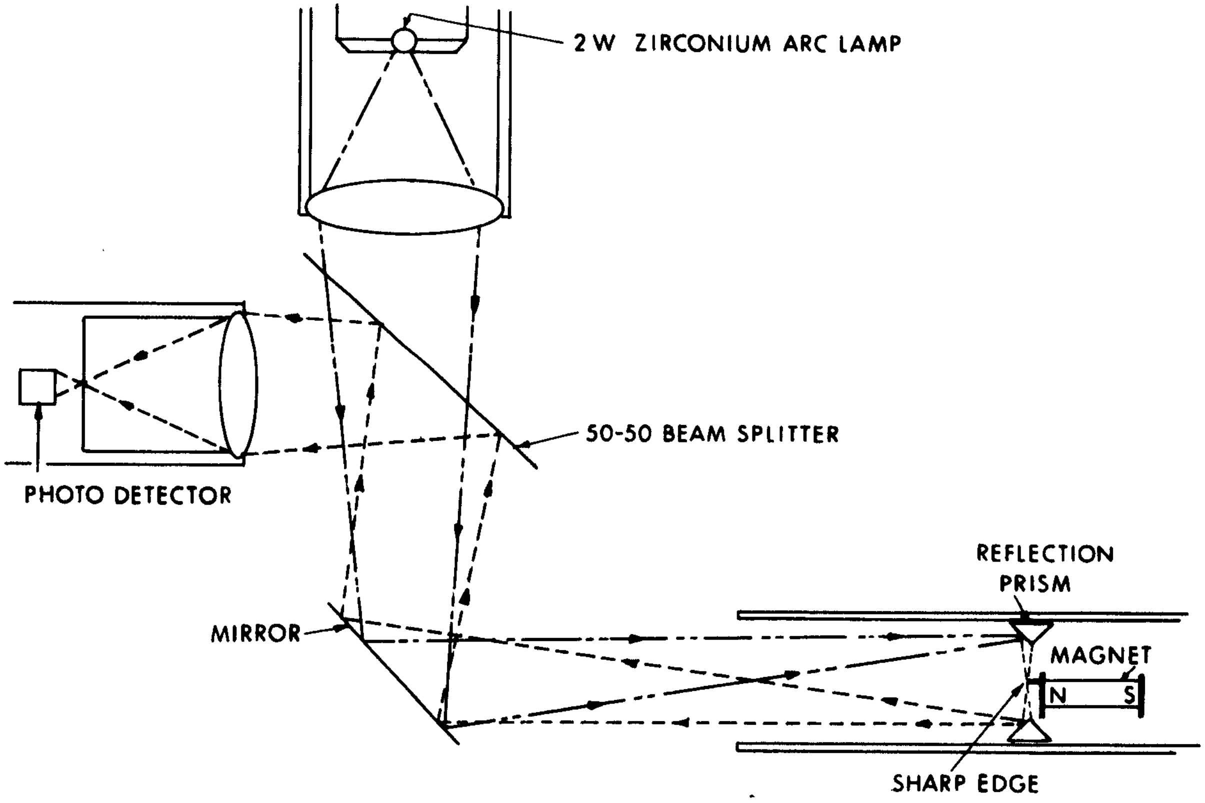

Fig. 3.12 Spot Occultation Displacement Detector (early version)

The size of the IDD optics is dictated by the tolerance allowed for the rotation of the test mass about transverse axes and the path length in each arm. The optical components close to the test mass are smaller than the ones further away. For a ± 1 degree rotation of the test mass the size of the main beam splitter must be at least 3 cm x 3 cm for a magnet-beam splitter separation of 100 cm. Experiments showed that rotation angles were less than ± 1° so that smaller size optics can be used. The SODD requires smaller size components because the beams are fixed in position. The detectors for each displacement detector are separated as shown in Fig. 3.13.

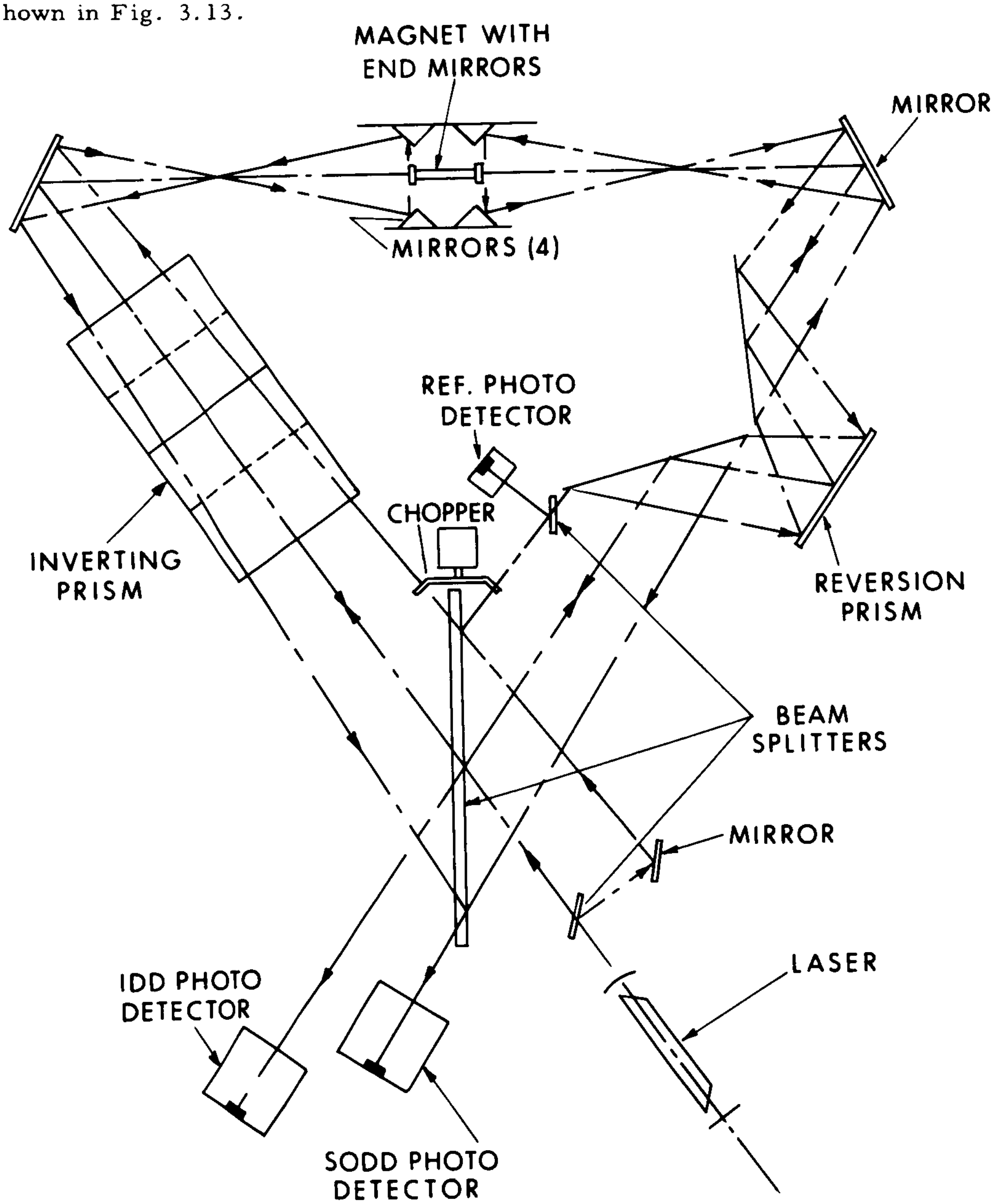

Fig. 3.13 Configuration for SODD-IDD Combination

CHAPTER IV

TEST MASS CONTROL

4.1 General

The LLAMA test mass is operated in a null configuration. Information about any displacement of the test mass is used to control a force that can restore the test mass to the null position.

At low acceleration levels (10^{-6} - 10^{-9} g) restoring forces of 10^{-3} - 10^{-6} dynes are required to maintain the 1 gm. test mass at null.

4.2 Magnetic Restoring Force

Sources of low level force have been investigated in Ref. (18). It was evident that the simplest way of controlling the test mass was by magnetic force exerted by means of two coaxial coils inside the superconducting cylinder, one on either side of the magnet. The two coils can be used for both end effect compensation as well as test mass control. The force exerted on the magnet by the coils according to the Appendix is of the form

$$F_c = -\beta I \sinh c_1 x$$

when the coils carry equal currents, I.

In order to maintain the magnet at null ($x = 0$) in the presence of acceleration, unequal currents must flow in the coils and the force becomes

$$F_c = -\frac{\beta}{2} [(I + \Delta I) \; e^{c_1 x} - (I - \Delta I) \, e^{-c_1 x}]$$

$$= -\beta \; I \sinh c_1 x \; -\beta \; \Delta I \cosh c_1 x$$

where $I + \Delta I$ is the current in one coil and $I - \Delta I$ is the current in the other coil. If I iskept constant, ΔI can be varied at will according to the gain in the feedback system.

That part of the magnetic force due to I, i.e., $-\beta I \sinh c_1 x$ is termed the common mode force because I flows in both coils. The force due to ΔI, i.e., $-\beta \Delta I \cosh c_1 x$ is termed the differential mode force.

The common mode force is free from dynamics since I remains constant. The differential mode force is associated with a lag due to the inductance of the coils.

Because of the complex field inside the superconducting cylinder an accurate estimation of the restoring force is not possible and a means for calibration is required; see Chapter VIII.

4.3 Length of Stable Region

End effect compensation was discussed in Section 2.5. A sketch of the uncompensated axial suspension force and the compensating effect of the coils for small displacements from null is shown in Fig. 4.1. For a suitably chosen common mode current in the coils, a small region exists around null where the magnet is axially stable; outside this region the suspension is unstable. The length of this stable region (taken as the distance between the peaks, e.g., p-p' in Fig. 4.1) corresponding to a desired spring constant at null is shown in Fig. 4.2. The smaller the desired spring constant, the shorter the stable region and hence the more sensitive the displacement detector has to be. One way of lengthening the stable region for a given spring constant is to reduce the inherent suspension spring constant as illustrated by the dotted curves in Fig. 4.2.

4.4 Block Diagram for Preliminary Accelerometer

Using the information developed in preceding chapters for the various components, an overall block diagram for an accelerometer is presented in Fig. 4.3.

An input acceleration, a, acts on the mass of the magnet, m, to produce a force, ma. This force causes the magnet to displace from null which calls into play suspension forces, and common mode magnetic force due to a constant standing current, I. The displacement is sensed by the displacement detector which puts out an output voltage. After amplification, this voltage generates a differential mode magnetic force due to a differential current ΔI, in the coils. This force tends to drive the magnet back to null.

The suspension damping, common mode, and differential mode forces are all summed at one junction together with ma and a tilt component $mg\theta$ due to a tilt angle θ of the superconducting tube.

This model of the accelerometer has many nonlinear elements--including the fact that the displacement detector has a finite range.

Since, for closed loop behavior, only small displacements are dealt with, the accelerometer model may be linearized and simplified by absorbing the minor feedback loops as shown in Fig. 4.4.

The open loop transfer function for the linear model is

$$\frac{\frac{\beta}{2} K_a K_d K_c \frac{1}{m}}{\left[S(S + \frac{K_f}{m}) + \frac{1}{m} (\frac{\beta c}{2} - 2 \alpha c)\right] (\tau_d S + 1)(\tau_c S + 1)}$$

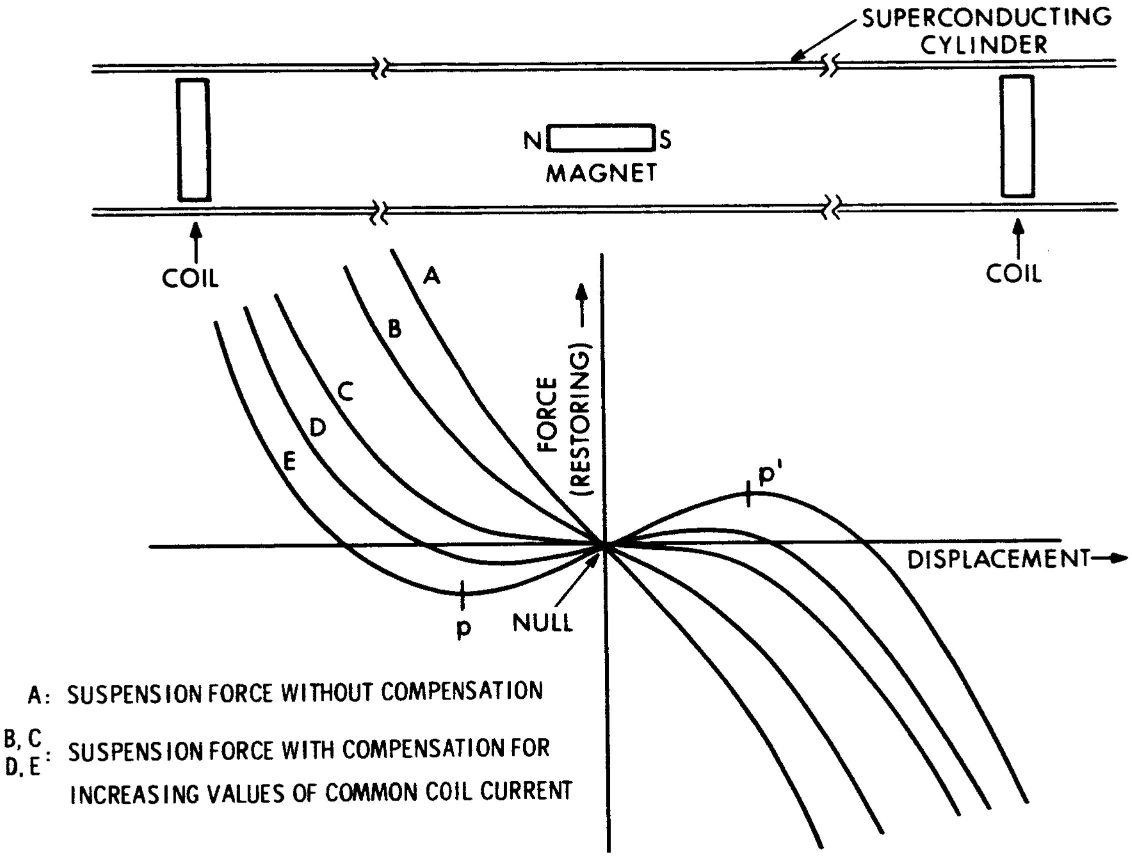

Fig. 4.1 Axial Force on Magnet Close to Null

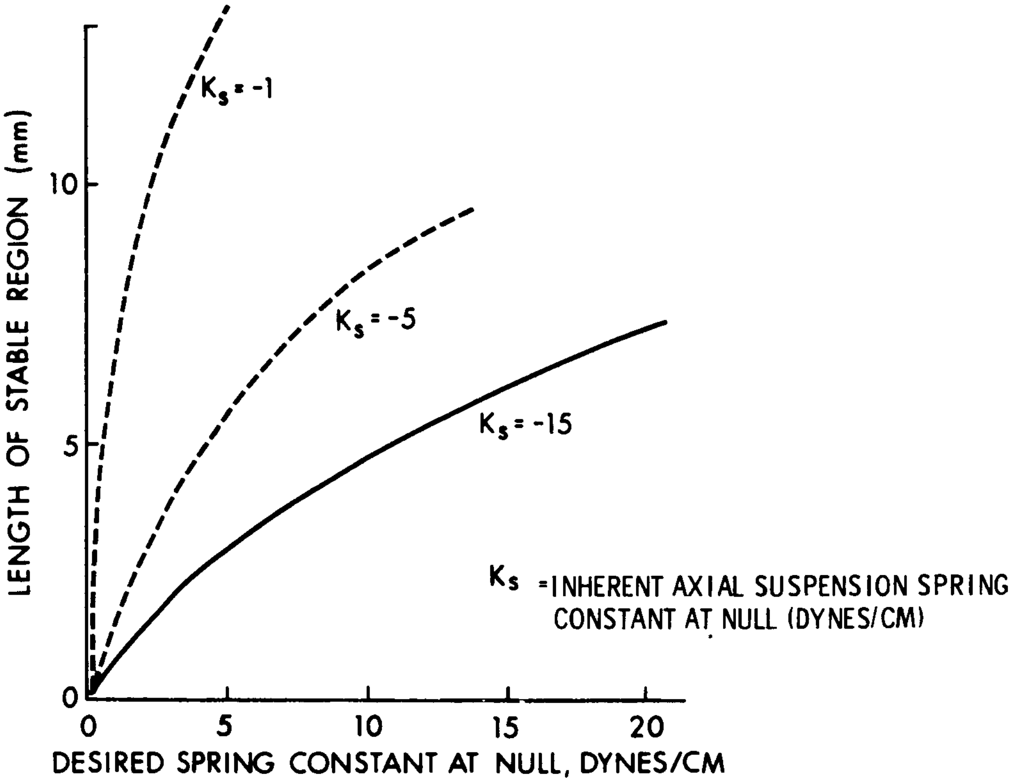

Fig. 4.2 Length of Stable Region vs. Desired Spring Constant at Null

m = mass of magnet

k_f = suspension damping coefficient

k_c = gain of coils

k_a = gain of amplifier

k_d = gain of displacement detector

τ_c = time constant of diff. mode force

τ_d = time constant of displacement detector

I = standing current in coils

θ = tilt error angle (small)

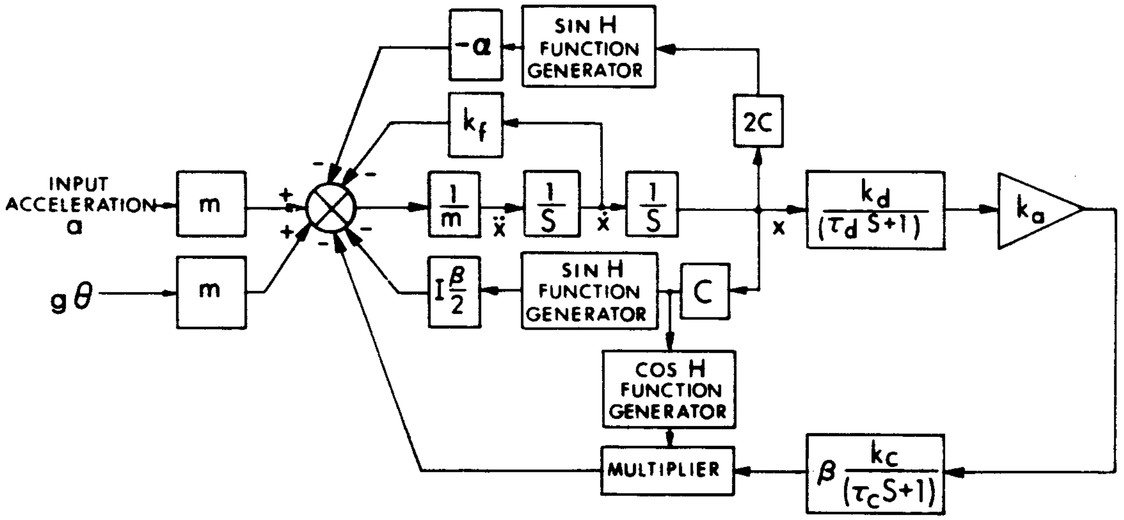

Fig. 4.3 Overall Block Diagram for Accelerometer

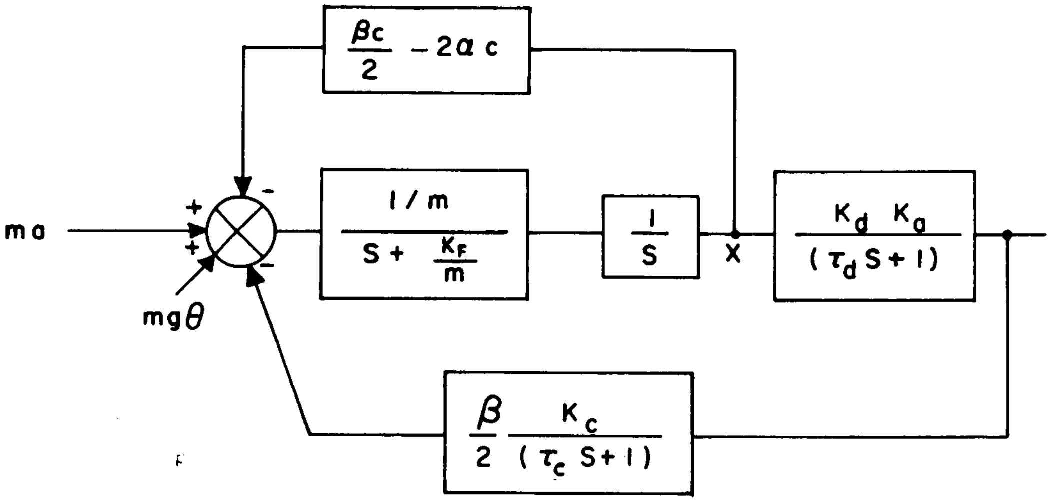

Fig. 4.4 Simplified Linearized Model

$G_1(S)$ = AXIAL DYNAMICS OF SUSPENSION
$H_1(S)$ = ROTATIONAL DYNAMICS OF SUSPENSION
$AG_2(S)$ = GAIN AND DYNAMICS OF SERVO
a_1 = DETECTOR AXIAL SENSITIVITY
a_2 = DETECTOR ROTATIONAL SENSITIVITY

γ = CONSTANT: AXIAL FORCE/DIFFERENTIAL CURRENT
K = CONSTANT: TORQUE/DIFFERENTIAL CURRENT
u = NOISE
v = DISTURBANCE FROM ENVIRONMENT

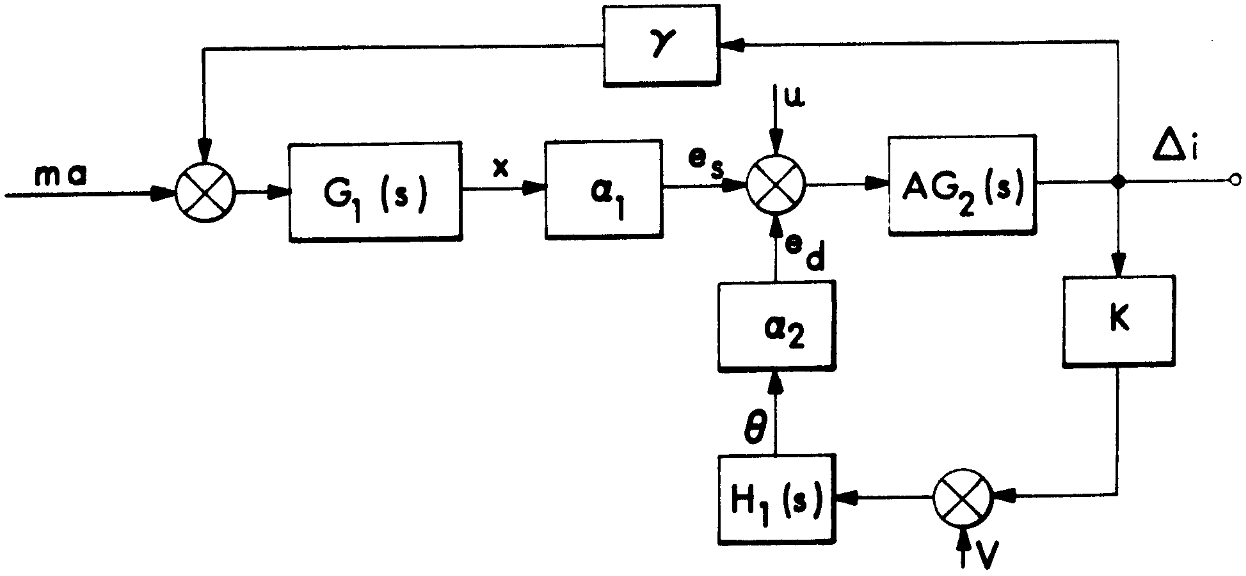

Fig. 4.5 Coupling of Oscillatory Modes

With the absence of damping K_f and suspension and common mode magnetic forces, the transfer function would be that of a type-2 servo, which is inherently unstable. Including K_f and the other forces neglected above, the system becomes stable only for very low gain. Clearly then, some form of compensation is needed. If a pure lead compensation is incorporated, the root locus diagram is modified by the lead network zero on the negative real axis to give a system that is stable for higher gain than previously. The open loop transfer function becomes

$$\frac{\frac{\beta}{2} K_a K_d K_c \frac{1}{m} (\tau_L S + 1)}{\left[S^2 + \frac{K_f}{m} S + \frac{1}{m} \left(\frac{\beta}{2} C - 2 \alpha c\right)\right] (\tau_d S + 1)(\tau_c S + 1)}$$

where τ_L = lead compensation time constant

The steady state displacement error for a step input is given by

$$x_{ss} = \frac{A}{\frac{\beta}{2} K_a K_d K_a \frac{1}{m}}$$

so that x can be small for a high loop gain. If the steady state error is to be zero, a pole at the origin has to be added and this brings another stability problem.

The differential current in the coils is a measure of the applied acceleration.

The output of the accelerometer is obtained by measuring this current or less accurately, by measuring the voltage output of the amplifier in the loop.

4.5 Effect of Rotation of Test Mass

The excitation of rotary oscillation of the test mass is possible, see Chapter VII, and is partly due to the magnetic axis of the test mass not coinciding with its principal axis. This causes the axial restoring force from the coils to apply the torque to the magnet. If the displacement detector is sensitive to rotation, an oscillatory condition can exist.

Fig. 4.5 shows the coupling of the oscillatory mode for a given detector rotational sensitivity α_1, and a torque/differential current ratio K. The only place where compensation is feasible is in the servo block $AG_2(s)$, in the main accelerometer loop.

By reducing the detector rotational sensitivity α_2, see Chapter III, the problem of oscillatory modes may be eliminated.

CHAPTER V

HARDWARE DESIGN

5.1 Dewar Design

The dewar design is a modification of a standard type made by the Janis Research Co., of Stoneham, Massachusetts. The brass block with the superconducting assembly and the window assemblies were made by EAL (See Fig. 5.1).

The dewar weighs about 35 pounds (empty) and has a helium capacity of about 3 liters. Except for the magnet, no magnetic materials were used in the dewar.

The heat of vaporization of helium is so low that great care is required in the dewar design to minimize the inward flow of heat. In Fig. 5.1 the inner container is for liquid helium and is of thin-walled welded stainless steel construction. The only metallic thermal conducting path for the flow of heat is in the filling neck at the top. A teflon "bolt" is normally inserted to fill the entire neck. This "bolt" has a coarse pitched thread so as to lead the cold escaping helium gas in a helical path in intimate contact with the filling neck. This technique removes much of the heat flowing down the stainless filling tube.

The bottom of the helium flask has a 1/2" thick copper disk silver soldered to the stainless steel cylinder. This disk has a 1/2" wide by 4" long through slot to allow liquid helium to fill the brass block. A recess is cut around the slot so that the superconducting assembly in the brass block can be soft soldered to this disk to obtain a helium tight joint with good thermal contact. This design--a relatively large mass suspended a substantial distance below a flexible joint--is a crude pendulum. To eliminate any unwanted oscillations a vertical 3/8" diameter pin is attached rigidly to the bottom of the brass block and it is fitted to a lucite bushing which is rigidly attached to the bottom plate of the radiation shield. Care has been used in the design to minimise thermal conduction.

A copper shield is used external to and concentric with the helium flask to minimise radiative heat transfer. This shield is not pressure tight and a common vacuum exists on both sides to prevent conductive heat transfer. This subassembly is also pendulous and 2 similar 3/8" vertical pins are used to prevent relative

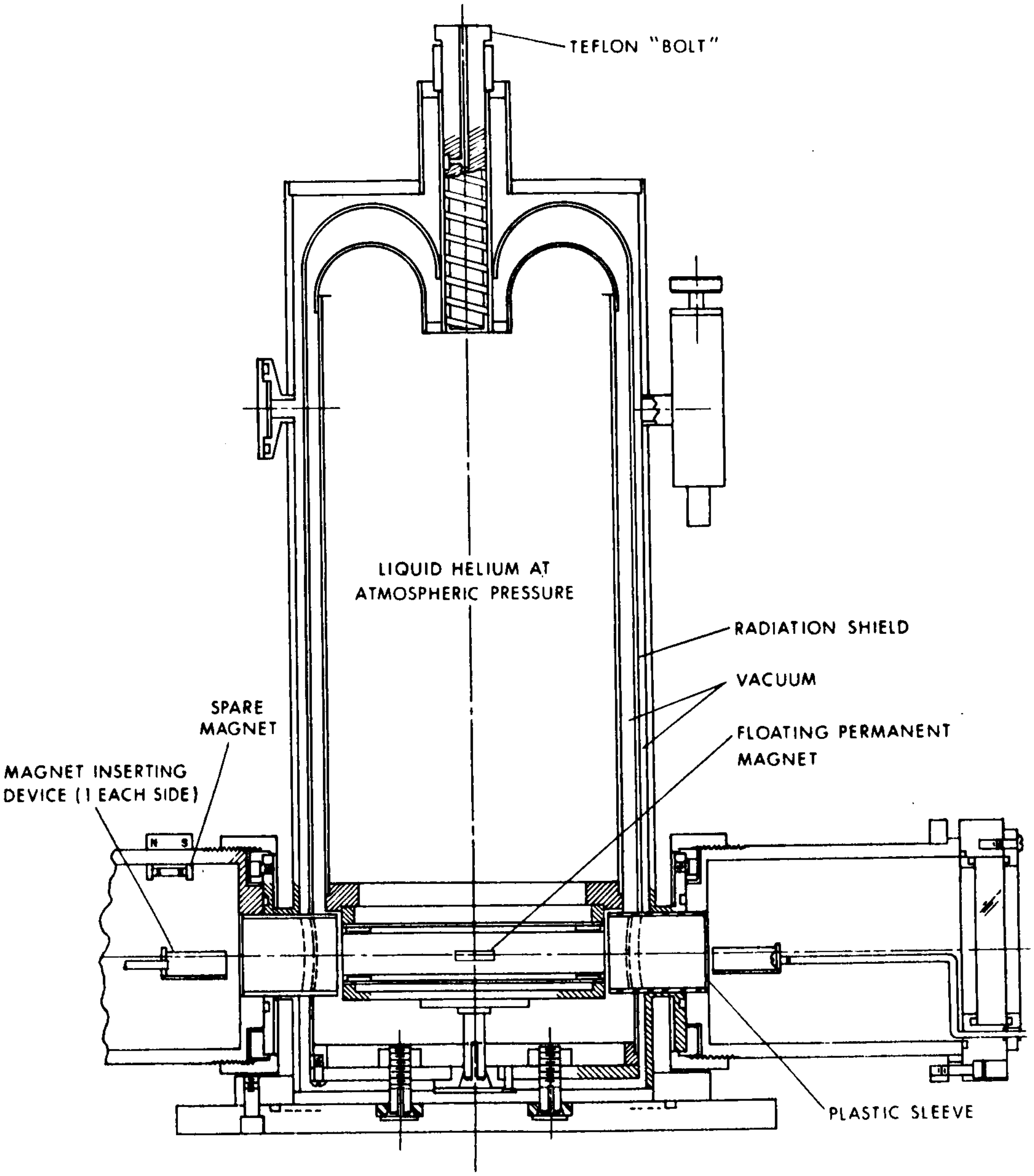

Fig. 5.1 Section Through Helium Dewar

motion between the radiation shield and the outer shell. The outer shell is a vacuum tank made of heavy gauge stainless steel. The axis of the flanged holes is in the same horizontal plane as the axis of the superconductor but the two axes are displaced 2° about the tank vertical center line. A hermetically sealed electrical feed through plug and an "O" ring sealed safety relief cap are also used.

As far as practical all stainless surface are buffed and polished and the outermost surface is chrome plated and polished to minimise the radiant transfer of heat. The insulation of the dewar is such that the outer shell reaches a temperature of about 5° C below room temperature.

The dewar manufacturer advised against using a liquid nitrogen cooled radiation shield because the increased cost, weight, and complexity of operation would not be justified. The manufacturer estimated that the dewar would cause about 1 liter of helium to boil off in 2 hours but if the windows were omitted 1 liter should last 6 to 8 hours. By contrast, the liquid nitrogen shielding 25 liter helium storage dewars will boil off liquid helium at about 1 liter in 48 hours. It is apparent that most of the heat comes in via the windows in the form of radiation. The use of infrared reflecting coatings on the optically flat windows needs to be investigated.

For reasons explained under "operating procedures" it is considered necessary in the setup to have the floating test mass 4" above the surface plate. To accomplish this an aluminum plate 1/2" inch thick by 16" square is bolted-with spacers- to the dewar base. The dimensions are chosen so that the superconducting axis would be a nominal 4.22 inches above the surface plate. This plate has 3 height adjusting and leveling screws. The screws may be used to tip the dewar about either of 2 orthogonal axes, one-axis normal to but not intersecting the superconducting tube axis.

5.2 Superconducting Assembly Design

The superconducting assembly is mounted in the brass block which is readily removable from the dewar by means of a soft soldered joint. (Fig. 5.2).

Two other designs for a superconducting cylinder were made but they proved unsatisfactory.

The first system consisted of a copper tube and brass block as shown in Fig. 5.2 except that the inside of the tube was coated with niobium (also known as columbium). The coating work was carried out by National Research Co. by vacuum evaporation. The adhesion was not satisfactory and, in fact, niobium particles could be dusted off. This lack of cohesion was evidentally due to the copper oxide coating on the copper, even though great care was used to avoid it.

The second system was similar to Fig. 3 except the copper tube was lead plated about .004" thick on the outside and a 1/8" gap was cut through the lead on top of the tube. This scheme also failed because the lead coating was not satisfactory.

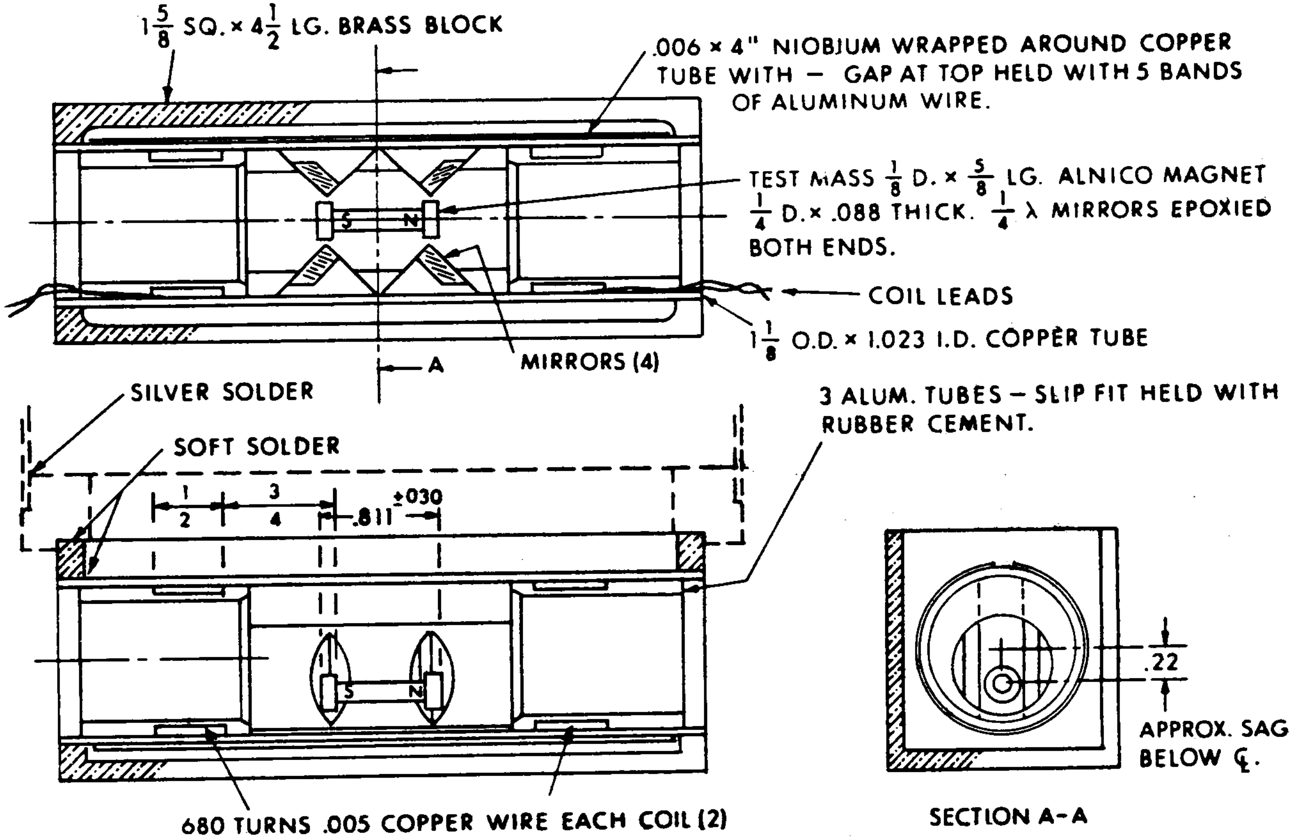

Fig. 5.2 Detail of Superconducting Block and Mirror Assembly

The third superconductor design is shown in Fig. 5.2. The design features niobium in contact with the liquid helium. The temperature tolerance and the maximum permissible magnetic flux are much greater for niobium than other practical materials. A .006" thick sheet of niobium was wrapped around a copper tube and a 1/8" longitudinal gap was left at the top. The reason for this gap is discussed in Section 2.4. The niobium sheet is held in place by 5 equally spaced .040" dia. aluminum wire bands wrapped around the sheet and twisted at the top to secure. It is important that the niobium take the form of part of a perfect cylinder, see Chapter II. The copper tube has an accurately turned cylindrical outside diameter and is an integral part of the helium flask. Inside the copper tube a coil is placed near each end, wound with about 680 turns of enamelled (HF) .005" copper wire. The coils are wound in slots in separate thin walled aluminum tubes which are a slip fit in the copper tube and are anchored in place with a daub of rubber cement. The four leads were connected to the electrical feedthrough plug. Each coil has a room temperature resistance of about 80 ohms and a cold resistance of about 8 ohms.

Each coil repels the test mass magnet and in combination they may be used to center the magnet axially in the tube with a spring constant dependent on the coil currents, suspension geometery, etc. (See Chapter IV). Damping of axial motion of the magnet is provided by (a) eddy currents set up in the copper tube and (b) the servo. Other motions of the magnet are satisfactorily damped by eddy currents only. However, rotation of the magnet about the longitudinal axis is not damped so well. A pendulous oscillation was noticed with periods of 1 to 2 seconds and required from 5 to 10 minutes to dampen out (See Chapter VII). The coil axes are concentric with the superconductor axis but the magnet with 1/4" diameter mirrors floats about 0.22 inch below this axis. The longitudinal axis of the SODD displacement detector was lowered about 1/8" to be more nearly concentric with the magnet axis. The reflecting planes of the mirrors were set at 43° 55' from the superconductor axis by accurately milled locating surfaces in the aluminum mirror holder. Another lineup requirement--not built in--is that the straight edges of the mirror must be normal to the dewar base within ± 2°. The mirror sleeve is anchored in the copper tube with rubber cement. Originally, the mirrors were epoxied in their respective slots but unequal contraction of the glass and aluminum broke the glass. Now the mirrors are held in place with brass clips and a drop of epoxy is used at one end of the each mirror. To disassemble, the mirror assembly and coil arbors may be pushed out by hand. If they are too tight they may be jacked out by an improvised screw-washer-tube assembly in which the reaction force must be applied against an end of the brass block.

5.3 Antechambers Design

It is required to insert test mass magnets into the copper tube and between the restoring coils after the superconducting state has been established. To do this and to keep both ends free for optical and visual control,it was necessary to use an offset inserting device. To accomplish this, two aluminum antechambers of roughly 3-1/4" inside diameter and 4-7/16" long were made and spoons on offset rods were provided. A test mass may be moved about the inner cylindrical surface of the antechamber by an external magnet and maneuvered into a spoon lying against the inner antechamber wall. With the spoon the test mass is lifted away from the wall and inserted into the superconducting region. The spoon shaft, 1/8" diameter, extends through the antechamber cover plate and is sealed by an "O" ring which permits rotation, axial motion, and a limited amount of wobble. One spoon was replaced with an electromagnetic coil which serves the same purpose but is narrow enough to fit between the mirrors. This coil is wound on a relatively heavy copper core which serves as a heat sink. This coil has a room temperature resistance of 45 ohms and may be energized with 350 m.a. for one minute maximum. The coil current should be shut off quickly in order to drop the magnet without introducing angular accelerations.

The antechambers are equipped with 1/2" thick x 3" dia. optically flat glass windows. These windows and the entire antechambers are skewed in a horizontal plane 2° off the superconductor axis to prevent confusing reflections in the interferometer system. The antechambers are equipped with quick disconnect flanges to provide ready access to the test area. All separable joints are sealed with "O" rings.

Additional magnets may be stored about the perimeter of the antechamber. These test mass magnets can be held in place by external magnets holding through the 1/4" aluminum antechamber wall. Experience has shown that the internal magnets are difficult to keep apart and once they touch they can be separated only by removing the antechamber. The use of only 2 or 3 magnets per run is suggested.

5.4 Lessons Learned From Early Experimentation

In the earlier runs some trouble was experienced with the test mass magnets falling into the gaps between the brass block and radiation shield and between the radiation shield and the outer shell. To prevent this,thin-walled lucite sleeves were installed in each end. These were anchored to the outer shell flanged holes with rubber cement and almost touched the superconducting block assembly.

Another difficulty experienced was that of helium leakage. By means of a mass spectrometer leak detector a leak was found between the helium flask and the vacuum compartment. The superconducting assembly was resoldered two times, checked with a leak detector, and tested with a helium run each time. The tests were repeated twice with the dewar inverted and the base plate and radiation base removed to check rigorously the brass block assembly for leaks but none could be found. The helium leak detector did not indicate a leak because the helium was not flowing downward into the deep blind annular hole. Finally, by means of water traps and leak detectors it was possible to demonstrate that helium was leaking around the toroidially shaped top of the helium flask. This defect required replacement of the top at the factory. The manufacturers attributed the leak to corrosion of the stainless cap due to spilling of the non-corrosive soft soldering flux--known commercially as "No-Corrode." This damaged piece was examined and on visual inspection no defects could be seen. This half toroid was spun from a piece of stainless sheet and required very severe cold working and frequent annealing. This leak had a very deceptive behavior and appeared to be a "cold leak". These are supposed to be cracks, etc., which leak at very cold temperatures only and are notoriously difficult to locate. The leakage of the air and nitrogen were not noticed because the mechanical pump was used until liquid helium was transferred. If helium gas leaks into the evacuated space, however, it does not freeze but increases the pressure.

A third difficulty which also appeared to be a cold leak was caused by the cold helium gas flowing downward and freezing the "O" ring in the safety valve. The cold gas flowed downward because the rags that are wrapped around the top of the dewar were allowed to hang down near the valve.

At all times, the vacuum pressure was monitored with a National Research Company model 501 thermocouple vacuum gauge with a useful range of 2 to 500 x 10^{-3} mm Hg. having essentially the same calibration curve for helium and air. This gauge may be used indefinitely with high off-scale vacuums.

At one time, a glass antechamber window was replaced by a lucite window equipped with a National Research Company # 507 ionization pressure gauge. The pressure with the dewar cooled to the liquid nitrogen temperature and the mechanical pump running was about 2 x 10^{-3} mm. Hg. but when the pump inlet was closed and liquid helium added the pressure dropped to 1 x 10^{-6} mm Hg. This drop in pressure is caused by cryopumping: the air in the vacuum chamber and the air leaking in are frozen on contact with the cold helium flask.

5.5 Optical Systems Design

Both optical systems are sensitive displacement detectors and as such they must be free of all extraneous motions. The dewar and all optical components were set up on a 1200 pound, 4 foot square cast iron surface plate. Each critical optical component was of heavy steel construction and had a 3 point support.

All beam splitting mirrors were specified to have equal transmittance and reflection for 45° incident unpolarized light except the beam splitter closest to the laser. This beam splitter has a transmission to reflection ratio of four to one. Protective coatings were not used.

Fig. 5.3 shows the combined layout of the spot occultation displacement detector (S. O. D. D.) and the interferometer system. The S. O. D. D. system was designed to provide independent beam splitting mirrors and to avoid passage of beams through the dove prisms. The angle between the interferometer axis and the S. O. D. D. axes was fixed by the dewar mirror design at 2° 10'. This angle and the design of the chopping wheel for a preferred angle of about 90° limit the overall configuration to the approximate dimensions and angles shown on Fig. 5. 3.

The light source is a Perkin Elmer model 5200 gas laser and a model 5201 power supply. The laser has a wavelength of 6328 Å, a beam intensity of .5 milliwatts, and has a collimated polarized beam of .15 diameter. A plot of intensity distribution across the beam would give essentially a gaussion curve. The laser is mounted on an aluminum frame and may be rotated and locked in any position about its longitudinal axis. The frame also has height and level adjusting screws. Provision is made for mounting 2 microscope objectives, usually 16 mm. or longer focal length. These lenses give good control over focusing and were used to obtain a small .01 inch beam diameter at the points where they were occulted by the test mass in the S. O. D. D. system. By controlling the beam diameter at these points adjustment of the S. O. D. D. sensitivity may be achieved, (see Chapter III). Next in the optical path a beam splitter--mirror assembly was used to give adjustable separation and relative angle to the interferometer and S. O. D. D. beams.

In the following assembly a 3" diameter optically flat beam splitter was used for the interferometer beam and was coated on the side nearer the laser. This mirror was equipped with horizontal and vertical adjustments which affect only the reflected beam component. On either side of this 3" beam splitter were 5/8" dia. beam splitters for the S. O. D. D. system. These mirrors were also adjustable about 2 axes. A motor driven chopping wheel was then used to interrupt alternately the right and left beams of the S. O. D. D. system at 16 c.p. s. before they entered the dewar. A small beam splitter and photovoltaic cell were used in the right beam to obtain a phase reference. The next optical components are the two dove prisms--one in the left and one in the right interferometer leg. These prisms are aligned so that 4 long sides are parallel to and equidistant from the axes of the beams going toward the dewar. Next, the optically flat mirrors are set up so they are in line with and make a 67 1/2° angle to the superconducting tube centerline. These mirrors reflect both the incoming and outgoing interferometer and S. O. D. D. beams. The mirrors have spring loaded conical pivots near the spot where the interferometer beams are reflected to minimize the axial mirror motion during angular adjustments. The angular changes are made by 2 micrometer heads which will rotate the mirror about a vertical and horizontal axis.

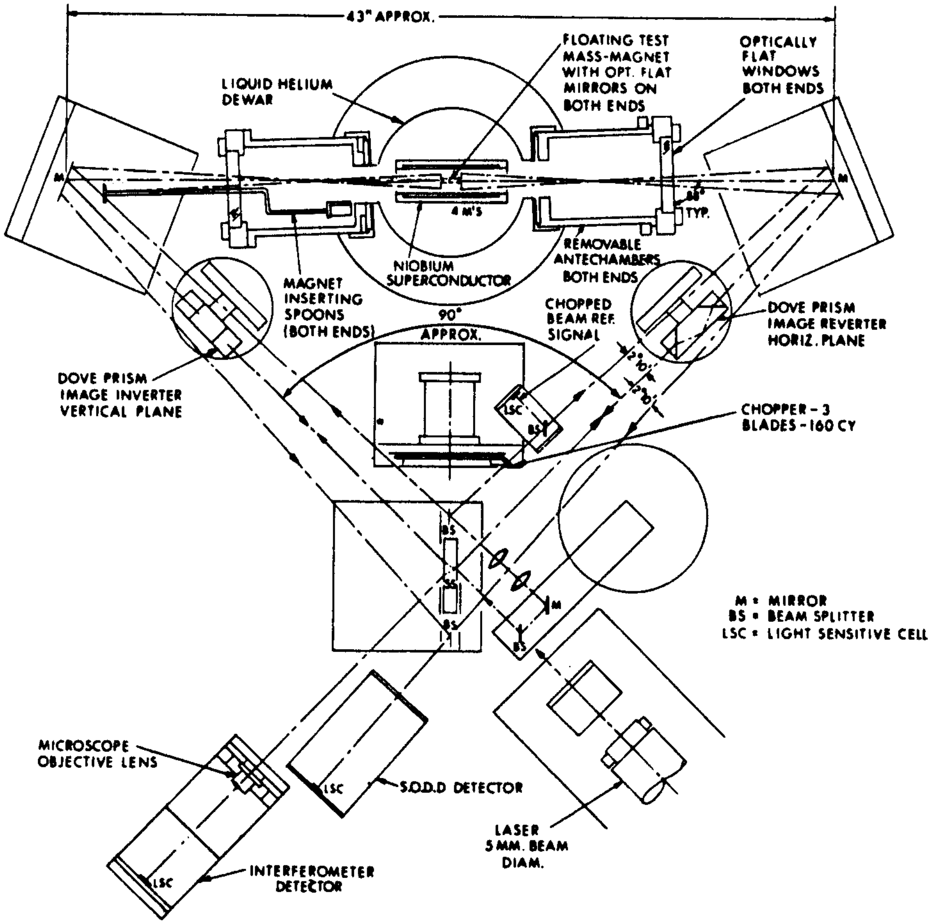

Fig. 5.3 Layout of Two Optical Systems

Because rotation of the test mass about transverse axes will cause the reflected beams to separate in opposite directions (i. e., if one reflected beam goes up the other comes down) the use of inverting mirrors is required, (see Chapter III). Originally, two inverting mirror assemblies were made, each with 3 mirrors, for each interferometer leg. These assemblies were mounted so that their axes were concentric with the interferometer beams going toward the dewar. This technique worked well as far as keeping the interfering spots superimposed during test mass rotation but the setting up procedure was too cumbersome. Two dove prisms about 1" square by 3" long replaced the mirror assemblies and were found to be adequate.

The light sensitive photovoltaic cells were made by Hoffman Electronics Corp. and are available in a wide range of sizes. Tests were made on the cells which showed the output voltage to be relatively independent of spotsize or position Obviously the .5 milliwatt laser beam is well collimated and the spot should not be so small that local heating will become a factor. Permanent damage to the cell will be caused by local temperatures of 100° C. It is suggested that the image be not smaller than .02 inch in diamter unless better advice or test results become available.

The interferometer test results were quite unsatisfactory even when the test mass simulator was used. It was possible to adjust the simulator to achieve spot brightness variations but superimposed on the steady state brightness was a random low frequency intensity modulation.

5.6 Test Mass Design

The test masses were made as follows:

Two mirrors 1/4" diameter by .088" thick and flat to 1/4 wave were aluminized but were not given a protective coating. These mirrors were epoxied onto the ends of an Alnico V magnet 1/8" diameter by 5/8" long. As the epoxy cured the mirrors were held against optically flat windows which were accurately spaced with 3 sets of gauge blocks each stack .8110" high. A fixture was provided which was a 1" diameter x 3/4" high steel cylinder with a 1/8" diameter through hole in which each end was counterbored to .250" diameter x 5/32" deep. The axes of these holes were accurately concentric and normal to the cylinder ends. A 90° segment was cut from this cylinder and as a fixture it was held magnetically to the magnet. The magnet axis was then normal to the optically flat window, the two 1/4" diameter mirrors were held concentric to the magnet, and enough space was left about the small mirrors to allow a brass leaf spring to hold them against the optical windows to obtain accurate parallelism.

5.7 Test Mass Simulator Design

To calibrate the optical systems two test mass simulators were used in place of the dewar and test mass. The first simulator, designed to calibrate the less sensitivie S.O.D.D. system, consisted of a magnet mounted above a heavy two axis micrometer fed microscope slide. See Chapter III for discussion of results.

The other simulator has a positioning requirement to detect wave interferences of about .02 wave length.

In effect the sensitivity is doubled (1 mirror advances as the other retreats) so it is required to move the mirrors through distances as small as 5×10^{-7} cm. or, .2 micro inch. When used in the servo the output error signal is effective for a displacement of about 1.5×10^{-5} cm. and cannot distinguish between positions 3×10^{-5} cm. part.

The test mass simulating mirror was a 1/4 inch diameter by 3/4 inch long cylinder of glass with the ends parallel, polished, and aluminized to optical flat standards. This double mirror was mounted on a 3" dia. x 3/8" thick aluminum platform which had 4 integral legs approx. 5/16" square x 1-3/16" long equally spaced and enclosed within a 2-1/2" diameter. The legs were also integral with a heavy base and in effect the platform could be displaced horizontally with respect to the base with a very stiff spring constant. A screw and coil spring assembly were attached to the base in such a way that the spring would exert an adjustable horizontalforce on the platform. The spring constants were such that 1 pound would deflect the platform 5 micro inches and the coil spring 4×10^{4} micro inches. It can be shown that the coil spring may be compressed by 1600 micro inches to displace the table .2 micro inch. With suitable preloading the mirror may be moved axially in either direction and the system is free of backlash and hysteresis. This testing fixture also had a provision for rotating the mirror about a vertical diameter so that test mass wobble could be simulated.

5.8 Liquid Level Sensing Devices

A helium level sensing probe was made by soldering a 1/8" OD x 30" long stainless steel tubing to a drawn copper sweat fitting adapter 5/8" ID to 1/8" ID. A .005" thick x 5" square rubber sheet was wrapped over the large end and in "O" ring was wrung over the 3/4" OD cylindrical diameter so as to hold the rubber tight and flat over the large end. When the small end of the sensor is immersed in liquid helium and withdrawn slowly, the rubber diaphragm will vibrate with a large amplitude at a frequency of about 6 cps. As the tube is withdrawn, the frequency increases to about 20 cps and it suddenly stops when the tube end is no longer immersed in liquid helium.

The same tube assembly may be used to sense liquid nitrogen levels if the rubber diaphragm and "O" ring are removed. If the tube is about room temperature and the small end is lowered slowly into LN_2 small drops will fly out the top just as the tube contacts the liquid surface.

5.9 Electronics

The SODD control loop is shown in Fig. 5.4.

The output of the SODD photo detector, a solar cell, was fed into a preamp followed by a power amplifier and a phase sensitive demodulator. The reference to the phase sensitive demodulator was obtained from the output of the reference photo detector shown in Fig. 5.3. The output of the demodulator was fed into a variable gain operational amplifier with variable lead-lag capability. The output of this amplifier drove a differential transistor stage which controlled the currents in the coils on either side of the magnet inside the superconducting cylinder. Means are provided for feeding only one coil and for the external adjustment of the currents in either coil.

A switch after the servo amplifier allowed open loop or closed loop operation.

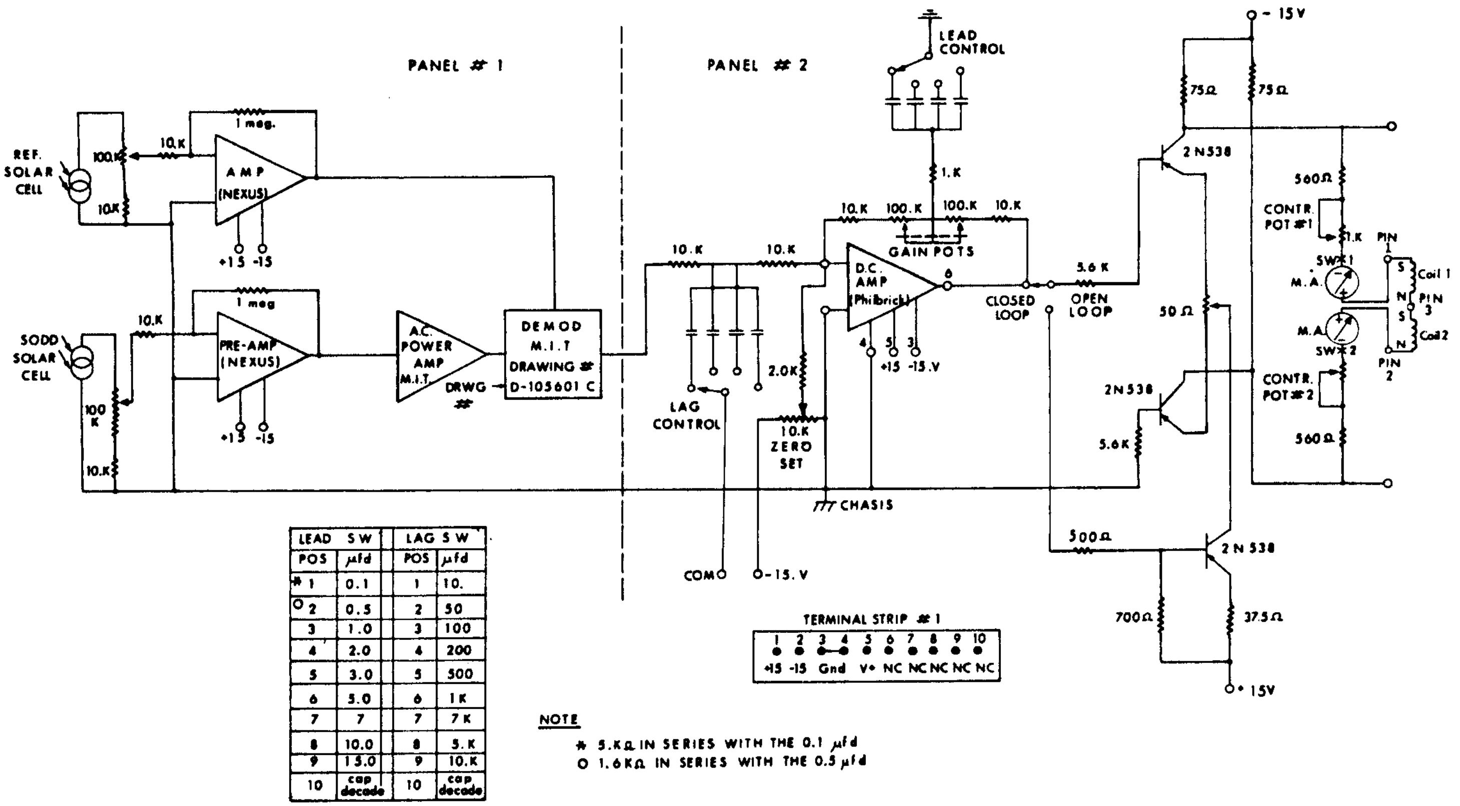

LEAD SW		LAG SW	
POS	μfd	POS	μfd
* 1	0.1	1	10.
O 2	0.5	2	50
3	1.0	3	100
4	2.0	4	200
5	3.0	5	500
6	5.0	6	1K
7	7	7	7K
8	10.0	8	5.K
9	15.0	9	10.K
10	cap decade	10	cap decade

TERMINAL STRIP # 1

1	2	3	4	5	6	7	8	9	10
+15	-15	Gnd		V+	NC	NC	NC	NC	NC

NOTE

* 5.KΩ IN SERIES WITH THE 0.1 μfd
O 1.6KΩ IN SERIES WITH THE 0.5 μfd

Fig. 5.4 SODD Control Loop

CHAPTER VI

OPERATIONS PROCEDURE

6.1 Equipment Requirements

For a helium run in the LLAMA dewar the following supplies are required:

1. Mechanical vacuum pump capable of 5×10^{-3} mm Hg. including a suitable vacuum hose.
2. National Research Co. #501 Thermocouple pressure gauge.
3. National Research Co. #701 Vacuum gauge control.
4. 25 liters of liquid helium in a storage dewar.
5. 15 liters of liquid nitrogen in a storage dewar.
6. Pressurized helium gas in bottle equipped with regulator valve and pressure gauge to use in the 1-10 psi range.
7. Liquid helium transfer tube. Janis Research Co. #FHT
8. Liquid nitrogen tranfer tube. Janis Research Co. #RHT
9. Liquid helium level sensing tube.
10. Helium storage dewar "reamer." (3/8" dia. x 3 ft. long alum.tube).
11. 3 or 4 cotton rags.
12. 1/4" I.D. x 20 ft. long rubber tubing suitable for 10 psi.
13. 2 flashlights.
14. Thermos bottle of 1 to 2 liters capacity with large mouth.
15. 6 Alnico V magnets about 1/4" diameter x 1-1/4" long.
16. A magnetic compass--cheap pocket type about 2" diameter.

6.2 Preliminary Optical Alignment

Both optical systems should be aligned before the dewar is cooled. The LLAMA dewar must be set up on a large stable platform, preferably a 4 ft. x 4 ft. or larger surface place, as shown in Fig. 5.3.

The larger (10" diameter) base plate on the dewar and the surface plate should both be leveled within ± 3 arc minutes in a direction parallel to the superconductor axis.

The interferometer is more critical and should be aligned first. The reflecting test mass mirrors will not be in place and as a substitute the laser beams entering each end of the dewar must pass through and be coaxial with each other and parallel with the superconductor axis at an elevation approximately equal to the floating test mass center line. This requirement is most easily met if all interferometer beams are confined to one plane. Another reason to limit the beams to a plane, is because the overlapping beams would otherwise have a wedge effect.

The alignment was made easier by using a mask with a 3/32" diameter clearance hole set at 4" above its base. This mask could be inserted in the beam path at any one of several points so that one beam would pass through the hole concentrically. The other beam approaching from the opposite direction could then be adjusted to pass through the same hole. Both beams should then be combined so they are parallel and concentric when they fall on the light sensitive cell in the interferometer detector. Lack of concentricity may be detected by alternately interrupting each beam and observing whether the spot on the light sensitive cell appears to jump.

The S. O. D. D. system should then be set up but the micrometer adjusted mirrors are common to both systems and any angle changes must be compatible with both.

6.3 Cooling of the Dewar

Before cooling, the vacuum jackets of the dewar and the liquid helium transfer tube should be evacuated to about 10 microns. The next step is to transfer liquid nitrogen to the dewar for precooling. The input end of the liquid nitrogen transfer tube is immersed in the liquid nitrogen L. N_2 storage dewar and the neck of the dewar is sealed to the outer jacket of the transfer tube with a rubber hose. The output end is inserted in the LLAMA dewar and the storage dewar may then be pressurized with about 4 psi of helium gas. The flow of L. N_2 will start and should be continued until the dewar is at least half full--5" deep. This transfer requires about 4 to 6 minutes and as there is no visible indication of the dewar nitrogen level we watch for drops of L. N_2 to spill out the top of the dewar. This begins when about 1 liter has been transferred. The filling should continue for another minute or so then the flow of L. N_2 should be shut off. This is accomplished by turning off the helium gas supply and venting the storage dewar to atmosphere. We find that the L. N_2 level may be estimated by using the liquid nitrogen level sensing probe as described in Chapter V.

The L. N_2 should then be allowed to remain in the dewar for at least half an hour and may then be removed by reversing the transfer tube end for end. The LLAMA dewar may then be pressurized and the process repeated. This reverse transfer will still leave about 100 cc. of L. N_2 in the brass block assembly. To remove the remaining liquid a vigorous blast (6-10 psi) of gaseous helium impinging on the slot will be helpful. Next the valve on the dewar leading to the vacuum pump should be closed and the vacuum hose removed. The pressure gauge should still be operative and the indicated pressure should remain below about 5×10^{-3} mm. Hg. for the entire run.

It should be noted that any air finding its way into the L. He dewar will freeze. For this reason, the helium dewar reamer, an aluminum tube 3/8" diameter by 3 ft long, is used to clear the neck of frozen substances before each transfer. The operator should also be aware of the possibility of the transfer tube becoming obstructed by frozen particles. Neither the liquid helium nor liquid nitrogen storage dewars should ever be exposed to internal pressures greater than 10 psi gauge. It is considered good practice to blow helium gas through the transfer tube to minimize the amount of air trapped in the flexible tubing convolutions and to check for obstructions.

The input end of the helium transfer tube should then be inserted in the helium storage dewar and the sliding sleeve sealed to this dewar with rubber tubing. This sleeve should be adjusted so the input end of the transfer tube is about 1" above the bottom of the dewar. About 3 psi of helium gas pressure is then applied to the storage dewar to cause the liquid helium to flow. It is helpful to immerse the output end of the transfer tube in a large mouthed thermos bottle so the flow of LHe may be confirmed before inserting the tube into the LLAMA dewar. If the outside of the transfer tube should reach a temperature more than about 10° C below ambient the vacuum is not sufficient for good thermal insulation.

When the liquid helium flow through the transfer tube has been confirmed the output end is then inserted into the LLAMA dewar. Rags should then be wrapped tightly about the dewar-transfer tube joint.

No outward indication exists for the amount of liquid helium in the dewar. At first a thin white smoke-frozen water vapor-will rise as the cold helium gas passes through the rags and cools the surrounding air. After about 5 minutes a dense white smoke made up of frozen particles of air will appear. The transfer should be continued for another 4 to 5 minutes. After shutting off the helium gas supply and venting the storage dewar to atmosphere to stop the liquid helium flow, the transfer tube should be removed from the LLAMA dewar and the liquid helium level sensing probe used to find the liquid depth. Three inches of depth represents one liter which should maintain the superconducting state for about 1-1/2 hours. Normally, about 10 liters of liquid helium are required to charge the dewar to this level. Finally the Teflon "bolt" is inserted in the LLAMA dewar filling neck and the dewar is ready to use.

6.4 Test Mass Insertion

It was found in practice that the insertion of the test mass into the operating position is a difficult process. It should be emphasized that the polarity of the test mass magnet must be compatible with each coil. The adopted convention was that the operator looking at the electrical feedthrough side of the dewar would always have the north pole of the test mass magnet pointing toward the right end of the dewar and the confining coils and the electro magnetic inserting device would have their north poles pointing to the left. Each test mass had a daub of yellow or white paint near its north pole end.

If both confining coils are energized the magnet will have 3 stable axial positions. The normal position is equidistant between the 2 coils and the magnet is repelled by both. The other 2 positions are the central position in each coil. To insert a magnet from one end first block the opposite end with the unused spoon or coil, and energize the farther confining coil with about 40 m.a. The spoon containing the magnet is then pushed gently inside the superconductor about 1/16" less than its limit. The exposed end of this loading spoon is then tapped to kick the magnet out and the nearer coil is then energized immediately with about 40 m.a. to capture the floating magnet between the coils. The electromagnetic inserting device may be used in a similar fashion except the magnet may be inserted close to the axial center of the superconductor. Both confining coils may then be energized to about 40 m.a. each and the inserting device may then be de-energized with a switch. It is important to open this coil circuit quickly so both ends of the magnet will drop at the same time.

Experience has shown that a magnet approaching a repelling coil with sufficient speed may flip over end-for-end or become wedged crosswise in the tube. A flipped magnet should be removed to an antichamber, reversed end-for-end with an external magnet and re-inserted. To minimize the above difficulties both ends of the superconducting tube were blocked with the spoons and by using minimum coil current and manual amplitude and balance controls, it was possible to center and stabilize the magnet.

The spoons may then be withdrawn and the servo position controls turned on. The servos will not operate if the spoons block the optical sensing paths.

6.5 Final Optical Alignment

Two possibilities for leveling the superconductor axis now are available: One the leveling of the LLAMA dewar; and the other the leveling of the entire surface plate including all optical components. The floating test mass magnet should be centered with the S.O.D.D. position sensing system by means of the dewar leveling screws when both coil currents are equal and have an amplitude of about 10 m.a. If the magnet now has a longitudinal tilt the interferometer beams cannot be contained within a plane unless the entire surface plate is tipped and the dewar tipped an equal angle in the opposite direction to maintain the superconducting axis level.

Fig. 6.1 is a photograph of the latest verison of the LLAMA dewar and Fig. 6.2 shows the dewar with one ante-chamber taken out to reveal one end of the superconducting cylinder and the construction of the lucite spoon.

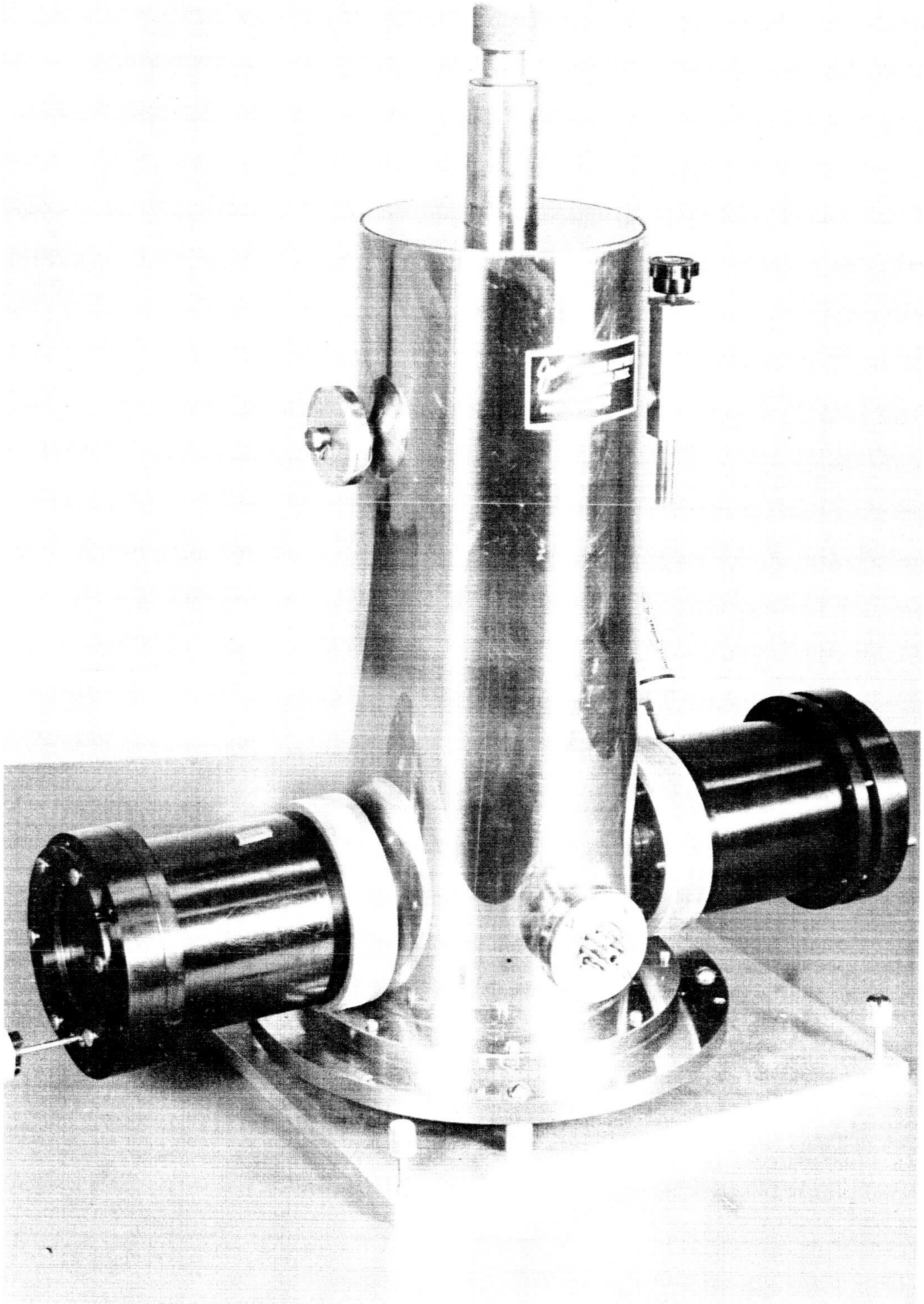

Fig. 6.1 The LLAMA Dewar (present model)

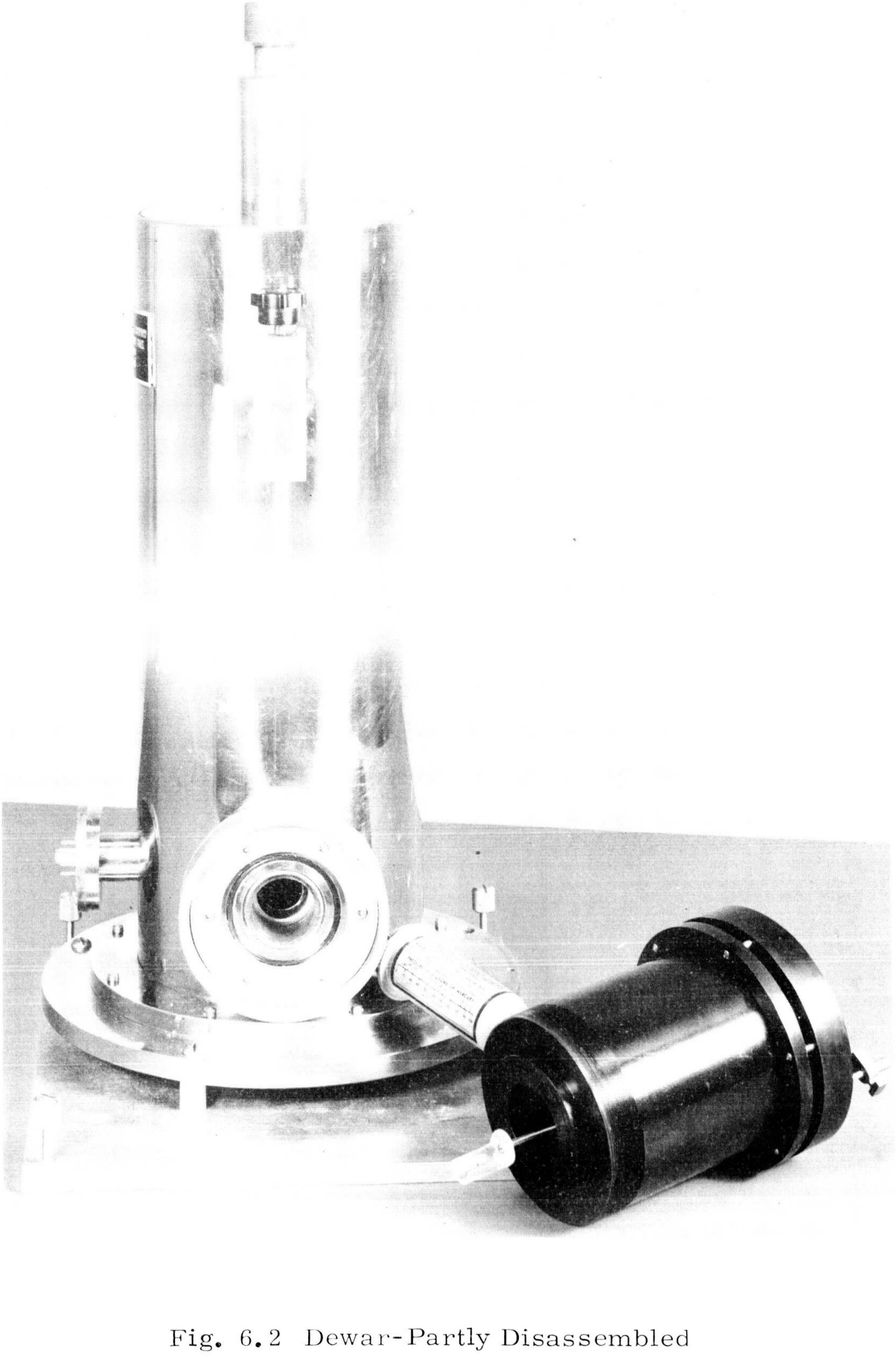

Fig. 6.2 Dewar-Partly Disassembled

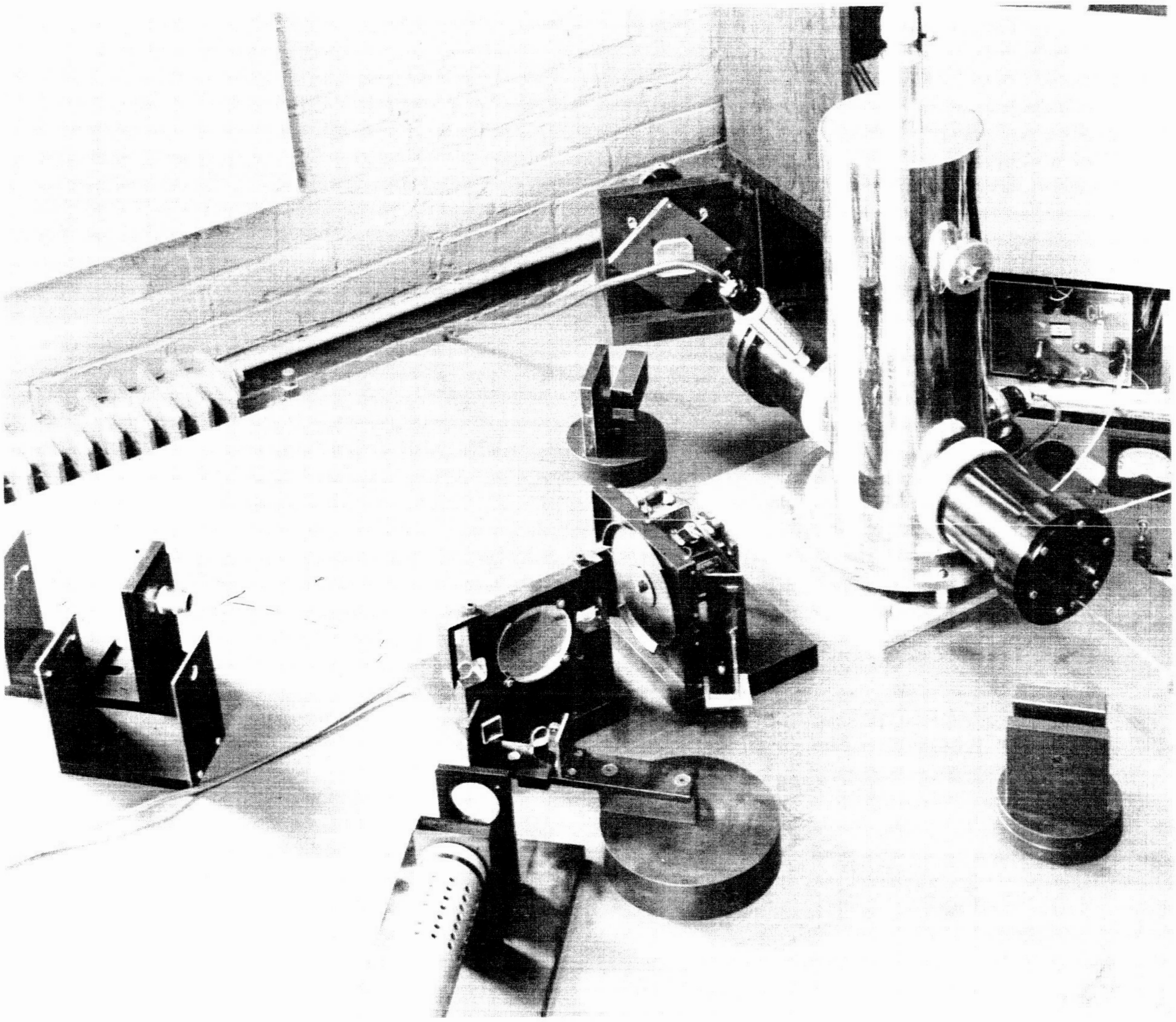

Fig. 6.3 LLAMA Setup

Fig. 6.3 is a photograph of the layout of the LLAMA system during operation. A corner mirror at bottom right is not shown in the photograph.

CHAPTER VII

PERFORMANCE OF THE EXPERIMENTAL SUSPENSION

7.1 Introduction

The LLAMA suspension dewar, in its present form, demonstrates the feasibility of stably supporting a magnetic test-mass in a superconducting cylinder. However, the technique used for making the tube (see Section 5.2) leaves a great deal to be desired and was adopted only as a simple expedient for checking the design concepts. It is therefore not to be expected that the present suspension should approach the theoretical limits derived in Chapter IX. Modifications to improve the performance are also discussed in Chapter IX.

The best method of testing the supsension would be to observe the performance of the complete LLAMA system. Pending the availability of the other components, an attempt was made to measure the inherent (negative) spring constant of the suspension. There are some problems in making this measurement, which will be clarified by considering the idealized model discussed in the Appendix.

There is serious doubt as to the applicability of the theoretical model in the present suspension; however, conclusions drawn from it do prove to be of some value in interpreting the test data.

7.2 The Effect of Axial Non-Linearity

Since measurements could of course be made only when there was sufficient current flowing in the coils to ensure stability, the method used to determine the initial spring constant due to end effects in the suspension consisted of plotting the square of the observed natural frequency of axial oscillation as a function of the current, and extrapolating the resultant curve to zero current. The force on the magnet due to the coils certainly varies linearly with the current, so this method, on the surface, seemed capable of good accuracy, as long as small oscillations were used.

Assuming that the same current is flowing in each coil, and that the coils are equally displaced from the center of the suspension, the maximum tolerable amplitude of oscillation in these tests may be estimated by using Eqs. (2.5) and (2.6). Neglecting damping, the equation of axial motion of the test-mass is

$$m\ddot{x} + \beta I \sinh c_1 x - \alpha \sinh 2c_1 x = 0 \qquad (7.1)$$

For small oscillations, the motion is of course simple harmonic, with a spring constant given by

$$K_o = c_1 (\beta I - 2\alpha) \tag{7.2}$$

provided that I is sufficiently large for this quantity to be positive.

For larger oscillations, (7.1) shows that the stiffness of the equivalent spring at first increases with displacement and then starts to decrease, eventually becoming negative. By differentiating the restoring force in (7.1) with respect to x, it is easy to show that maxima of the force occur when

$$\cosh^2 c_1 x - \frac{\beta I}{4\alpha} \cosh c_1 x - 1/2 = 0 \tag{7.3}$$

The force is zero when

$$\cosh c_1 x = \frac{\beta I}{2\alpha} \tag{7.4}$$

and beyond this point is negative, so that this gives an absolute upper limit on the permissible amplitude of oscillation. In practice, it was found that the magnet did not necessarily fly out of the suspension when the displacement exceeded this limit: the restoring force increased rapidly when the magnet approached one of the coils (where the assumptions underlying (A.3.7) of the Appendix become invalid, even in the idealized model), so that it was possible for three stable positions of the magnet to exist inside the suspension.

In order to estimate the effect of the amplitude of oscillation on the measured value of the initial negative spring constant K_s, consider the average spring constant for an oscillation of amplitude x_o, which is given by (7.1) as

$$\overline{K} = \frac{1}{x_o} (\beta I \sinh c_1 x_o - \alpha \sinh 2c_1 x_o) \tag{7.5}$$

Use of this parameter of course implies that the motion is sinusoidal, which is, in general, a very crude approximation, but it will suffice for an order of magnitude estimation.

Now from (7.1)

$$K_s = -2\alpha c_1 \tag{7.6}$$

and so

$$\overline{K} / |K_s| = \frac{\beta I}{2\alpha} \frac{\sinh c_1 x_o}{c_1 x_o} - \frac{\sinh 2c_1 x_o}{2c_1 x_o} \tag{7.7}$$

If the measured value of $\overline{K}$ (i.e., the square of the measured angular frequency of oscillation) is plotted against I, the intercept of the resulting line with $\overline{K}$ axis will thus give the correct value of K_s if the oscillations are sufficiently small, but in general it will be in error in the ratio $(\sinh 2c_1x_o)/2c_1x_o$.

This expression is plotted in Fig. 7. 1 as a function of x_o. It is clear that the amplitude of the oscillations must be kept below about 0. 25 cm if this technique is to give a reasonable accuracy.

The implication of this result is that some form of displacement detector is a prerequisite for determination of the inherent spring constant, as visual observation of the test-mass did not allow sufficiently accurate estimation of the oscillation amplitude.

7.3 Experimental Results

In order to make the measurement described above, a simple optical displacement detector was constructed and attached to the dewar, see Chapter III. The output characteristics showed a linear range of approximately 1 mm. The axial position of the null inside the suspension was determined by the location of a small prism assembly mounted inside the copper tube.

The prisms were moved until the output null was as close to the center of the superconducting tube as possible. The stabilization coils were fixed in position near the ends of the suspension: when the magnet was inserted, it was found that a coil current of 11 mA was the minimum for stability. The levelling of the base of the dewar was then adjusted, causing the magnet to move into the linear range of the detector, until an output close to null was obtained.

The test mass was displaced to one end of the linear range by bringing an external magnet near one of the dewar windows and then released. The output of the detector due to the resultant damped axial oscillation was recorded, and the experiment repeated for several different values of the coil current. A typical record is shown in Fig. 7. 2.

The first parameter that could be determined from these tests is the damping due to eddy current generation in the copper tube. The amplitudes of successive cycles of the oscillations are plotted in Fig. 7. 3 as functions of the time. The time constant was found to be approximately 3 seconds.

Secondly, the spring constant corresponding to each record (i.e., $m\omega^2$) was computed and plotted as a function of the coil current, as shown in Fig. 7. 4. The inherent suspension spring constant was found to be approximately -15 dynes/cm.

From Eqs. (7. 6) and (7. 2), the values of the constants in Eq. (7. 1) are

$$\begin{aligned} \alpha &\cong 2.5 \text{ dynes} \\ \beta &\cong 0.5 \text{ dynes/mA} \end{aligned} \qquad (7.8)$$

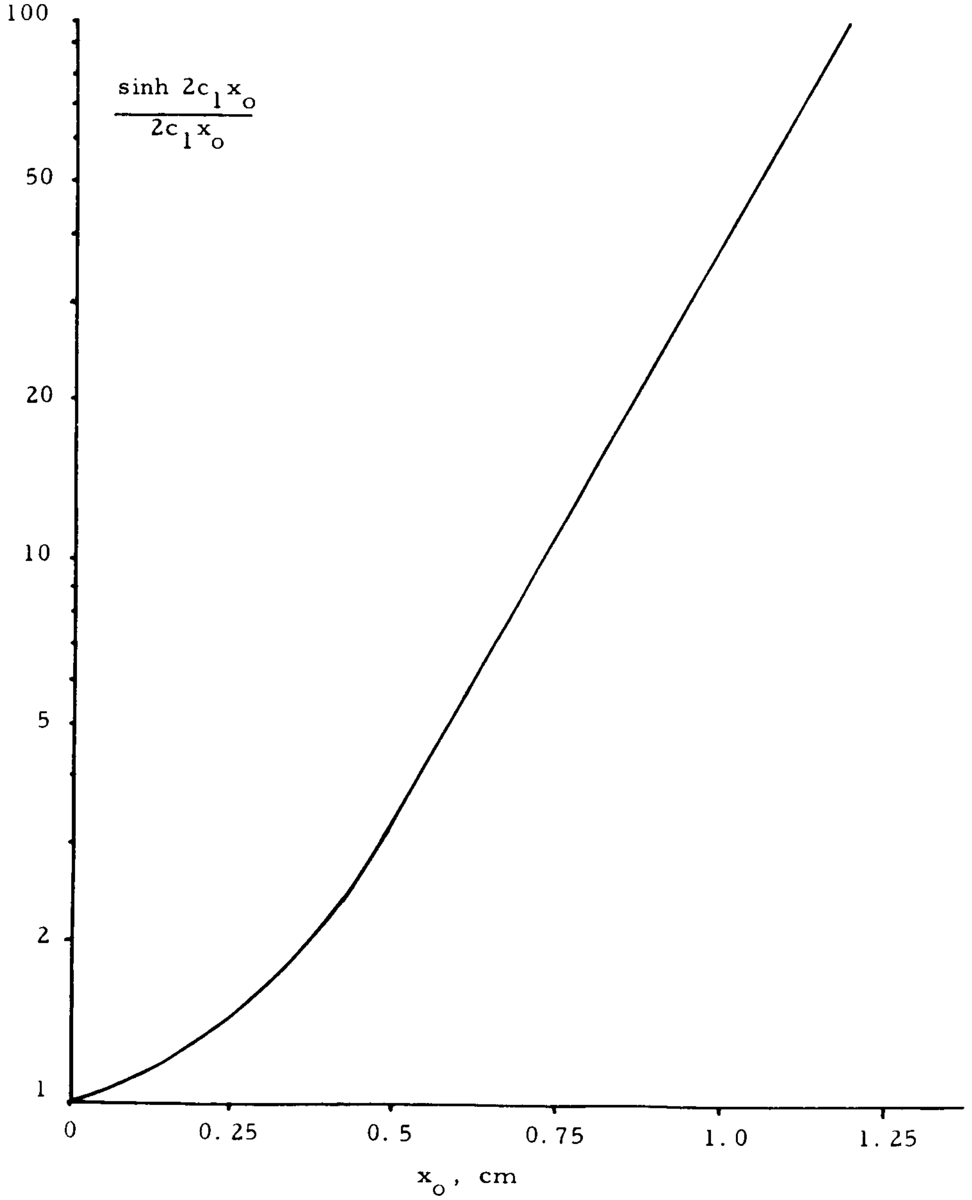

Fig. 7.1 Effect of Oscillation Amplitude on Accuracy of Spring-Constant Measurement

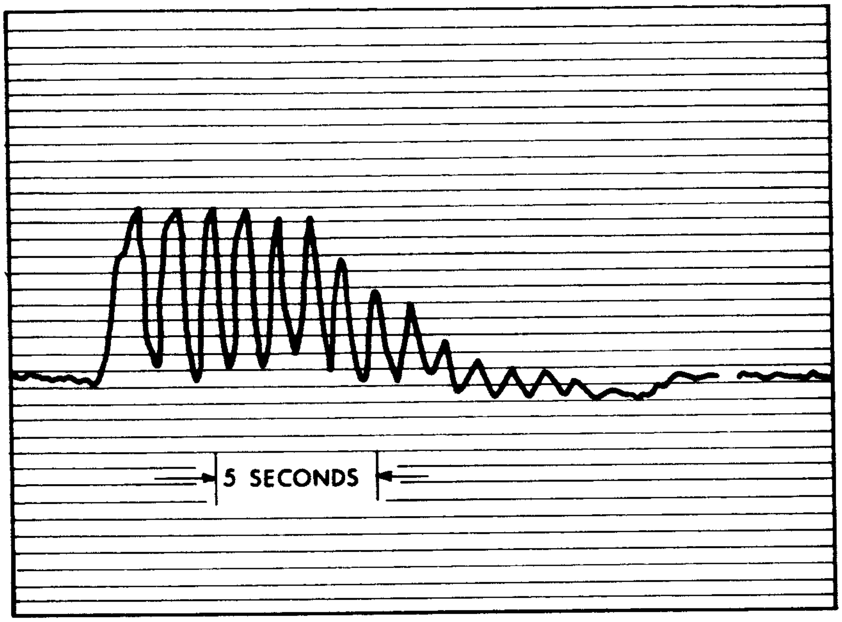

Fig. 7.2 A Typical Test Record

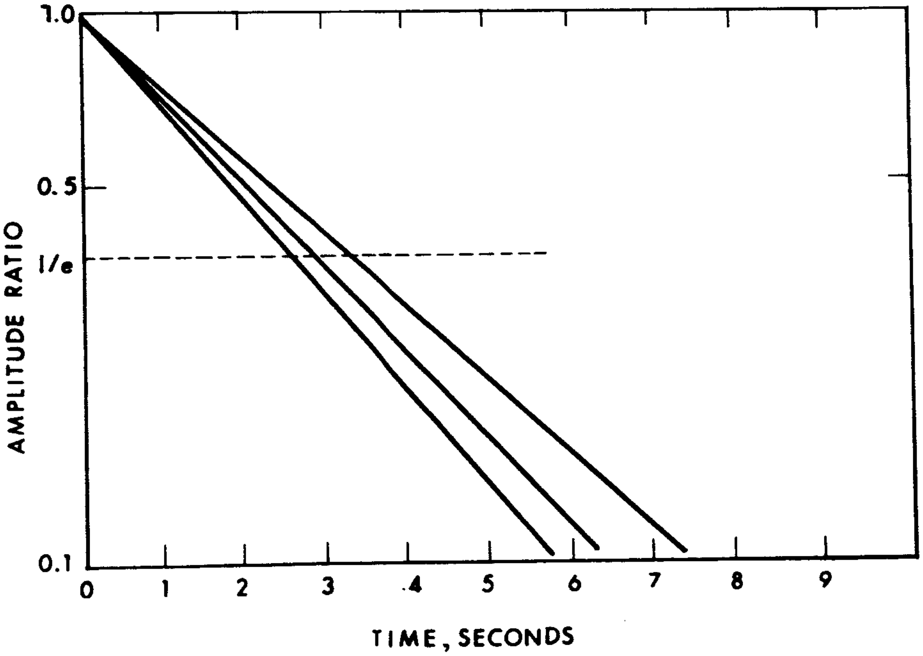

Fig. 7.3 Damping of Axial Oscillation

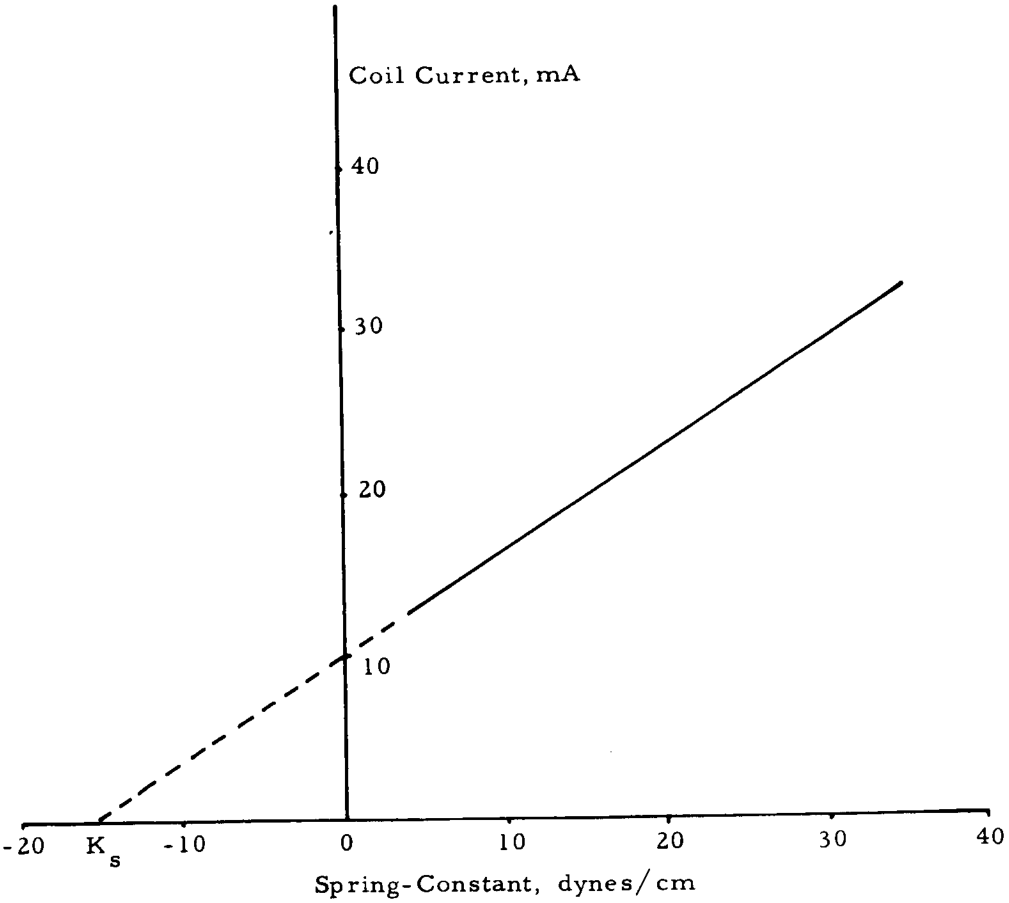

Fig. 7.4 Suspension Axial Spring-Constant vs. Coil Current

Two more simple tests were preformed as an aid in evaluating the suspension. In the first of these, the base of the dewar was suddenly tilted through 12 arc seconds, with a current of 15 mA flowing in the coils. It was found that this produced a very easily observable change in the detector output, as shown in the record of Fig. 7.5. The record was to some extent corrupted by noise due to shaking of the test fixture, but it was estimated that a tilt of 2 arc seconds, corresponding to 10^{-5}g. would be well above the threshold, even without the rest of the LLAMA system.

As a check on this result, the current in one of the coils was increased suddenly, when the magnet was floating near null. From Eq. (A.36), the force on the magnet was due to a step ΔI in one of the coils is $\frac{\beta}{2} \Delta I$: it was found that a change of 0.05 mA was readily observable, corresponding to a force of 0.013 dynes, equivalent to12 x 10^{-6}g. The agreement with the preceding result was surprisingly good.

The results of the tests are tabulated in Table 7.1, for ready reference.

It is also clear that the present suspension incorporates a very useful amount of damping, which should make it a relatively simple matter to close the restoring force feedback loop.

7.4 Interpretation of Test Results

The observed initial spring constant, K_s, is of the same order as that which would be obtained if the magnet were placed in free space between two vertical soft iron plates, separated by the length of the LLAMA suspension. It is considered that the numerical value observed does not have great general significance, as it is undoubtedly greatly affected by the width of the slit along the top of the suspension. However, the observed conditions for stability do lend some support to the belief that the displacement dependence of the axial forces does follow the hyperbolic form derived in the Appendix.

In any case, the end-effect compensation coils performed extremely well, as evidenced by the low acceleration threshold when the suspension was used as an elementary accelerometer. It is quite surprising that the present instrument, which was designed for checking feasibility, not for high performance, should do so well, without any of the other components of LLAMA.

7.5 Closing the Loop

In order to close the loop around the magnet, the output of the displacement detector was fed into a variable gain operational amplifier, see Fig. 7.6. The amplifier output drove a differential transistor stage. The two coils were connected in series across the two collectors of the transistors and the point between the coils was connected to a variable voltage supply.

In the open loop mode, the input to the amplifier was grounded by closing switch S_1 and the input to the differential stage was also zero. The common mode current in the two coils was adjusted by means of the applied voltage at the center position between the coils.

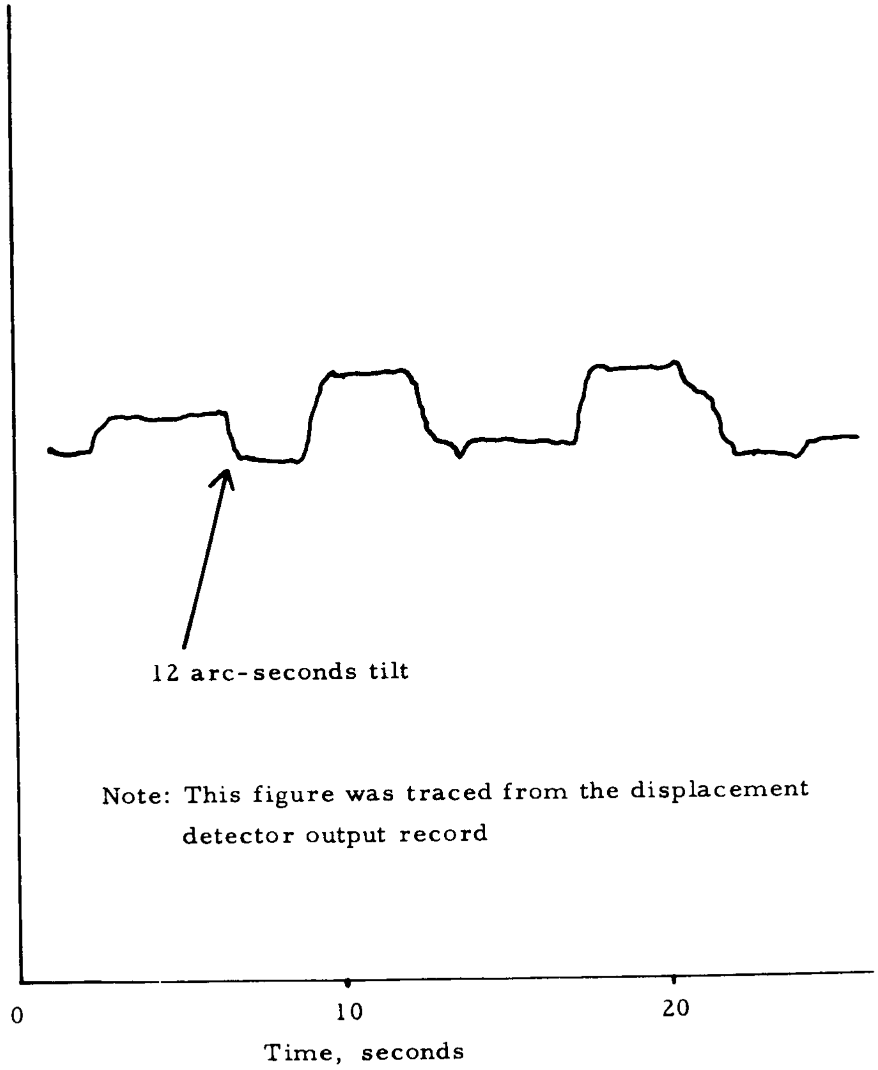

12 arc-seconds tilt

Note: This figure was traced from the displacement detector output record

Fig. 7.5 Response to Steps in Input Acceleration

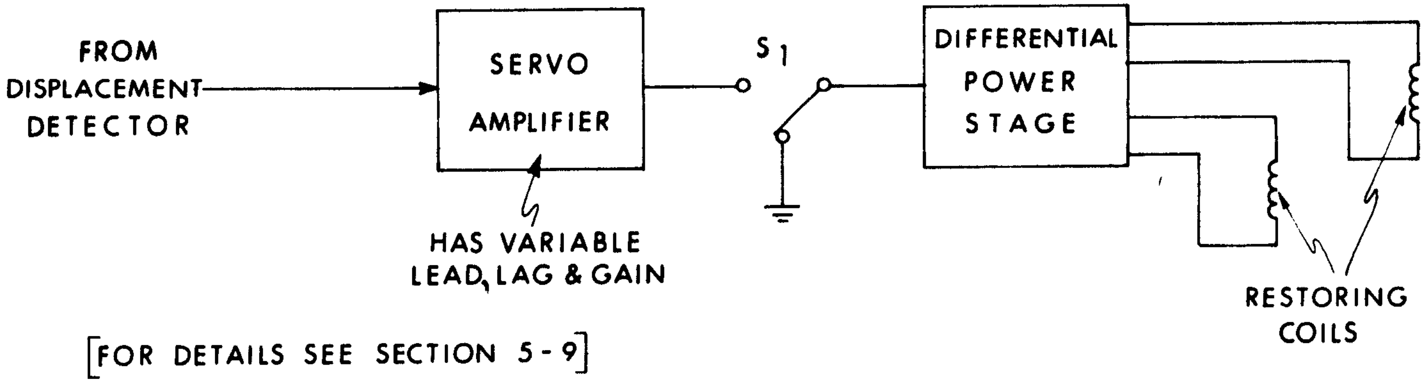

Fig. 7.6 Feedback Loop

In the closed loop mode, switch S_1 was opened so that a displacement detector output would cause a differential current in the coils.

Starting with the same procedure as for Section 7.3, the magnet was brought into the linear range of the detector and the loop was closed.

The output of the displacement detector was monitored on a recorder. The output clearly indicated the presence of a limit cycle shown in Fig. 7.7 due to the limiting property of the detector. Turning the gain down only reduced the frequency of the oscillation.

By applying some lead compensation and adjusting the gain, the oscillation began to damp out, see Fig. 7.8, as was predicted in Chapter IV. However, before the loop was stabilized completely, the magnet was excited into another mode of oscillation--about a horizontal axis normal to the tube, as shown by the sudden appearance of a high frequency oscillation, which will be investigated later in this section. This mode of oscillation was eliminated by the application of a low pass filter in the feedback loop, and the loop was finally stabilized. The magnet was quite stationary, with the usual slight oscillation about the sensitive axis since damping is not provided for this mode in the present suspension.

The application of dewar tilt angles of about 50 seconds of arc gave noticeable change in the detector output but an accurate closed loop response to step acceleration inputs has yet to be determined.

The variation in the frequency of the damped oscillation in Fig. 7.8 may be explained as follows: for small amplitudes, well within the linear range of the displacement detector, the frequency was about 2.5 c/s due to a fairly tight loop with an effective spring constant of 250 dynes/cm. As the amplitude increased, the curvature of the detector output, Fig. 3.11, had the effect of decreasing the net gain in the loop thus decreasing the spring constant and hence the natural frequency.

The excited mode of oscillation was most probably caused by the detector being sensitive to rotations and displacements about other axes, as explained in Section 4.5.

When the improved version of the SODD, Fig. 3.10, was used the loop was closed without any noticeable excitation of other modes of oscillation. The threshold acceleration was below 10^{-6} g, limited by the present test environment.

When the interferometer displacement detector was used with the floating magnet several problems came to light. Because rotation of the magnet about the sensitive axis is very lightly damped, magnet rotation about this axis never quite damped out and any slight inherent misalignment of the principal mirrors on the magnet prevented the interfering spots from overlapping on the screen. Extra care was then taken in attaching the mirrors to the magnet so that they were as concentric as possible with the magnet. Pendulosity effects which caused the oscillations about the sensitive axis were reduced in this way.

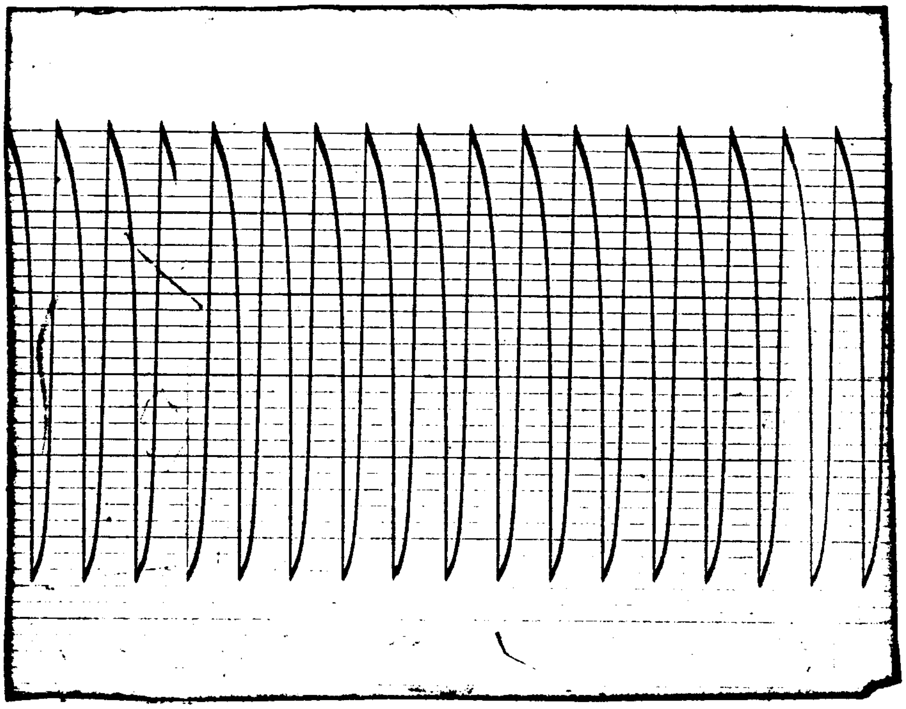

Fig. 7.7 Closed Loop Limit Cycle

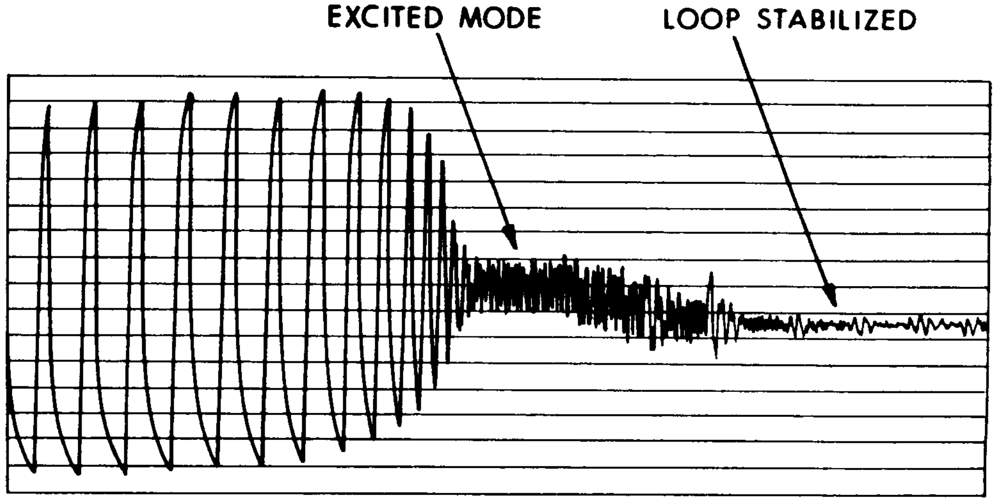

Fig. 7.8 Damping of Closed Loop Oscillation

Ideally, it would be desirable to have the principal mirrors integral with the magnet. Grinding the ends of the magnet flat and parallel to act as mirrors is worth exploring. The pendulosity effect that would remain in this case would be that due to the separation of the center of gravity of the magnet from its magnetic axis.

On several occasions spot overlap of the IDD spots was possible but the interferogram was not stable due to noisy environment. Very quiet conditions are extremely important in the test of a suspension of this kind.

At the present stage of development, LLAMA has shown considerable promise of exceptional sensitivity. There is little doubt that the value of the measured acceleration threshold is determined by the limitations of the displacement detector used and the stability of the test fixture rather than by the suspension itself. It is expected that use of the interferometer and creation of a more stable environment by mounting the instrument on a suitable seismic pier would enable the threshold to be lowered by several orders of magnitude, even without improving the rather primitive arrangement of the superconductor.

Table 7.1: Characteristics of Experimental Suspension

Initial inherent suspension spring constant (K_s)	-15 dynes/cm
Force constant of suspension (α)	2.5 dynes
Force constant of stabilizing coils (β)	0.5 dynes/mA
Natural axial damping time constant	3 seconds
Threshold as an elementary accelerometer	10^{-5} g

CHAPTER VIII

CALIBRATION

8.1 General

As was mentioned earlier, the force generated by the restoring coils cannot be accurately determined. The steady state differential current in the coils, when in closed loop operation, is a measure of the applied acceleration. For the purpose of calibration, an external force of known magnitude is exerted on the magnet and the corresponding differential current recorded. This can be repeated for other magnitudes of the force to obtain a calibration curve.

Since the mass of the magnet is 1 gram, an external force of 10^{-3} dynes corresponds to an acceleration of 10^{-6}g.

Considering the methods of generating small forces outlined in Ref. 22, and keeping in mind that the range of interest extends below 10^{-6}g, the photon force provides a feasible solution.

Possible methods for generating a suitable photon force for LLAMA application are examined in the following sections.

8.2 Requirements for Application of Photon Force

The force F available from electro-magnetic radiation is given by(22)

$$F = \frac{EA\,(1+r)\cos^2\theta \times 10^7}{c}$$

F = force exerted by beam of light in dynes.

E = power in incident beam in watts.

c = velocity of light = 3×10^{10} cm/sec.

r = reflectivity of surface on which the beam is incident.

θ = angle of incidence of beam on surface.

A = area of surface in cm^2

The magnitude of this force is 0.66×10^{-3} dynes if the energy in the beam is 1 watt falling normally on a perfectly reflecting surface.

Several requirements have to be met for the application of photon force.

(a) The available surface area dictates the power density in the beam. In LLAMA, because of float height limitation in the present setup, the available surface is a disc 1 cm in diameter or an area of 0.78 cm^2. The area of the largest square incribed in the disc is 0.51 cm^2. To generate low forces is simple. To generate 10^{-3} dynes requires 1.5 watts, (see Section 3.3.1 of Ref. 22) for a perfectly reflecting surface and the power density is 2-3 watts/cm^2 depending on the cross-section of the beam. Possible sources are discussed in Section 8.3.

(b) A high vacuum below 10^{-5} torr must prevail to avoid thermal effects, (see Section 2.3.3 of Ref. 22). The vacuum surrounding the liquid helium inner bottle is excellent since after a short period of time only helium gas can exist in this region, since all other gases liquify due to the cryopumping action of the liquid helium. To ensure the absence of helium gas, the enclosure can be flushed with, say nitrogen. However, in the present system, air which is rich in helium due to the evaporation of liquid helium from the inner bottle, can leak in from outside via the "O" ring feed throughs and a helium atmosphere can build up. If found necessary, a low pressure pump can be permanently incorporated so as to keep the vacuum as low as desired.

(c) The surface must have a high work function so as to reduce the generation of photo-electronics (see Section 3.3.2. of Ref. 22).

(d) The surface must have high reflectivity to maximize the force and minimize heat absorption.

8.3 Criterion for Choice of Source

A good source of photons is a light source. Sources of light vary in brightness, size of source, spectral distribution of the radiated energy, the direction of the radiation and so on.

In the case of LLAMA, the photon beam not only has to be squeezed on to an area less than 1 cm^2, but also has to meet a beam angle requirement imposed by the geometry of the suspension.

In order to develop a criterion by which various sources may be judged, a simple optical configuration is assumed, (see Fig. 8.1) where

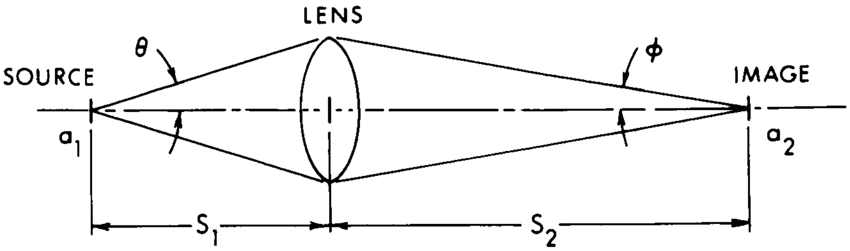

Fig. 8.1 Optical Configuration for Comparison of Sources

a_1 = projected area of source normal to optical axis

a_2 = projected area of image normal to optical axis

θ = angular semi-aperture of lens from source

ϕ = angular semi-aperture of lens from image

s_1 = distance of source from lens

s_2 = distance of image from lens

Assuming the source emits equally in all directions, i. e., a Lambert's Law radiator, the flux collected by an elemental ring at the lens is given by

$$\delta F = B_1 a_1 \cos \psi \, \delta\omega$$

where

B_1 = brightness of source

F = flux collected by lens

ψ = angle subtended by ring

$\delta\omega$ = solid angle subtended by ring

r = distance of any element of ring from source

and

$$\delta\omega = \frac{2\pi r \sin \psi \, r \, \delta\psi}{r^2}$$

The total flux collected by the lens is

$$F = 2\pi B_1 a_1 \int_0^{\theta} \sin\psi \cos\psi \, d\psi$$

$$= \pi B_1 a_1 \sin^2 \theta$$

Now substituting for $\sin\theta$ and noting that $\frac{a_2}{a_1} = \frac{s_2^2}{s_1^2}$

$$F = \pi B_1 a_1 \frac{\tan^2 \phi}{\frac{a_1}{a_2} + \tan^2 \phi} \tag{8.1}$$

The flux collected by the image is FT where T is the transmission factor of the lens, provided the image is smaller or equal to the available image area.

For a given ϕ, Eq. (8.1) shows that F is increased if the product $B_1 a_1$ is maximized and $\frac{a_1}{a_2} = \frac{1}{(\text{magnification})^2}$ is minimized.

For a given lens, there is a definite limit on the magnification for each value of ϕ. Fig. 8.2 shows the magnification for different values of ϕ for an f/1 lens. Another limit on the magnification is the size of the target area.

Using Eq. (8.1), the limitation on magnification from Fig. 8.2, and assuming a target area of 0.25 cm^2, three promising sources were compared. All three were high pressure mercury arc lamps and their characteristics are given in Table 8.1:

Source	Power Watts	Source Dimensions mm	Brightness $cdls/cm^2$
I	100	0.25 x 0.25	170,000
II	200	0.6 x 2.2	33,000
III	500	1.1 x 4.1	30,000

Table 8.1

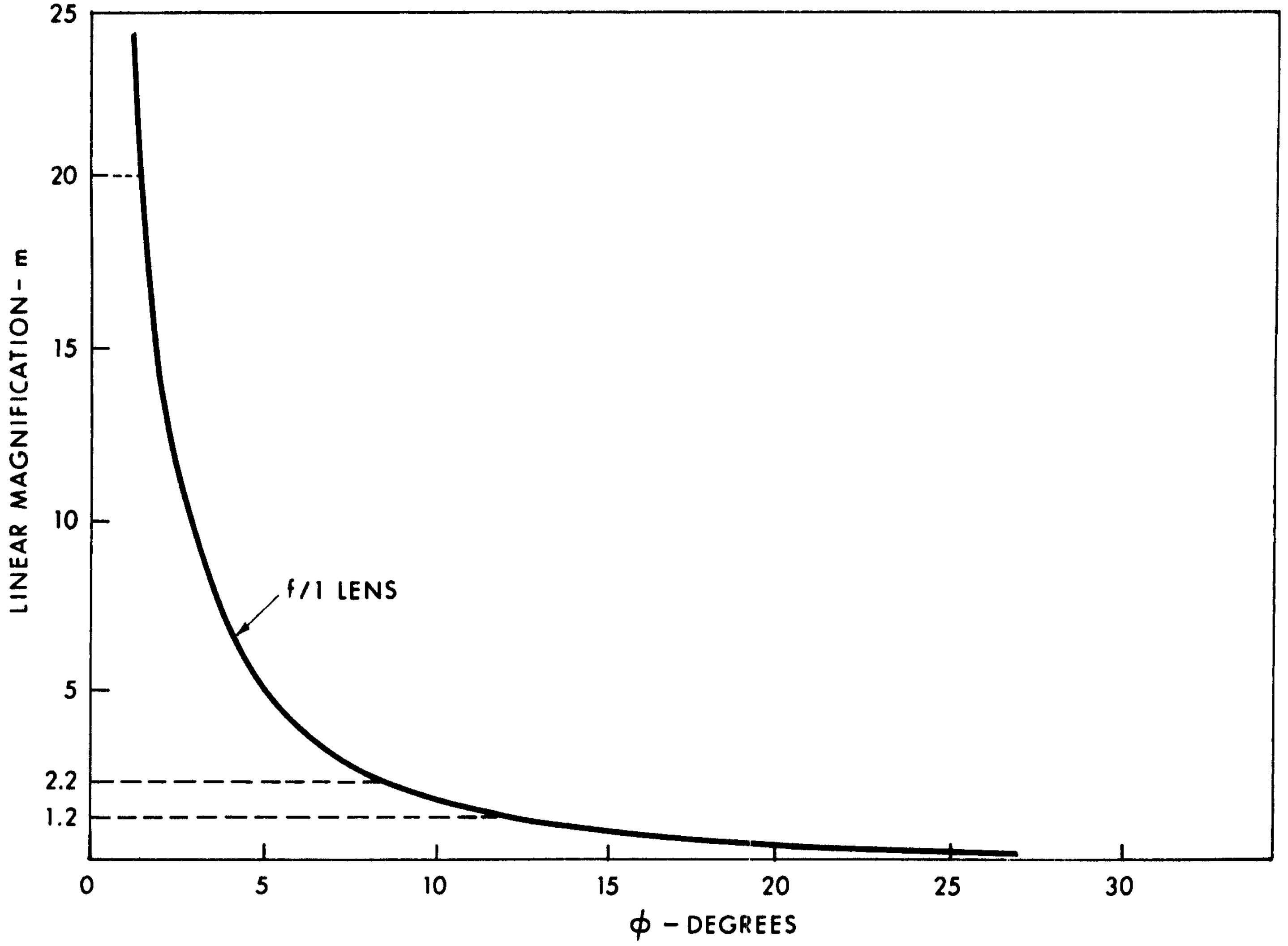

Fig. 8.2 Magnification Against ϕ

Fig. 8.3 shows a plot of the flux collected by an f/1 lens (in arbitrary units) against ϕ for the three sources.

With a 5 cm diameter f/1 lens, the LLAMA geometry dictates a ϕ less than 6°. Fig. 8.3 shows that the 100 watt lamp collects the most flux in the region where ϕ is below 6 degrees.

8.4 Force Available From 100 Watt Arc Lamp

The optical configuration for the measurement of the power from the 100 watt arc lamp is shown in Fig. 8.4. The lamp was an Osram HB0-109 mercury arc lamp.

The radiation from the lamp was collected by an f/1 lens and focussed on a thermopile 20 cm away after attenuation by a neutral density filter. The back radiation was made use of by placing a spherical reflector with the source at its center of curvature. The image size was less than 0.25 cm^2 and the measured power was 3.5 watts. (This takes into account the attenutation of the filter.)

The lens used was uncoated and made from ordinary lens glass. A coated quartz lens would have increased the power by reducing the reflection at the lens, and the ultra violet absorption by the lens. The line spectra of the lamp extended to below 2900 Å.

To increase the power even more, a good quality aluminized elliptical reflector with an equivalent speed of f/ $\frac{1}{2}$ can be used with the lamp at one focus and the target at the other focus.

Already the measured power of 3.5 watts is equivalent to more than 2×10^{-3} dynes.

A UV source is preferred so as to minimize the heating effect inside the cryogenic environment to conserve the helium.

Another advantage for using a UV source is its compatability with the 6328 Å wavelength of the helium-neon laser that is proposed for use in the interferometer. The filtering problem is eased when the wavelengths of the sources are widely separated.

Other sources that can give a slightly higher power density in a beam angle of less than 6° are available in the form of high intensity carbon arc lamps that consume around 14,000 watts.

8.5 Measurement of Photon Force

By measuring the power in a photon beam, the force it can exert can be calculated from Eq. (8.1).

The ideal detector is one that has a flat response for all wavelengths in the beam, a high signal to noise ratio and a short time constant.

Quantum detectors such as photo-electric, photo-conducting and photo-voltaic cells where the incident photons change the detector characteristic directly

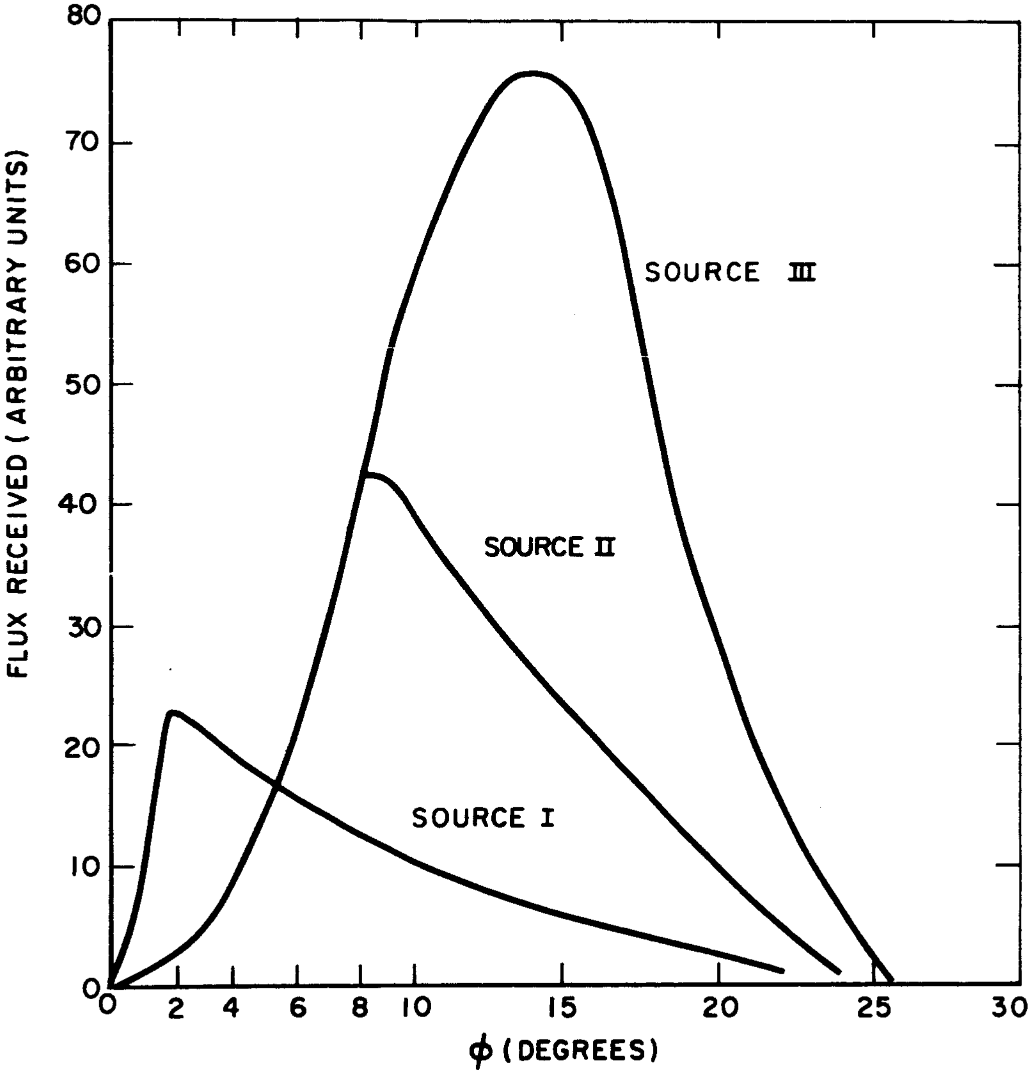

Fig. 8.3 Flux Received Against ϕ

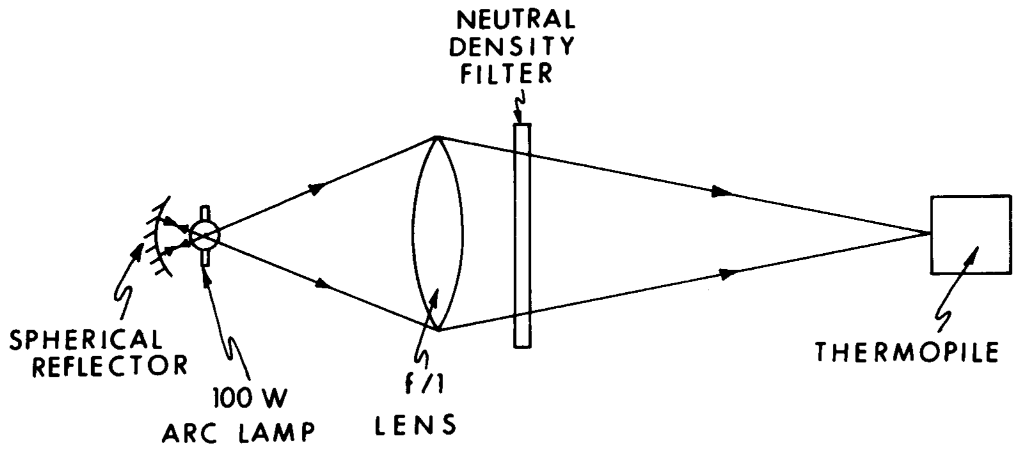

Fig. 8.4 Configuration for Measurement of Power From 100W Lamp

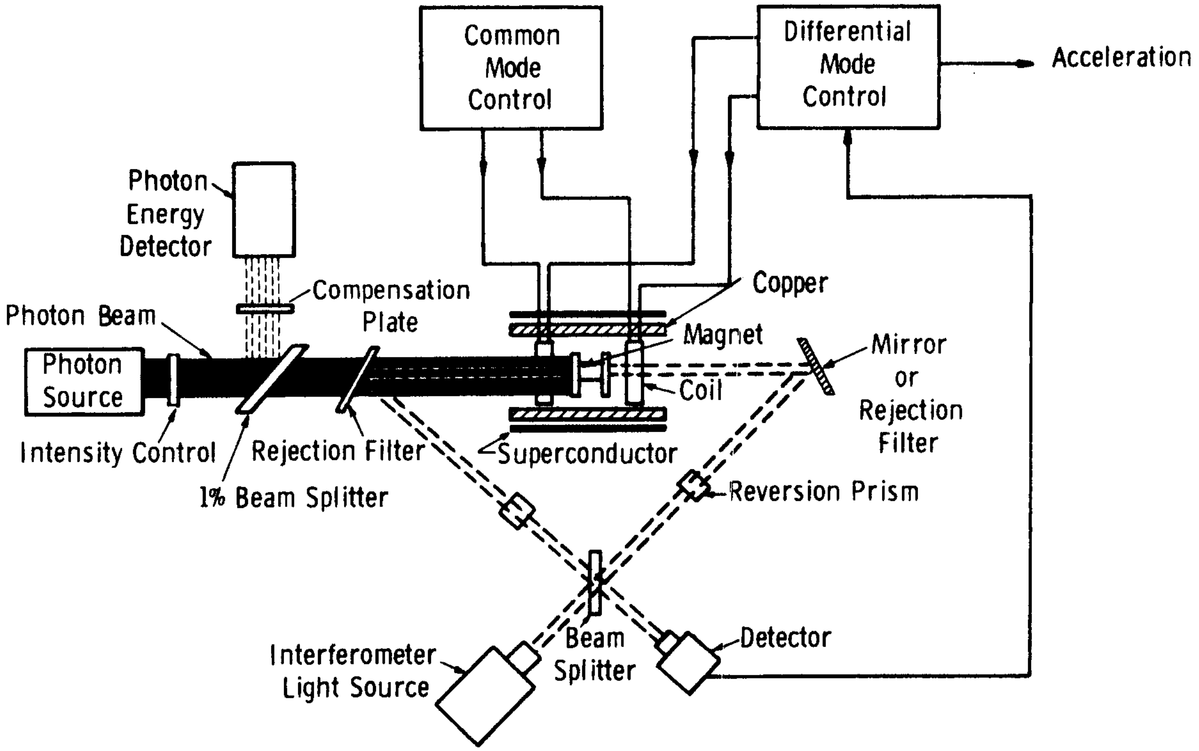

Fig. 8.5 The LLAMA System

exhibit different sensitivities for different wavelengths. This property is undesirable unless the beam is monochromatic.

Thermal detectors, such as a thermopile, absorb the radiation in a black surface and detect the temperature rise in the surface by the Peltier Effect. A surface such as lamp black absorbs equally over a wide range. One disadvantage with thermal detectors is the inherent time constant of the order of a second which can become troublesome when the beam is modulated. The noise level is neglibile since the signal is high.

8.6 Modulation of Photon Force

The search for a simple nonmechanical method for the control of the intensity of a photon beam is intense.

Electro optical techniques, however, do exist using the Kerr cell(26) or the Pockels effect where the light is first polarized by a 0° polarizer, passes through $0^\circ \rightarrow 90^\circ$ variable polarizer and finally through a 90° polarizer. By varying the angle of the polarization(27) in the middle polarizer, the intensity of the beam can be modulated. The maximum transmission is about 25%.

Mechanical shutters are numerous and can be used either as aperture controllers or as choppers. A suitable method for generating pulses of varying widths from a constant beam can be achieved using a stepping motor.(28)

Sources such as flash tubes can be easily controlled by varying the flash rate but the average power output for a period time is below 1 watt with present devices.

The application of lasers is discussed in the next section.

8.7 Laser Application

Injection lasers are ideal for the generation of photon force. The beam is narrow, intense and can be electronically modulated. The radiation need not be highly monochromatic or coherent for this application.

Present injection lasers have reached an output power of 3 watts(29) continuous--but these devices are still in the experimental stage.

The cryogenic cooling that is required for the lasers presents no problem in this case since liquid helium and nitrogen are already available for the suspension.

Presently, molecular gas lasers such as the N_2-CO_2 laser(30) are generating powers of the order of tens of watts (cw) and promise even more. So far, molecular gas laser frequencies are in the far infrared and great care would have to be taken not to introduce excessive heat input into the dewar.

8.8 Possible Calibration Method

To generate a low level force of 10^{-3} dynes and less of known magnitude is one problem, to use this force for calibration on earth is another problem.

Assuming ideal conditions where the outside interference is negligible during the time needed for calibration, a possible method is shown in Fig. 8.5.

The photon beam is directed at an aluminum deposited disc attached at one end of the magnet. A well-calibrated beam splitter deflects 1% of the beam onto a thermopile. This deflected beam is made to pass through identical windows, rejection filters, and so on as those in the main beam for compensation. The intensity of the beam can be varied by neutral density filters and the differential current required to keep the magnet at null is recorded so as to obtain a calibration curve. If the differential current is too small, the number of turns in the coils can be reduced.

If the isolation is not ideal, an alternating force can be applied by chopping the photon beam. The frequency has to be chosen so that it can be easily filtered out. The choice of frequency depends on the statistical behavior of the interference for the particular environment selected and on the bandwidth of the accelerometer. A survey of various disturbances and a means for building an isolation platform is given in Ref. (31).

CHAPTER IX

FUTURE DEVELOPMENTS OF THE LLAMA SYSTEM

9.1 Ultimate Limits of Performance

The most significant feature of the LLAMA suspension is that there is no mechanism present which might cause "stiction". The threshold sensitivity which might conceivably be attained is therefore limited by other factors, such as the sensitivity of the displacement detector and the geometric perfection of the superconducting surface.

One possible limiting factor is thermal fluctuation of the test-mass position (i.e., Brownian motion of the test-mass). If the threshold sensitivity of the displacement detector is x_o cm, and it is required to detect an acceleration of a_o cm/sec^2, then it is clear that the maximum spring constant of the accelerometer (whether it be generated by feedback or by open-loop forces) is given by

$$K = \frac{ma_o}{x_o} \qquad (9.1)$$

The mean amplitude x_n of Brownian oscillation of the test-mass is then given by the equipartition theorem as

$$\frac{ma_o x_n^2}{2x_o} = \frac{kT}{2} \qquad (9.2)$$

where k is Boltzmann's constant, 1.38×10^{-16} ergs/degree, and T is the absolute temperature.

Assuming that measurement is possible when the amplitude of the Brownian oscillation is one half the displacement threshold, the acceleration threshold is given by

$$a_o = \frac{4kT}{mx_o} \qquad (9.3)$$

The implication of this equation is that this limit is minimised by allowing a large x_o; but unfortunately the natural period τ, and hence the settling time of the instrument, is proportional to $\sqrt{x_o}$. The limitation is therefore likely to be the patience of the observer (or perhaps the supply of helium!). Putting x_o = 1 micron and $T = 10^{\circ}$ in (9.3) gives

$$a_o = 5 \times 10^{-12} \text{ cm/sec}^2 \tag{9.4a}$$

$$\tau = 8 \text{ hours} \tag{9.4b}$$

From (9.1),

$$\tau = 2\pi \sqrt{\left(\frac{x_o}{a_o}\right)} \tag{9.5}$$

so that (9.3) may be written

$$a_o = \frac{2\pi}{\tau} \sqrt{\left(\frac{4kT}{m}\right)} \tag{9.6}$$

Thus the acceleration threshold imposed by thermal fluctuation varies inversely as the allowable natural period. Increasing x_o to 1 mm would improve the value of a_o given in (9.4a) by a factor of one thousand, but it would also increase the natural period to about one year. For most cases, then, 10^{-12} cm/sec^2 may be taken as a practical limit on the sensitivity.

Another possible limit is imposed by thermal fluctuation of the current in the restoring coils, which is given by

$$\Delta I = \sqrt{\left(\frac{4kTB}{R}\right)} \tag{9.7}$$

where R is the output resistance of the current supply, and T is now room temperature. Because of (9.6) there is no point in having a large value of the bandwidth B.

For small displacements, the corresponding change in the spring constant is given by (2.6) as

$$\Delta K = c_1 \beta \Delta I \tag{9.8}$$

in the experimental suspension, $c_1\beta = 1.5$ dynes/cm/mA (see Section 7.3). Taking as an example $B = 0.001$ c/s, $R = 10\text{k}\,\Omega$, Eqs. (9.7) and (9.8) give for this case

$$\Delta K = 2.10^{-7} \text{ dynes/cm} \tag{9.9}$$

For comparison, the spring constant in the Brownian motion limited case of (9.4) is given by (9.1) as

$$K = 5.10^{-8} \text{ dynes/cm} \tag{9.10}$$

It should not be difficult to decrease ΔK by two orders of magnitude, by increasing R and decreasing β (according to (A.37) of the Appendix, β decreases exponentially with separation of the coils). The conclusion is therefore that thermal fluctuation of the spring constant imposes a sensitivity limit which is of the same order as that imposed by the Brownian motion effect.

The limitation imposed by distortion of the superconductor is not expected to be significant at the above levels. Large scale distortion (buckling) simply modifies the inherent spring constant of the suspension, at least for small displacements, and hence may be compensated by adjusting the current in the stabilizing coils. Surface roughness is averaged over a distance of the order of the float height, so that, again for small displacements, it too is seen simply as a variation of the spring constant. If the surface finish is held to (say) 5 microinches, these effects should be negligible.

Finally, the experimental suspension is grossly overdamped for operation at the levels considered in this section. This is due to eddy current generation in a copper liner inside the superconducting tube. In the ideal case of a magnet floating inside a superconducting tube, with no other metal present, the only damping would be due to eddy current generation in the metal of the magnet itself, since eddy currents in a superconductor can dissipate no energy. The resistivity of Alnico V is 2500 times that of copper, so that it is expected that a suspension of this type would not be limited by damping at the levels considered.

In view of the above results, it is clear that the ultimate limit on sensivity, at least in a terrestrial installation, will be due to external vibration, microseisms, etc. It is only in a space application that LLAMA will ever be able to approach its maximum performance potential.

In this discussion of limits on performance, it has been assumed that the only variation of the currents in the coils is due to thermal noise. If end effect compensation requires a current which is large compared to the position control (restoring force) currents, it may be impossible to regulate the current sufficiently for this to be so. This is not regarded as a fundamental limitation, however, since it is possible to reduce the required stabilizing currents to an arbitrarily low level, by increasing the length of the suspension or by one of the end effect compensation schemes discussed in Section 9.2.

9.2 Suspension Modification for Improved Performance

The test mass suspension discussed in this report was intended only to demonstrate the feasibility of the LLAMA concept, and does not approach the theoretical performance limits presented in the previous section. There are a number of modifications which could be made to the system, which would be expected to decrease susbstantially the measurement threshold of the accelerometer.

In the first place, the measured value of the (negative) axial spring constant of the suspension alone (i. e., without end effect compensation) is considerably higher than the theoretical analysis presented in the Appendix would lead one to expect. The reason for this is almost certainly buckling of the niobium sheet used to form the superconducting tube. In order to overcome this problem, it is suggested that a suspension be constructed in which niobium is plated or vacuum-deposited on the outside of a finely-lapped copper tube. This technique would allow much tighter control of distortion of the superconducting surface, and would also, if desired, allow a non-developable surface to be employed. This latter possibility may be of interest in connection with one of the end effect compensation schemes mentioned below.

The following methods of reducing the end effects encountered in the experimental suspension seemworthyof further study: i) At the present time, the superconducting surface is singly-connected, which is achieved by leaving a narrow gap along the top of the niobium tube. It is possible that performance could be improved by using a multiply-connected surface. For example, if narrow bridges of superconductor were placed across the top slit at either end of the tube, the total fluxes through the slit and through the ends of the tube would be held constant at the values which existed at the time of transition of the superconductor. The effect expected is a repulsion of the floating magnet from the ends of the tube, with a consequent decrease in the negative spring constant. A variant of this idea is the use of superconducting guard rings at each end of the tube, insulated from the superconducting suspension proper. ii) If the outside of a copper tube were turned to a slightly bulbous shape and then plated with niobium, it would be possible, at least in principle, to produce a suspension with a "flat" region over a considerable axial distance near the center. Determination of the optimum shape would require and extensive study of the perturbed field equations, together with appropriate experimentation, but this technique might allow the elimination of other forms of end effect compensation altogether.

As a general rule, it is preferable to vary the geometry of the superconducting surface in order to control end effects, instead of using the coils in the present apparatus. The primary reason for this is that the force on the magnet due to an adjacent superconductor is proportional to the square of the magnetic field, whereas the force from a current-carrying coil is simply proportional to the field. The former technique therefore allows matching of the compensation to the end effect over a larger region. In addition, of course, Joule dissipation in a compensation coil adds to the rate of loss of helium from the dewar.

Finally, it is recognized that the cryogenic requirements of the LLAMA suspension, which are acceptable in the laboratory environment, would cause considerable difficulty in deploying the system for any length of time on a space mission, where many of the most interesting applications of low-level accelerometry occur. Fortunately, the support forces required in space are generally much lower than in the terrestrial case, so that a suspension using other diamagentic materials than superconductors may be feasible. In particular, a thick-walled bismuth tube, of the same internal diameter as the present suspension, would support the LLAMA test mass in a transverse field of at least 10^{-4}g. This figure could be improved by using a smaller diameter tube and a more powerful magnet, such as a platimum-cobalt alloy rather than Alnico V.

9.3 Sensitive Displacement Detection

So far the LLAMA system has been limited by the external environment and the spot occultation displacement detector has been adequate for preliminary evaluation. Interferometeric measurements of displacement, although verified using a test mass simulator, performed poorly when using the floating magnet because of the noisy environment.

In order to appreciate the capability of the LLAMA system an elaborate quiet test facility must be set up. With path length modulation, interferometric techniques can be used to measure displacements down to 10^{-3} -10^{-5} fringe.

More exotic schemes may utilize frequency rather than the phase measurements used in interferometry. For example, each end mirror on the floating magnet can be made a part of a Fabry-Perot cavity with an active laser medium shown in Fig. 9.1. If the two lasers are operated in a single longitudinal mode then displacement of the magnet would cause the frequency of one laser to increase and the other to decrease. The beat frequency gives a measure of the displacement. A 1 kc/s change in the beat frequency corresponds to a displacement of 10^{-7} microns for a laser in the visible with a cavity length of 10 cm.

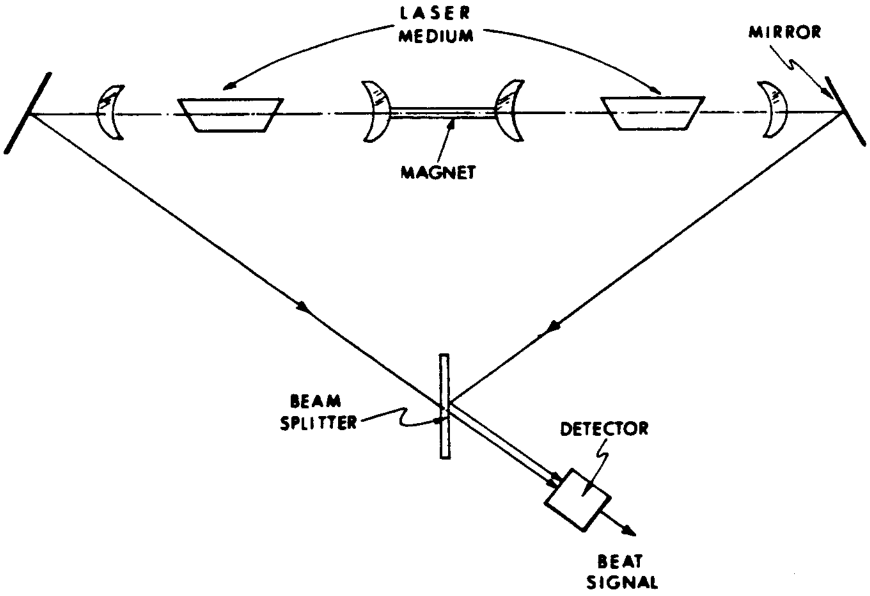

Fig. 9.1 Exotic Scheme for Displacement Measurement

$$\frac{1}{r}\frac{d}{dr}\left(r\frac{dR}{dr}\right) + k^2 R = 0 \qquad \text{(A. 4a)}$$

and

$$\frac{d^2Z}{dz^2} - k^2 Z = 0 \qquad \text{(A. 4b)}$$

are obtained, where k^2 is the separation constant.

Eq. (A. 4a) is a Bessel equation, and (A. 4b) gives trigonometric or hyperbolic solutions, depending on whether k is imaginary or real. In order to specify the solutions further, it is necessary to consider the boundary conditions.

At the superconducting surface, because the magnetic field cannot penetrate and because there are no magnetic poles there, the normal component of the field is

$$H_r = -\frac{\partial\Omega}{\partial r} = 0 \qquad \text{(A. 5)}$$

so that homogeneous Neumann boundary conditions obtain on the curved surface of the cylinder.

As the tube is of infinite length, the boundary condition at the ends is of course that Ω be zero there.

Strictly speaking, the source of the field is the magnetostatic potential distribution over the surface of the magnet. Eq. (A. 1) should be solved by finding the Green's function corresponding to a source point $\underline{r}_o$ on the surface of the magnet, weighting this with the potential distribution, and integrating in the source coordinates over the magnet. However, since the diameter of the magnet is very much less than the diameter of the tube, an adequate approximation is obtained if the magnet be idealized so that it consists of a pair of poles, of strength $\pm p$ at $(0,0,\pm d)$. The Green's function is then a solution of

$$\nabla^2 G = -4\pi\delta \qquad \text{(A. 6)}$$

where δ is a "volume" delta function at one of the poles (i. e., the volume integral of δ is unity). Note that Gaussian units are employed in this equation.

The choice of a form for the trial solution of this equation is guided by the following considerations:

i) As z has an infinite range, and since Ω is continuous and has a finite mean value, a Fourier integral representation of the z-dependence is appropriate.

ii) Because of the radial symmetry, only zero-order cylindrical harmonics are required. In addition, since Ω must be finite on the z-axis, only Bessel

APPENDIX

THE FIELD INSIDE THE LLAMA SUSPENSION

A. 1 Introduction

The purpose of this Appendix is to derive expressions for the field inside several mathematical models which represent in some sense the LLAMA Meissner effect test-mass suspension. Because of the rather highly idealized nature of the models used, the results can be applied to the present suspension only with considerable caution. However, they are useful in the discussion of ultimate performance limitations in Chapter IX and again in the interpretation of the test results in Chapter VII.

A. 2 A Suspension of Infinite Length

The simplest case to be considered is that of a magnet which is stationary on the axis of a superconducting cylinder of infinite length (the steady-state case in free fall). The effects of the slit along the top of the suspension are ignored.

In this static situation, the magnetic field $\underline{H}$ may be set equal to the negative gradient of a scalar potential Ω. For the region internal to the tube but external to the magnet, Ω is a solution of Laplace's equation.

$$\nabla^2 \Omega = 0 \tag{A. 1}$$

subject to the applicable boundary conditions.

Set up a circular cylindrical coordinate system r, θ, z with the z-axis along the axis of the cylinder. Since by symmetry there is no variation of Ω with θ, the above equation becomes

$$\frac{1}{r}\frac{\partial}{\partial r}\left(r\frac{\partial \Omega}{\partial r}\right) + \frac{\partial^2 \Omega}{\partial z^2} = 0 \tag{A. 2}$$

which may be solved by the standard separation of variables technique. Putting

$$\Omega = R(r)\ Z(z) \tag{A. 3}$$

the pair of equations

functions of the first kind will appear.

The trial solution is therefore

$$G = \sum_s J_o(c_s r) \int_{-\infty}^{\infty} A_s(k)\ e^{-jkz}\, dk \qquad \text{(A. 7)}$$

where, if a is the radius of the tube, $c_s a$ is the s^{th} root of the equation

$$\frac{d}{d\lambda} J_o(\lambda) = 0 \qquad \text{(A. 8)}$$

thus satisfying the required Neumann conditions at the superconductor.

Inserting (A. 7) in (A. 6) and carrying out the indicated differentiation gives

$$\sum_s J_o(c_s r) \int_{-\infty}^{\infty} (k^2 + c_s^2)\, A_s(k)\, e^{-jkz}\, dk = 4\pi\,\delta \qquad \text{(A. 9)}$$

which may be solved for $A_s(k)$ by making use of the properties of the Fourier transform and the orthogonality of the Bessel functions. Multiplying both sides of (A. 9) by $J_o(c_s r)\ e^{jkz}$ and integrating over the volume of the cylinder gives the result

$$2\pi^2 a^2 J_o^2(c_s a)\ (k^2 + c_s^2)\ A_s(k) = 4\pi\ e^{jkd} \qquad \text{(A. 10)}$$

where the delta function has been taken at the positive pole. Eq.(A. 7) then gives

$$G = \frac{2}{\pi a^2} \sum_s \frac{J_o(c_s r)}{J_o^2(c_s a)} \int_{-\infty}^{\infty} \frac{e^{-jk(z-d)}}{(k^2 + c_s^2)}\, dk \qquad \text{(A. 11)}$$

The integral is readily evaluated as $\frac{\pi}{c_s} \exp(-c_s|z-d|)$.

Thus

$$G = \frac{2}{a} \sum_s \frac{J_o(c_s r)}{c_s a J_o^2(c_s a)} \exp(-c_s|z-d|) \qquad \text{(A. 12)}$$

The potential Ω is obtained by summation of the Green's functions corresponding to the two poles, weighted by the pole strengths. Thus

$$\Omega = \pm \frac{4p}{a} \sum_{s=1}^{\infty} \frac{J_o(c_s r)}{c_s a J_o^2(c_s a)} e^{-c_s |z|} \sinh c_s d \tag{A. 13}$$

for $z > d$, where the postive sign is to be used when the nearest pole is positive, and conversely.

A. 3 A Finite-Length Case

The purpose here is to find the way in which the potential distribution of Eq. (A. 13) is modified when the tube is of finite length, and hence to develop an approximate expression for the axial force on the test-mass due to end effects.

In order to solve Laplace's equation for this case, it is of course necessary to assign definite boundary conditions at the ends of the tube. If homogeneous Neumann conditions are chosen (e. g., plane superconducting ends) a configuration results which is clearly stable with respect to all displacements of the test-mass from the center. Conversely, homogeneous Dirichlet conditions (e. g., plane high permeability ends connected by an external low-reluctance path) produce an axially unstable situation.

The actual end boundary conditions lie somewhere between these extremes, but their precise nature is unknown. Since the real suspension is unstable, but the best approximation available is that of a tube with Dirichlet ends. This is not too unreasonable, because the lines of force are parallel to the axis of the tube at the superconducting surface and close to the axis, so that the field emerging from the ends should be largely perpendicular to the ends, as required by Dirichlet conditions.

Since the forces due to end effects are not expected to depend very strongly on the precise height at which the magnet is floating, it is again assumed to be on the axis of the tube.

A circular cylindrical coordinate system r, θ, z is set up, with the origin at the center of the tube. The magnet is again idealized so that it consists of a pair of poles of strengh $\pm p$, located at $(0, 0, x+d)$, where x is the axial displacement of the center of the magnet.

The development is similar to that in the preceding section except that a Fourier series, rather than integral, representation of the z-dependence is now appropriate. The trial solution of (A. 6) is therefore now taken as

$$G = \sum_{k, s} A_{ks} J_o(c_s r) \sin\left(\frac{k\pi}{2L}(z+L)\right) \tag{A. 14}$$

which goes to zero at z = ± L, the ends of the tube, and satisfies homogeneous Neumann conditions at the curved surface.

Inserting this expression in (A. 6) gives the result

$$\sum_{k,\,s}\left[\left(\frac{k\pi}{2L}\right)^2 + c_s^2\right] A_{ks}\, J_o(c_s r)\, \sin\left[\frac{k\pi}{2L}(z+L)\right] = 4\pi\,\delta \qquad \text{(A. 15)}$$

This equation is now multiplied by $J_o(c_s r)\, \sin\left[\frac{k\pi}{2L}(z+L)\right]$ and integrated over the volume of the cylinder, to obtain

$$\pi L a^2 J_o^2(c_s a)\left[\left(\frac{k\pi}{2L}\right)^2 + c_s^2\right] A_{ks} = 4\pi \sin\left[\frac{k\pi}{2L}(x+d+L)\right] \qquad \text{(A. 16)}$$

where the delta function has been taken at the positive pole. Then

$$G = \frac{4}{La^2}\sum_s \frac{J_o(c_s r)}{J_o^2(c_s a)}\sum_{k=o}^{\infty}\frac{\sin\left[\frac{k\pi}{2L}(x+d+L)\right]\sin\left[\frac{k\pi}{2L}(z+L)\right]}{\left(\frac{k\pi}{2L}\right)^2 + c_s^2} \qquad \text{(A. 17)}$$

As before, the magnetostatic potential is found by taking the weighted sum of the Green's functions corresponding to the two poles. Using the trigonometric identity

$$\sin\left[\frac{k\pi}{2L}(x+L+d)\right] - \sin\left[\frac{k\pi}{2L}(x+L-d)\right] = 2\cos\left[\frac{k\pi}{2L}(x+L)\right]\sin\frac{k\pi d}{2L} \qquad \text{(A. 18)}$$

the potential is found to be

$$\Omega = \frac{4p}{La^2}\sum_s \frac{J_o(c_s r)}{J_o^2(c_s a)}\sum_{k=-\infty}^{\infty}\frac{\sin\left[\frac{k\pi}{2L}(z+L)\right]\cos\left[\frac{k\pi}{2L}(x+L)\right]\sin\frac{k\pi d}{2L}}{\left(\frac{k\pi}{2L}\right)^2 + c_s^2} \qquad \text{(A. 19)}$$

where the sum over k has been extended to -∞ by virtue of the evenness of the terms with respect to k.

It is possible, although somewhat involved, to obtain a closed form representation of the z-dependence. To simplify the algebra, the products of trigonometric functions are first expanded:

$$\sin\left[\frac{k\pi}{2L}(z+L)\right]\cos\left[\frac{k\pi}{2L}(x+L)\right]\sin\frac{k\pi d}{2L} = \frac{1}{2}\left[\sin\left[\frac{k\pi}{2L}(2L+x+z)\right]+\sin\left[\frac{k\pi}{2L}(z-x)\right]\right]\sin\frac{k\pi d}{2L}$$

$$= \frac{1}{4}\left[\cos\left[\frac{k\pi}{2L}(2L+x+z-d)\right]-\cos\left[\frac{k\pi}{2L}(2L+x+z+d)\right]\right.$$

$$\left.+\cos\left[\frac{k\pi}{2L}(z-x-d)\right]-\cos\left[\frac{k\pi}{2L}(z-x+d)\right]\right]$$

(A. 20)

The problem has therefore been reduced to evaluating sums of the form

$$S = \sum_{k=-\infty}^{\infty}\frac{\cos\frac{k\pi q}{2L}}{\left(\frac{k\pi}{2L}\right)^2+c_s^2} \qquad \text{(A. 21)}$$

which may be achieved by use of Poisson's sum formula$^{(21)}$

$$\sum_{n=-\infty}^{\infty} f(\lambda n) = \frac{\sqrt{(2\pi)}}{\lambda}\sum_{m=-\infty}^{\infty}\Phi\left(\frac{2m\pi}{\lambda}\right) \qquad \text{(A. 22)}$$

where Φ is the Fourier transform of f.

For the present application, put

$$f(n) = \frac{\cos nq}{n^2+c_s^2} \qquad \text{(A. 23)}$$

and

$$\lambda = \frac{\pi}{2L} \qquad \text{(A. 24)}$$

Then

$$\Phi(\omega) = \frac{1}{\sqrt{2\pi}}\int_{-\infty}^{\infty}\frac{e^{j\omega n}\cos nq}{n^2+c_s^2}\,dn$$

$$= \frac{\sqrt{\pi}}{2c_s\sqrt{2}}\left(e^{-c_s|\omega+x|}+e^{-c_s|\omega-x|}\right) \qquad \text{(A. 25)}$$

so

$$\sum_n f(\lambda n) = \frac{L}{c_s} \sum_m \left(e^{-c_s |4Lm+q|} + e^{-c_s |4Lm-q|} \right) \qquad \text{(A. 26)}$$

An examination of (A. 20) shows that, for all the sums of interest, $|q| < 4L$. Thus

$$\sum_{n=-\infty}^{\infty} f(\lambda n) = \frac{2L}{c_s} \left(e^{-c_s |q|} + 2\cosh c_s q \sum_{m=1}^{\infty} e^{-4c_s Lm} \right)$$

$$= \frac{2L}{c_s} \left(e^{-c_s |q|} + 2\cosh c_s q \, \frac{e^{-4c_s L}}{1 - e^{-4c_s L}} \right)$$

$$= \frac{2L}{c_s} \, \frac{\cosh c_s (|q| - 2L)}{\sinh 2c_s L} \qquad \text{(A. 27)}$$

Substituting the various values of q from (A. 20) and inserting the results in (A. 19) gives the following expressions for the potential after some algebraic reduction:

$$\Omega = \frac{8p}{a} \sum_s \frac{J_o(c_s r) \sinh c_s d \sinh c_s (L - z) \cosh c_s (L + x)}{c_s a J_o^2 (c_s a) \sinh 2c_s L} \qquad \text{(A. 28a)}$$

for $z > x + d$ and

$$\Omega = -\frac{8p}{a} \sum_s \frac{J_o(c_s r) \sinh c_s d \sinh c_s (L + z) \cosh c_s (L - x)}{c_s a J_o^2 (c_s a) \sinh 2c_s L} \qquad \text{(A. 28b)}$$

for $z > x - d$

As a check on the algebra, note that (A. 28a) is zero at $z = L$ and (A. 28b) at $z = -L$. Also, both expressions have the limiting form

$$\Omega = \pm \frac{4p}{a} \sum_s \frac{J_o(c_s r)}{c_s a J_o^2 (c_s a)} \, e^{-c_s |z - x|} \sinh c_s d \qquad \text{(A. 29)}$$

as L approaches infinity, which is the correct value.

If $L >> a$, and the magnet is not near one of the ends of the tube, it is clear from Eqs. (A. 28) that only the first term in the sums over s will be significant.

At the ends of the tube, the magnetic field of course has only a z-component. The net force on the end at z = L is given by

$$F_1 = \frac{1}{8\pi} \int_S H_z^2 \, dS \tag{A.30}$$

where S is the area of the end. From (A.28a)

$$F_1 = \frac{-8p^2}{a^2 J_o^2 (c_1 a)} \; \frac{\sinh^2 c_1 d \cosh^2 c_1 (L + x)}{\sinh^2 2c_1 L} \tag{A.31}$$

Similarly, the force on the other end is

$$F_2 = \frac{8p^2}{a^2 J_o^2 (c_1 a)} \; \frac{\sinh^2 c_1 d \; \cosh^2 c_1 (L - x)}{\sinh^2 2c_1 L} \tag{A.32}$$

The net force on the magnet is of course the negative difference of these forces, or

$$F = \frac{8p^2}{a^2 J_o^2 (c_1 a)} \; \frac{\sinh^2 c_1 d}{\sinh 2c_1 L} \; \sinh 2c_1 x \tag{A.33}$$

A.4 Forces from Stabilizing Coils

Consider the infinite length tube of Section A.2, with the addition of single-turn coils of radius b at $z = \pm z_c$. The axes of the coils are coincident with the tube axis. With a current of I amperes flowing in one of the coils, the force on an element $\underline{dl}$ of it is given by

$$\underline{dF} = 10 \; I \, \underline{dl} \times \underline{H} \tag{A.34}$$

where $\underline{dl}$ is measured in cm and $\underline{H}$ is the magnetic field of the test-mass in oersteds.

By symmetry, radial forces will cancel, so the net force on the coil is in the axial direction:

$$F_z = 20\pi \; I b H_r \tag{A.35}$$

Assuming $(z_c - x)$ is fairly large (at least of the order of the tube radius), H_r may be calculated from (A.13) or (A.33), retaining only the first term of the sum

Thus

$$F_z = \mp \frac{80\pi\ b\ p}{a^2 J_o^2 (c_1 a)} \ J_1(c_1 b) \ \sinh c_1 d \ I \ e^{-c_1 \left| z_c - x \right|} \tag{A.36}$$

If the same current is flowing in each coil, the net force on the magnet is

$$F_c = \frac{160\pi\ b\ p}{a^2 J_o^2 (c_1 a)} \ J_1(c_1 b) \ \sinh c_1 d \ e^{-c_1 \left| z_c \right|} \ I \ \sinh c_1 x \tag{A.37}$$

REFERENCES

1. Brune, J.N., and Oliver, J., "The Seismic Noise of the Earth's Surface", Bulletin of the Seismological Society of America, Vol. 49, #4 October 1959, pp.349-353.
2. Roberson, R.E., "Attitude Control of Satellites and Space Vehicles", Advances in Space Science, Vol. 2, pp.351-436, Academic Press, New York, 1960.
3. Weber, J., "General Relativity and Gravitational Waves", Interscience Tracts on Physics and Astronomy, #10, 1961; Sec 8.2, p.126.
4. Tilton, Parkin, Covert, Coffin and Chrisinger, "The Design and Initial Operation of a Magnetic Model Suspension and Force Measurement System", M.I.T. Aerophysics Laboratory Technical Report #22, August 1962.
5. Gilinson, P.J., Jr., Denhard, W.G., and Frazier, R.H., "A Magnetic Support for Floated Inertial Instruments", M.I.T. Instrumentation Laboratory Report #R-277, April 1960.
6. Nordsieck, "Principles of the Electric Vacuum Gyroscope", Progress in Astronautics and Rocketry, Vol. 8, Guidance and Control, p.435, Academic Press, New York, 1962.
7. Martin Company, Orlando, Florida, Report OR 3673, "Analytical Report on Particle Reference Device".
8. Kamerlingh-Onnes, H., "Disappearance of the Electrical Resistance of Mercury at Helium Temperature", Commun. Phys. Lab. Univ. Leiden, #122b (1911); ibid, Supplement #34 (1913).
9. Quinn, D.J., III, and Ittner, W., III, "Resistance in a Superconductor", J. Appl. Phys., Vol. 33, 1962, p.748.
10. Bremer, J.W., "Superconductive Devices", McGraw-Hill, New York, 1962, p. 3.
11. Schawlow, A.L., Phys. Rev., Vol. 101, 1956, p.573.
12. Meissner, W., and Ochsenfeld, R., Ein Neuer Effekt bei Eintritt der Supraleitfahigkeit", Naturwissenschaften, Vol. 21, 1933, p.787.
13. London, F., and London, H, Proc. Roy. Soc. A, Vol. 149, 1935, p.71.

14. Bardeen, J., Cooper, L. N., and Schrieffer, J. R., Phys. Rev., Vol. 106, 1957, p.162; ibid, Vol. 108, 1957, p.1175.

15. Einstein, A., Ber. Berlin Acad. 261 (1924).

16. Schafroth, M. R., Phys. Rev. 100, 463 (1955).

17. e.g. Blatt, J. M., "Theory of Superconductivity" Academic Press, New York, 1964.

18. Arkadiev, V., Nature, Vol. 160, 1947, p.330.

19. Harding, J. T., and Tuffins, R. H., Advances in Cryogenic Engineering, (K.D. Timmerhaus, Ed.) Plenum Press, New York, 1961, Vol. 6, p.95.

20. Simon, I, J. Appl. Phys., Vol. 24, 1955, p.19.

21. Morse, P. M., and Feshbach, H., "Methods of Theoretical Physics," McGraw-Hill, New York, 1953, p.494.

22. Ezekiel, S., "Towards a Low Level Accelerometer," M. I. T. Experimental Astronomy Laboratory Report, TE-11, June 1964.

23. Born and Wolf, "Principles of Optics," McGraw-Hill 1964.

24. Scott, L. B., 1958, U.S. Patent No. 2,841,049.

25. Steel, W.H., Opt. Acta. 11, 211, (1964).

26. Electro-Optic Light Modulators, Bulletin 1201, ISOMET Corp., Palisades Park, New Jersey.

27. Shurcliff, W.A., "Polarized Light," Harvard University Press, 1962.

28. Cyclonome Stepping Motor, Sigma Instruments, Braintree, Massachusetts.

29. Hall, R. N. "Private Communication",

30. Patel, C.K.N., Phys. Rev. Letters, Vol. 13, No. 21, November 23, 1964.

31. Tsutsumi, K., "A Ground Tilt Isolation Platform," M. I. T. Instrumentation Laboratory Report E-1508, January 1964.

PUBLICATIONS

1. Chapman, P.K., "A Cryogenic Test-Mass Suspension for an Accelerometer," Thesis (S.M.), Department of Aeronautics and Astronautics, M.I.T., published as an Experimental Astronomy Laboratory Report, TE-10, June, 1964
2. Ezekiel, S., "Towards a Low-Level Accelerometer," Thesis, (S.M.), Department of Aeronautics and Astronautics, M.I.T., published as an Experimental Astronomy Laboratory Report, TE-11, June, 1964.
3. Chapman, P.K., And Ezekiel, S., "A Sensitive Cryogenic Accelerometer," M.I.T. Experimental Astronomy Laboratory Report, RE-13, October, 1964. This report was presented at the Proceedings of the 1964 Symposium on Unconventional Inertial Sensors, Polytechnic Institute of Brooklyn, Farmingdale, L.I., New York, October, 1964.
4. Chapman, P.K., and Ezekiel, S., "Une Technique Originale de Mesure par L'Inertie," ("An Unconventional Inertial Measurement Technique,") IV. 22, p. 589, Memorial de l'Artillerie Francaise, 3^e fasc. 1965.
5. Chapman, P.K., and Ezekiel, S., "Superconducting Suspension for a Sensitive Accelerometer," Rev. for Sci. Instru., Vol. 36, No. 1, 96, January, 1965.
6. Ezekiel, Shaoul, " Low Level Acceleration Measurement Apparatus, (LLAMA)," M.I.T. Experimental Astronomy Laboratory Report, (semi-annual status report), RN-6, June, 1965.
7. Ezekiel, S., Chapman, P.K., and Egan, J.T., "Analytical and Experimental Investigations of Low Level Acceleration Measurement Techniques," M.I.T. Experimental Astronomy Laboratory Report, RE-23, April, 1966.